FS Sonne Fahrtbericht / Cruise Report
SO213

SOPATRA:
South **Pa**cific Paleoceanographic **Tra**nsects
Geodynamic and Climatic Variability in Space and Time

Leg 1
Valparaiso/Chile – Valparaiso/Chile
27.012.2010 - 12.01.2011

and

Leg 2
Valparaiso/Chile – Wellington/New Zealand
12.01.2011 - 07.03.2011

Acknowledgements

We would like to thank the German Ministry of Education and Research (BMBF) for granting the SOPATRA & FOUNDATION proposals and for the possibility to carry out the scientific cruises SO213 Legs 1 and 2 into the South Pacific.

We are grateful to Captain Lutz Mallone and Oliver Meier, the officers and the crew onboard RV *SONNE* for their excellent support in all work done and for the splendid working atmosphere throughout the entire cruise, despite the length and sometimes adverse weather conditions. Maintaining shipboard harmony, safety standards, enthusiasm and high efficiency throughout a 9 week-long cruise is not an easy undertaking. Their high level of experience and unremitting engagement significantly contributed to the success of the SO213 cruise.

We would also like to express our gratitude to the Captain, officers and crew for their forbearance and assistance with the highly successful public open day held in Valparaiso at the beginning of the cruise.

SUMMARY

The R/V Sonne cruise SO213 comprised two expeditions into the South Pacific and combined a volcanological and a paleoceanographical program within the project SOPATRA (**So**uth **Pa**cific **Tra**nsects). The major paleoceanographic goals of SOPATRA were to reconstruct spatial and temporal changes of the oceanic frontal system, including the dynamic of the Humboldt Current, Pleistocene variations in dust transport, and changes in intermediate and deep water ventilation and circulation. Another task was to identify potential drill sites for the Integrated Ocean Drilling Program (IODP) and to support our IODP proposal CESOP (Cenozoic Southern Ocean Pacific) with seismic site survey data. The volcanology goals of the SO213 expedition were aimed at understanding how hotspots interact with spreading ridges, and if hotspots originate from shallow plate processes or from plumes upwelling from deep in the mantle. SOPATRA has been funded by the German Ministry for Education and Science. Major partners of the project are the Alfred Wegener Institute for Polar and Marine Research (AWI), Helmholtz Centre for Ocean Research (GEOMAR), Leibniz Institute of Marine Science (IFM-GEOMAR), Center for Marine Environmental Sciences (MARUM), GeoZentrum Nordbayern (University Erlangen-Nürnberg), Geomarine Research Auckland (New Zealand) and the University of Salamanca (Spain). Leg 1 (SO213-1) exclusively dealt with paleoceanographical topics. It started on December 27, 2010 in Valparaiso and ended on January 12, 2011 in Valparaiso (Chile). Leg 2 started on January 15, 2011 and ended on March 6, 2011 in Wellington (New Zealand). Leg 2 was multidisciplinary and pursued scientific targets that were related to the origin and development of the Foundation Seamount Chain and to the paleoceanographical history of the South Pacific.

Our working areas focused on five different regions: the Challenger Fracture Zone (CFZ), the Chile Rise (ChiRi), the East Pacific Rise (EPR, 36°S – 47°S), the Southwest Pacific Basin (SWB) and the New Zealand Continental Margin south of Chatham Rise (NZM). At the EPR, we had to abandon our initial plan of going farther south, since the weather forecast made it impossible for us to accomplish any research work on 50°S or even further south. Hence, we left this region and headed to our alternative research area– the New Zealand Continental Margin.

During the SO213 expedition, we successfully achieved our strategic goals of retrieving volcanic and other magmatic rocks from the Foundation Seamount Chain and the Pacific-Antarctic spreading axis, as well as water samples and sediment records along latitudinal and longitudinal transects from various water depths. In total, we performed 14 dredge stations, 10 rock corer stations and 7 CTD stations (including plankton net and multinet hauls), as well as 44 sediment core deployments (350 m of sediment recovery) and 35 multicorer operations (70 m of sediment recovery). In addition, we successfully recorded 1131 km of seismic reflection profiles in two different regions: the Central South Pacific west of the East Pacific Rise and along the Bounty Trough east off New Zealand.

The sediment records from CFZ, ChiRi, EPR and SWB are marked by low time resolution with sedimentations rates lower than 3 cm/1000 years. However, some of the records span the entire time interval of the last 5.5 million years or even provide insights into Miocene paleoceanographical changes. West of the Pacific rise, we performed a seismic pre-site survey for a potential IODP drilling location and identified a sediment sequence more than 100 m thick. With respect to the basement age and biostratigraphy, this sediment package most likely comprises an expanded Middle Miocene to Pliocene sequence. The sediment cores from the New Zealand continental margin are marked by high sedimentation rates (~20 to >100 cm/1000 years) and form a deep-water transect from 500 to 5000 m water depth. These records will provide detailed insights in the Holocene to Pleistocene variability in deep-water circulation and ventilation.

The most exciting and unexpected result of the volcanological operations was our mapping of the Westerly Seamounts and the Diagonal Ridges, which revealed for the first time that Volcanic Elongate Ridges (VERs) appear to have formed initially as chains of volcanoes that continued to grow and fill in the gaps between them to ultimately form volcanic ridges. This new insight is significant since it has broad implications for our understanding of age-progression in volcanic lineaments on the Pacific plate. This issue is especially important for determining whether Pacific intra-plate volcanism is caused by shallow plate tectonics or deep hotspots (mantle plumes).

During the transit to the New Zealand working area, we sampled the large guyot while marking the 'Young Bend' in the virtually un-sampled SE end of the Louisville hotspot trail. We recovered small rounded boulders with excellent potential for establishing the composition of the Louisville mantle (plume?) source, testing them for faster age-progression during the past 15-20 million years, and determining the age of the 'young Louisville Bend'.

CONTENTS

D. Core description
E. Core photos
F. Volcanology – Samplinfg summary
G. Volcanology – Rock description
H. Dredge samples – Paleontological information
I. Detailed results summary of foraminiferal biostratigraphy

1. INTRODUCTION

The R/V Sonne cruise SO213 comprises two expeditions into the South Pacific (Fig. 1-1) and interconnects a volcanologic and a paleoceanographic program within the project SOPATRA (**So**uth **Pa**cific **Tra**nsects), which is funded by the German Ministry for Education and Science. Leg 1 (SO213-1) exclusively deals with paleoceanographic topics. Leg 2 (SO213-2) is multidisciplinary and pursues scientific targets that are related to the origin and development of the Foundation seamount chain and to the paleoceanographic history of the South Pacific.

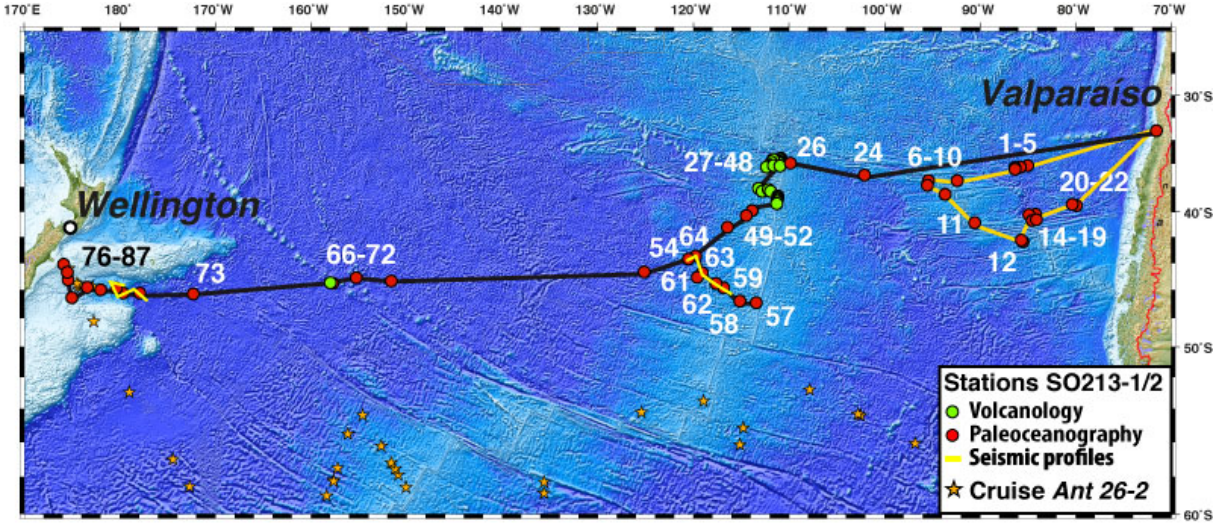

Fig. 1-1: SO213 cruise track of Leg 1 (dark yellow line) and 2 (black line). GEBCO map made by WTD on board RV SONNE.

1.1 PALEOCEANOGRAPHIC OBJECTIVES

Although the Southern Ocean represents a key component for understanding the processes of past climate variability, its largest region – the South Pacific - forms a blank spot on our paleoceanographic maps. Our project SOPATRA will contribute to close this gap in our knowledge. The main objective of the cruise was to collect sediment records for reconstructing changes in atmospheric and oceanic circulation patterns in the South Pacific. Leg 1 was designed to provide longitudinal and latitudinal transects of sediment records across the Humboldt Current, which stretch from the Robinson Crusoe Islands along the Challenger Fracture Zone to the Chile Rise and then south-eastward along the Chile Rise to the Valdivia Fracture Zone. Leg 2 extends the longitudinal transect further westward to the East Pacific Ridge. The major goal of Leg 2, however, was to provide both a deep-water transect of sediment records as well as a latitudinal transect along the East Pacific Ridge between 35°S and 55°S. Another, yet subordinated goal was to complete a deep to intermediate water transect of sediment records at the continental margin of New Zealand between Chatham Rise and Campbell Plateau, which was started with the Polarstern Expedition ANT26-2.

This framework of sediment records will be used to reconstruct changes in temperature, salinity, stratification of the upper water column, deep-water circulation, as well as changes in plankton productivity. These data will provide insights into the temporal and spatial dynamic of the South Pacific subtropical high, the Westerly Wind belt, the northern Antarctic Circumpolar Current (ACC) the cold Humboldt Current, and the South Pacific deep-water circulation. Thus, they will yield another important jigsaw piece for understanding the variety and interaction of climate processes, their causes and impacts.

In order to better understand the climatically relevant causal effects between oceanic, terrestrial, cryogenic and atmospheric processes and their effects on the Pliocene to

Holocene climatic evolution in the Subantarctic South Pacific, we will apply a variety of state-of-the-art paleoceanographic proxies to reconstruct climate and ocean variables. Our paleoceanographic studies will focus on the following topics:

- Position and extent of oceanic frontal systems (Subtropical Front, Subantarctic Front) in relation to the position and strength of the Subtropical High and the Westerlies
- Dynamic and heat transfer of the Humboldt Current
- Stratification of the upper water column and its impact on the oceanic-atmospheric gas exchange and the nutrient concentrations in the photic zone
- Deep-water formation, circulation, and carbonate chemistry
- Long-term changes in deep-water circulation as deduced from geometric changes in sediment deposits
- Identification of potential coring spots for IODP

1.2 PALEOCEANOGRAPHIC BACKGROUND

Relevance of the Southern Ocean for climate change – the Pacific sector as the missing link

The cryospheric, atmospheric and oceanic changes in the Southern Ocean are regarded as key components for understanding and explaining climate change on orbital and sub-orbital timescales. In comparison to the Atlantic-Indian sector of the Southern Ocean, the Pacific sector has been poorly investigated and thus forms a missing link in considering and understanding the entire circum-Antarctic pattern of climate change. Glacial to interglacial variations in sea-ice cover, upper ocean stratification, biological nutrient utilization and exposure rates of deep-water in the Southern Ocean have been considered to play a key role in explaining the variability in atmospheric CO_2 concentrations (Sarmiento and Toggweiler, 1987; Stephens and Keeling, 2000; Gildor and Tzipermann, 2001; Sigman et al., 2010). The Southern Ocean interaction with water masses from the Atlantic, Indian and Pacific oceans is a significant element of the global thermohaline circulation because it influences the salt, heat and nutrient balances of the world ocean and triggers climate

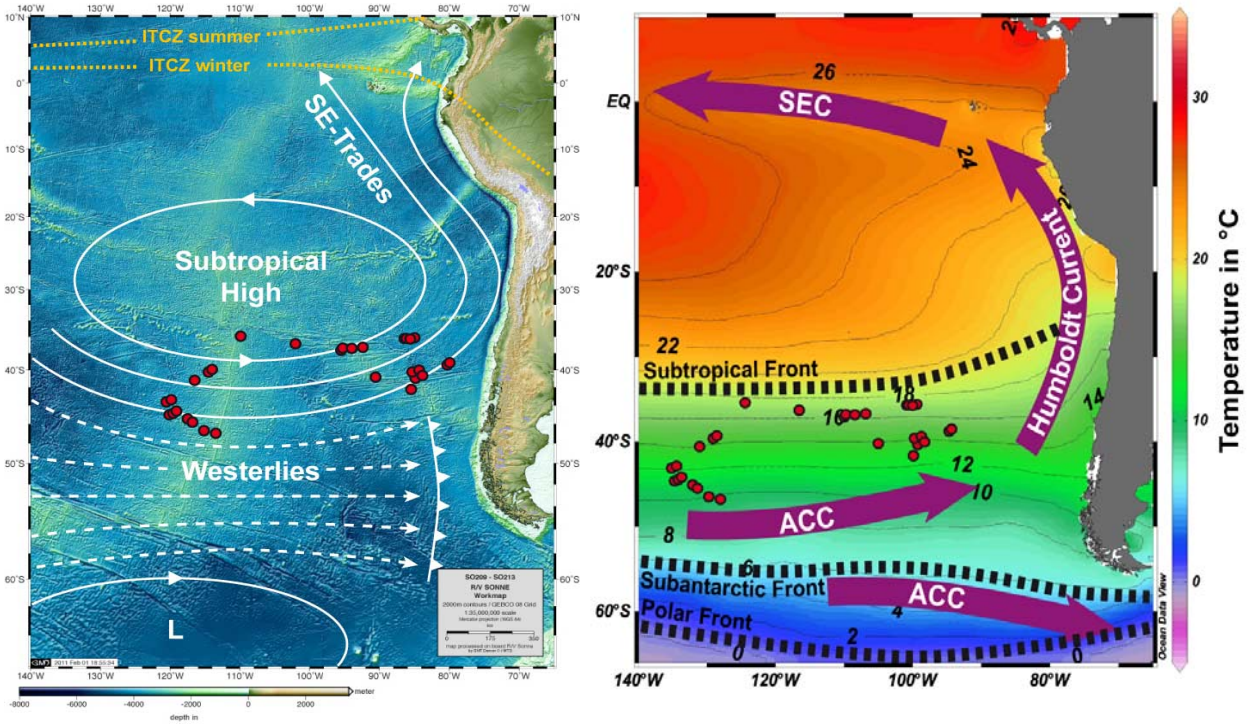

Fig. 1.2-1: Atmospheric (left) and oceanic (right) circulation patterns and fronts in the South Pacific. Red dots indicate paleoceanograhic stations of SO213 Leg 1 and 2.

feedbacks associated with heat transport and the carbon cycle. Latitudinal migrations of the oceanic fronts (Polar Front, Subantarctic Front, Subtropical Front), which are closely coupled to variations in the strength and position of the Westerly Wind belt, the subtropical high pressure cell and the Intertropical Convergence Zone exert a strong control on the northward export of subantarctic surface waters (e.g. the Humboldt Current) and newly formed subsurface water masses (Subantarctic Mode Water, Antarctic Intermediate Water, Antarctic Bottom Water).

Pleistocene migration of oceanic fronts and its implications

In the Southern Ocean, three oceanic frontal systems are commonly differentiated: the Antarctic Polar Front (APF), the Subantarctic Front (SAF), and the Subtropical Front (STF) (Fig. 1.2-1, 1.2-2) (Deacon et al., 1982; Belkin and Gordon, 1996; Orsi et al., 1995; Chaigneau and Pizarro, 2005). These oceanographic fronts are characterized by strong gradients in sea surface salinity and temperature, with increasing salinity and temperature towards the north. The STF separates cool, fresh and nutrient-rich subantarctic water masses in the south from warmer, saltier and nutrient-depleted subtropical water masses in the north, thereby affecting the position of the Westerlies. In the Pacific, the modern position of the STF occurs between 32°S and 37°S at 110°W (East Pacific Rise). Further eastward at 80°W, the STF is less well defined but is located further to the north between 25°W and 32°W (Schneider et al., 2003;

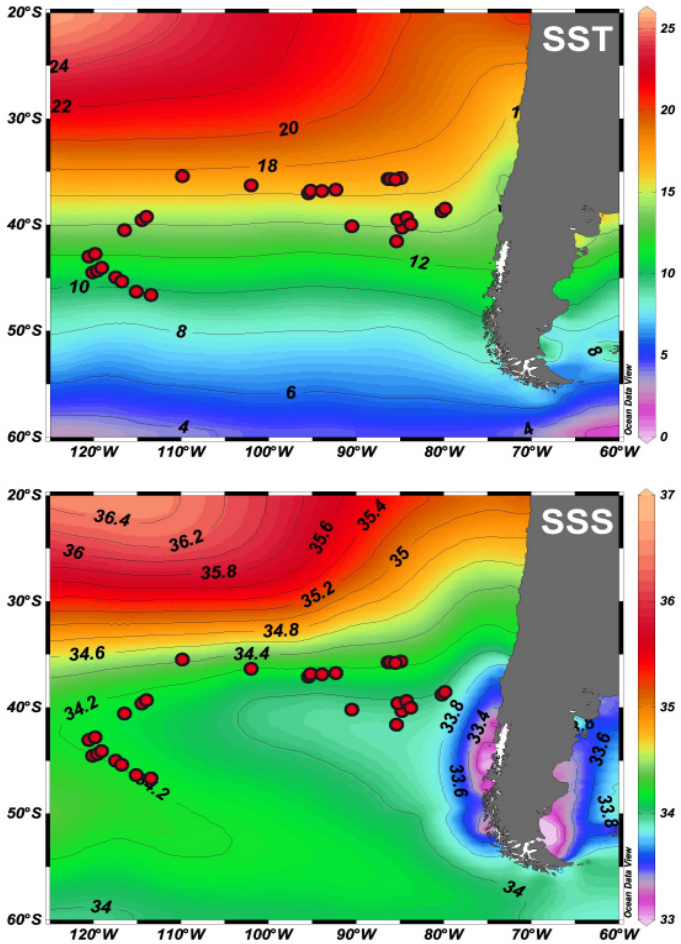

Fig. 1.2-2: Distribution of annual mean sea surface temperature (SST) and salinity (SSS) in the study area. Red dots indicate paleoceanograhic stations of SO213 Leg 1 and 2 in the SE-Pacific.

Chaigneau and Pizarro, 2005) due to the influence of the Humboldt Current, which transports subantarctic water masses equatorward along the coast of South America. Hence, the study area of Leg 1 and 2 is located within subantarctic water masses and thus, from an oceanographic point of view, belongs to the Southern Ocean (Fig. 1.2-1). South of the STF, the ACC, driven by the strong westerly winds, transports water mass signatures from the Pacific into the Atlantic via the Drake Passage. In general the SAF is located south of 55°S and the APF south of 60°S. Today, both fronts cross the Drake Passage. North of the SAF, Subantarctic Mode Water (SAMW) is formed due to strong wind-induced surface mixing and cooling during the winter months. Further to the south close to the PF Antarctic Intermediate Water (AAIW) is formed. The formation areas for both SAMW and AAIW are hence characterized by a deep thermocline. North of the SAF, however, the stratification in the upper oceanic mixed layer increases (seasonal thermocline, and permanent thermocline north of the STF).

Spatial changes in the STF and the PF on glacial/interglacial timescales have been described in detail for the Indian Ocean (Hays et al., 1976; Prell et al., 1979, 1986; Howard and Prell, 1992; Armand, 1997). For the South Atlantic, northward deflections of the PF during the glacials were reconstructed based on changes in sea surface temperature (Morley et al., 1988; Morley, 1989; Labracherie et al., 1989; Howard and Prell, 1992; Pichon et al., 1992) and marine productivity (e.g., Howard and Prell, 1992). The lateral extent of frontal movements, however, has remained speculative. For the last four glacial/interglacial cycles, Nürnberg and Groeneveld (2006) suggested that during interglacial times at the transition between Indian and Pacific oceans, the STC remained clearly south of Tasmania. During glacials, instead, subantarctic water masses might have moved northward up to <44°S. Around Tasmania, the frontal movement is relatively small, but is much more pronounced and synchronous in the subantarctic Indian Ocean and at Chatham Rise (New Zealand).

Based on faunal and floral assemblages, Gersonde et al. (2003) reconstructed a northward movement of the SAF by 5° in the Atlantic sector of the Southern Ocean and an extension of the winter sea ice coverage by 65% for the last glacial maximum (LGM). Since the STF only slightly moved northward during the LGM, largest temperature gradients occurred between the STF and the SAF (Gersonde et al., 2005; Nürnberg and Groeneveld, 2006).

Climate models suggest that the northward migration of the oceanic frontal system may provide a substantial mechanism to explain the glacial drop in atmospheric CO_2. The extended winter sea ice coverage and the strengthened ice-induced stratification of the upper water column during summer, in combination with a more effective biological pump, would clearly reduce the CO_2 flux from the ocean into the atmosphere (Stephens and Keeling, 2000; Sigman and Boyle, 2000; Sigman et al., 2004).

For the Pacific sector of the Southern Ocean, the glacial positions of the STF and the SAF are largely unknown, mainly due to the fact that appropriate sediment records are missing. Such records, in fact, are essential for successful paleoclimate modelling studies.

Paleotemperature reconstructions from a latitudinal core transect south of 60°S (Gersonde et al., 2005) suggest that the PF in the eastern Pacific (at ~120°W) only varied insignificantly on glacial/interglacial timescales. Other reconstructions from the Chilean margin (Kaiser et al., 2005), however, propose that the zone of the Westerlies shifted northward by 5° during the last glacial. This would also imply a northward shift of the SAF. In consequence, it might be hypothesized that the SAF remained north of the Drake Passage during the LGM. Such an oceanographic configuration should have reduced the surface water mass transport through the Drake Passage on one hand. On the other hand, it should have strengthened the Humboldt Current and, hence, the northward transport of cool and low-saline waters along the South American coast. Further, the glacial shift of oceanic fronts should have provoked the displacement of AAIW and SAMW formation areas towards the north, which in consequence should have reduced the flow of AAIW and SAMW from the Pacific into the Atlantic Ocean. Whether this scenario holds true for the northernmost areas of the Southern Ocean, or whether surface temperature and salinity gradients inclined during the LGM has yet to be verified.

Changes in deep water circulation

In comparison to the Atlantic and Indian Ocean sectors of the Southern Ocean, not much is known about the Pleistocene long and short-term changes in Pacific deep-water circulation. Thus, our picture about glacial/interglacial changes in deep water circulation and ventilation is incomplete and our understanding is mainly based on proxy-records from the Atlantic sector of the Southern Ocean. Expanding our knowledge into the Pacific sector may help to tackle some of the most pressing questions in paleoceanography.

The modern Southern Ocean releases deeply sequestered CO_2 into the atmosphere since the release through upwelled, nutrient-rich and old CO_2-charged deep-waters around Antarctica is not balanced by the biological pump, which acts to lower the partial pressure of CO_2 in the surface waters and consequently draws CO_2 out of the atmosphere. Growing evidence suggests that this Southern Ocean CO_2-leak was significantly reduced during glacial stages. The interplay between old upwelled deep-water masses and the efficiency of the biological pump is regarded to be one of the major drivers to explain the glacial decease in atmospheric CO_2-concentrations. However, whether the glacial leak was stemmed by enhanced upper ocean stratification or an increase in biological productivity is still a matter of debate. An increase in Antarctic surface water stratification during the last glacial would, in turn, reduce Antarctic deep to intermediate water formation and ventilation (Sigman et al., 2010). Support for this hypothesis is provided by the studies of Pahnke and Zahn (2005) and Pahnke et al. (2008). On the basis of benthic $\delta^{13}C$ records and Nd isotope records, they concluded that AAIW formation has been stronger during interglacials than during glacials. In contrast, new benthic $\delta^{13}C$ records from the Tasman Sea and modelling results from Steph et al. (submitted) question the hypothesis of Sigman et al. (2010), which proposes stronger water column stratification resulted in reduced production of glacial AAIW, indicating the continuous presence of well ventilated glacial AAIW. During glacials AAIW was shallower, fresher, more buoyant and possibly more vigorous than during interglacials. In addition, the majority of modeling studies support the hypothesis of enhanced Antarctic-sourced deep-water formation (e.g. Antarctic Bottom Water) (Liu et al., 2005) during the glacial, as the models balance the observed shoaling of the glacial North Atlantic Deep Water (NADW) by increasing the formation rate of Antarctic deep water. Consequently, the physical significance of one of the most prominent aspects of the ice age ocean remains in question.

Another aspect that may provide new insights into the stratification hypothesis is related to the supply of nutrients (and thus water) to the Antarctic surface from the deep ocean. Today, the nutrient concentration at the surface of the Southern Ocean contains ca. 90% of the global surface water nutrient reservoir. These high nutrient concentrations are related to the upwelling of nutrient-rich circumpolar deep-waters, which represent a mixture of old, southward flowing, re-circulated water masses that enter the Southern Ocean from the Atlantic, Indian and Pacific oceans. The nutrient contribution from the NADW is limited due to its relatively young age. However, the deep return flows from the Indian and Pacific oceans are characterized by high nutrient contents. Accordingly, one of the goals of the SOPATRA project is to collect sediment records that form a deep-water transect in the South Pacific. We are especially interested in the temporal changes of the flow dynamics and the nutrient contents of the Pacific Central Water (PCW), which flows from the North Pacific towards Antarctica (Fig. 1.2-3). It is the oldest water mass of the world, characterized by highest nutrient- and CO_2 contents, and thus forms a critical end-member of the global carbon cycle. Within the region of the Antarctic Polar Front, these water masses are exposed to the surface, and exchange their CO_2 with the atmosphere. During this exchange, great nutrient reserves are being released, which contribute to the richness in Antarctic surface nutrients, thereby stimulating the biological productivity. The glacial difference in nutrient concentrations between the PCW, just before it upwelled into the photic zone (preformed nutrients), and the AAIW, which is downwelled further north, would provide insights in both the glacial efficiency of the biological pump (e.g. a large difference would suggest a high efficiency) and/or the hypothesis of a stratified Southern Ocean during glacial times. Strongly

reduced exposure rates of PCW would increase its nutrient inventory due to the aging-effect of the water mass, which in turn would increase its ventilation age. In this scenario, the AAIW should provide lower ventilation ages, since an enhancement in upper ocean stratification would significantly reduce the PCW imprint of old CO_2 on the AAIW. De Pol-Holz et al. (2010) reconstructed the $\Delta^{14}C$ signature of Antarctic Intermediate Water off the coast of Chile for the past 20,000 years, using paired ^{14}C ages of benthic and planktonic foraminifera. In contrast to the above scenario, they find that the glacial $\Delta^{14}C$ signature of the Antarctic Intermediate Water nearly matches the modern one. This finding does not support the stratification hypothesis.

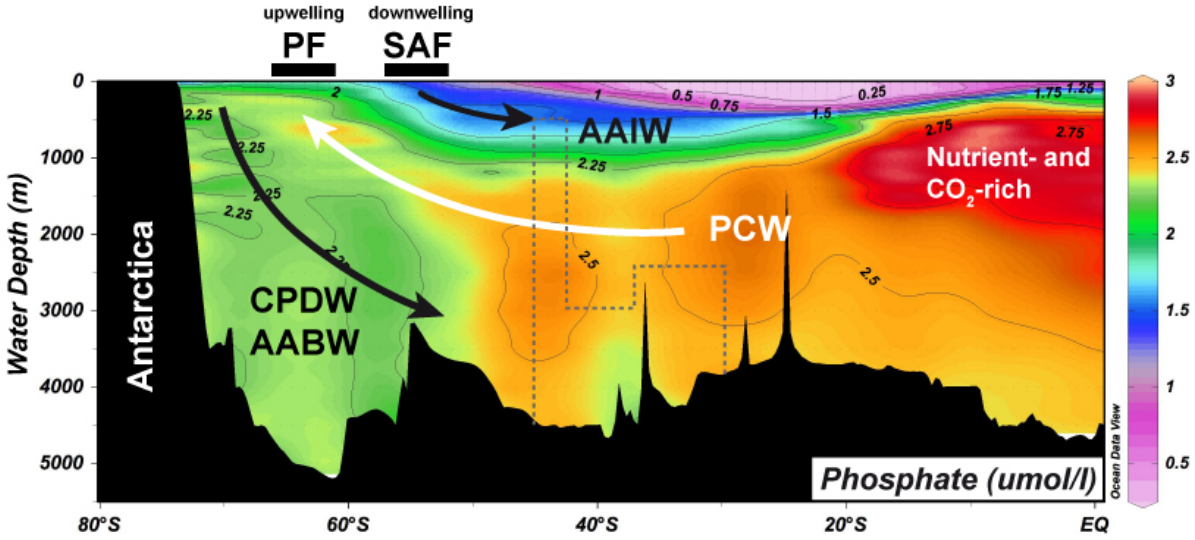

Fig. 1.2-3: North-South transect of nutrient concentration (PO_4) along 125°W reflects the flow of major deep and intermediate water masses: Pacific Central Water (PCW), Antarctic Intermediate Water (AAIW), Circumpolar Deep Water (CPDW), Antarctic Bottom Water. PF = Polar Front, SAF = Subantarctic Front. Grey dotted line indicates the deep water transect of SO213 sediment records (the depth interval from 2500-4000 m is covered by sediment cores from the SE-Pacific; the interval from 500-2500 m is covered with cores from the continental margin of New Zealand.

The glacial benthic foraminiferal $\delta^{18}O$ and $\delta^{13}C$ signatures of the world's major deep-water masses below 2500 m water depth (which are indicative of changes in deep-water temperature/salinity and ventilation) pose another enigma. Since all deep-water masses of the world ocean enter or leave the Southern Ocean, one can expect these values to plot on mixing lines between end-members that are located in the N-Atlantic, the Pacific and the Southern Ocean (Fig. 1.2-4). However, this relationship clearly isolates the water mass signatures of the Southern Ocean from the Pacific and Atlantic. One of the problems is that the Southern Ocean signatures only reflect the Atlantic sector of the Southern Ocean and so far, we have no information from the Pacific sector of the Southern Ocean. This diagram impressively highlights the need for establishing a circum-Antarctic network of proxy records. SOPATRA will contribute to close the Pacific gap.

A further step to solve the problem is the application of Nd-isotopes to trace the mixing of Atlantic and Pacific water masses (Rutberg et al., 2000; Piotrowski et al., 2005). The rare earth element Nd enters the ocean via continental weathering. Based on its oceanic residence time of 500-1000 years (Piepgras and Wasserburg, 1982; Jeandel, 1993; Frank et al., 2002) and the largely varying continental Nd-isotope signatures, the portion of Atlantic,

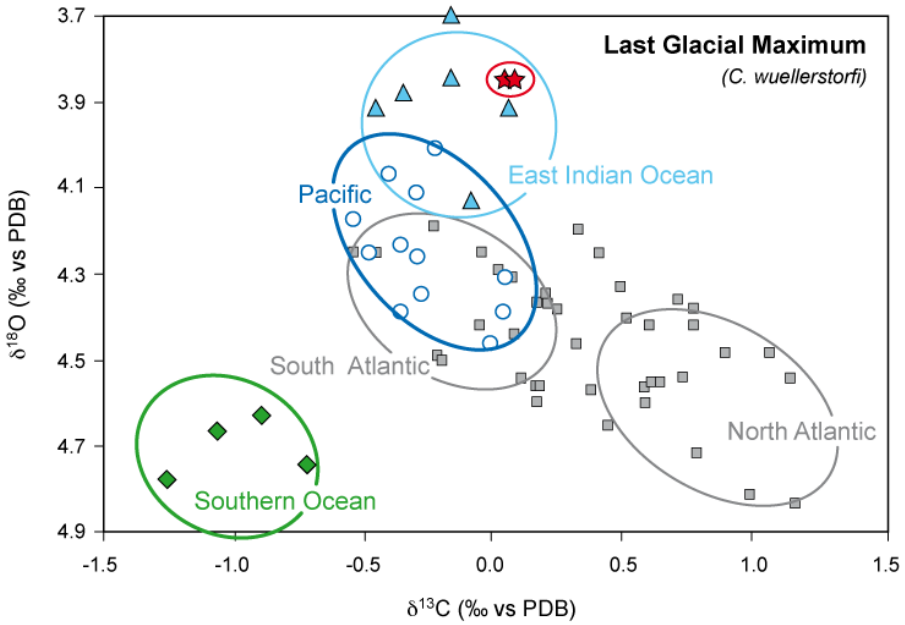

Fig. 1.2-4: Relationship between benthic foraminiferal $\delta^{18}O$ and $\delta^{13}C$ during the Last Glacial Maximum from sediment cores below 2500 m water depth (Duplessy et al., 2002; modified by Sturm, 2003)

Pacific and Antarctic deepwater masses in the Southern Ocean can be deciphered. In particular, the oceanic Nd-istope signature measured on sediments from different water depths should allow Pleistocene changes in deepwater circulation to resolve. Indeed, Nd-isotopes provide evidence that the glacial contribution of NADW was significantly reduced and further, that the changes in deep-water circulation lagged the large changes in global ice volume and the carbon cycle. From this point of view, the Southern Ocean is not expected to drive glacial/interglacial climate changes (Piotrowski et al., 2005).

However, it has not been considered so far whether the source signatures of the deepwater masses changed over time (Gutjahr et al., 2008). It is further not clear how variable the inflow of both Pacific water masses and newly formed deep-waters from the Ross Sea into the Southern Ocean was. It remains also speculative how such variability was in relation to circulation changes in the Atlantic sector of the Southern Ocean. The sediment records collected during the SO213 expedition are expected to provide insights into these questions.

Seismic surveys: Identification of IODP drilling locations and mapping the geometry of Cenozoic sediment deposits

Another task of the SO213 cruise is to identify suitable drill sites for the Integrated Ocean Drilling Program (IODP) and to support our IODP proposal CESOP (Cenozoic Southern Ocean Pacific). This proposal 625-Full (Gersonde et al., 2010) has been positively reviewed by the IODP-SSEP (Science Steering and Evaluation Panel), but recommended the generation of a comprehensive pre-site survey at the proposed sites. Besides sediment cores and bathymetric data, this especially includes seismic surveys, which are broadly lacking for the South Pacific. The high-resolution, multichannel seismic reflection measurements will enable to image the outline, thickness and internal structure of the entire sedimentary cover down to the basement. The reflection characteristics of the sedimentary layers offer indications on changes in deposition environment as well as on the sedimentary composition. The geometry of sediment drifts can be used for paleoceanographic reconstructions. Furthermore, the seismic mapping and documentation of the sedimentary layering will provide data for the selection of good quality locations to perform successful and save drilling.

The realization of an IODP-Leg in the South Pacific will fill a critical gap in the understanding of the Cenozoic climate evolution, especially in view of the Pacific Southern Ocean's role for climate change. The goals of this initiative are to understand and quantify (1) its response to the development of circum-antarctic water mass circulation and pathways related to plate tectonic opening and closure of deep and shallow gateways (Tasmanian Seaway, Drake Passage, Ross-Weddell Sea Passage) and development of South Pacific basin and ridge systems, (2) its implications for Antarctic continental ice sheet and ice shelf development, (3) its role in shaping global circulation and distribution of heat, vapor and nutrients, (4) its impact on global biogeochemical cycles through changes in productivity, nutrient cycling, burial of organic matter and ocean/atmosphere CO_2 exchange, (5) its response to orbital and solar forcing, (5) its impact and response on/to internal climatic relevant processes by looking at the phase relationship of South Pacific environmental change with records from other Southern Ocean sectors, the low and northern-high latitudes including Antarctic and Greenland ice core records.

An additional objective of the seismic reflection measurements is to detect and map sedimentary structures such as sediment drifts to image modifications in the bottom water circulation. In regions with strong changes of seafloor topography, the pathway of water currents changes and sediment drifts can build up. Such sediment bodies, also called contourites, are deposited and reworked by the sustained flow of thermohaline driven geostrophic bottom currents (Heezen et al., 1966; Faugeres and Stow, 1993) that are flowing parallel to bathymetric contours in deep sea basins. The structures of these drifts offer the opportunity to indicate and reconstruct the paleo-current activity. Additionally, these deposits are characterized by high sedimentation rates and thus provide high-resolution paleoceanographic archives.

Intermediate and deep-water masses are expected to form sediment drifts along the East Pacific Ridge, especially at fracture zones, which provide passages for deep-water flow. These passages result in acceleration and subsequent relaxation of deep-water currents where sediment drifts are then deposited. Potential locations of drifts are around the "Eltanin-Tharp Fracture Zone" (ETFZ) in the south of the East Pacific Ridge (ca. 57°S). Here, high-resolution sediment records have been recovered during "Polarstern" cruise ANT26-2, and a short seismic profile documents up to 1500 m sediment cover (Gersonde et al., cruise report, in prep.). Accordingly, we also expected sediment drifts in the area of the Menard Fracture Zone at ca. 50°S and at the intersection of the East Pacific Ridge with the Chile Rise at ca. 35°S (Fig. 1-1). A correlation of seismic data with ground-truth information of existing and future IODP drill sites will enable the development of a seismostratigraphic model for different sections along the East Pacific Ridge.

1.3 VOLCANOLOGIC OBJECTIVES OF CRUISE SO213 LEG 2

The Foundation Seamount Chain is one of the very few examples on earth where a hotspot trail intersects an active spreading axis (Fig. 1.3-1). The volcanology goals of the SO213 Expedition were to 1) map and sample in-situ volcanic and other magmatic rocks from seamounts and volcanic ridges extending diagonally from the northern and southern sides of the Foundation Chain towards the Pacific-Antarctic spreading axis (PAR) and 2) sample fresh volcanic glass from the active PAR where it is intersected by magmatic flow lines from the active Foundation hotspot. Major questions addressed by this project are aimed at understanding how hotspots interact with spreading ridges and if hotspots originate from shallow plate processes or from plumes upwelling from deep in the mantle.

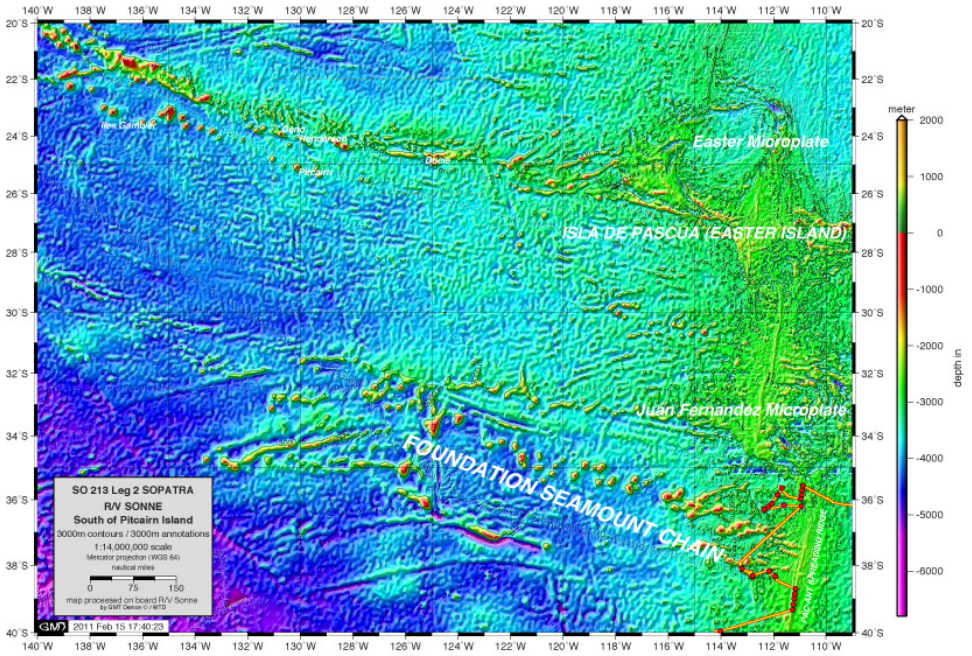

Fig. 1.3-1: Tectonic setting and bathymetry showing the fast to superfast spreading centres of the of the SE Pacific form a complex and dynamic tectonic environment that features two active microplates, Easter and Juan Fernandez, and two major hotspots, Foundation and Easter. The SO213 volcanology study region is where the Foundation Seamount Chain intersects the Pacific-Antarctic spreading axis. GEBCO 08 map made by WTD on board RV SONNE. SO213 rock sampling stations are shown as red discs (yellow line is ship's track).

1.4. VOLCANOLOGIC BACKGROUND

The Foundation Seamount Chain

The Foundation Chain was first detected using a combination of satellite altimetric and conventional geophysical data (Sandwell 1984; Mammerickx 1992) and described initially as a ~1350 km long chain of seamounts trending approximately in the direction of the absolute motion of the Pacific Plate (Mammerickx 1992). The Foundation hotspot trail was extensively dredge-sampled during the SO100 (1995) (Devey et al., 1997) and NO L'Atalante (1997) (Maia et al., 2000) expeditions (Fig. 1.4-1). The SO213 volcanology objective was to sample therefore un-sampled parts of the chain and the adjacent Pacific-Antarctic spreading ridge (PAR) in order to address important outstanding questions raised by the findings of the previous expeditions.

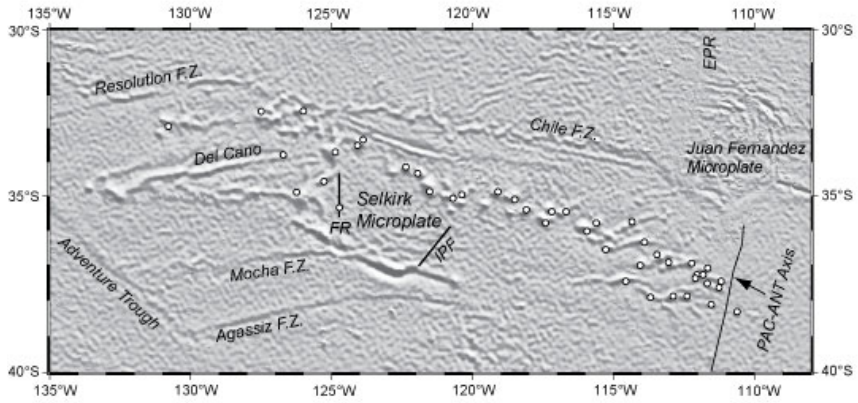

Fig. 1.4-1: Predicted topography map of the Foundation Chain (Smith and Sandwell 1997) showing the SO100 (1995) and NO L'Atalante (1997) dredge stations as white dots. IPF = Inner Pseudo Fault and FR = failed rift of Selkirk Microplate.

$^{40}Ar/^{39}Ar$ ages for rock dredge-samples show a linear trend of decreasing Foundation Chain age from the ~22 Ma northwestern end at a rate of 91±2 mm yr–1 (Fig. 1.4-2) (O'Connor et al. 1998, 2001, 2002, 2004). Age-progression, intraplate setting (Fig. 1.4-2) and hotspot-like composition (Devey et al. 1997; Hekinian et al. 1997, 1999; Hémond and Devey 1996; Hémond et al. 1999; Maia et al., 2001) show that the Foundation Chain is a hotspot trail comparable to the young end of the Hawaiian-Emperor Chain.

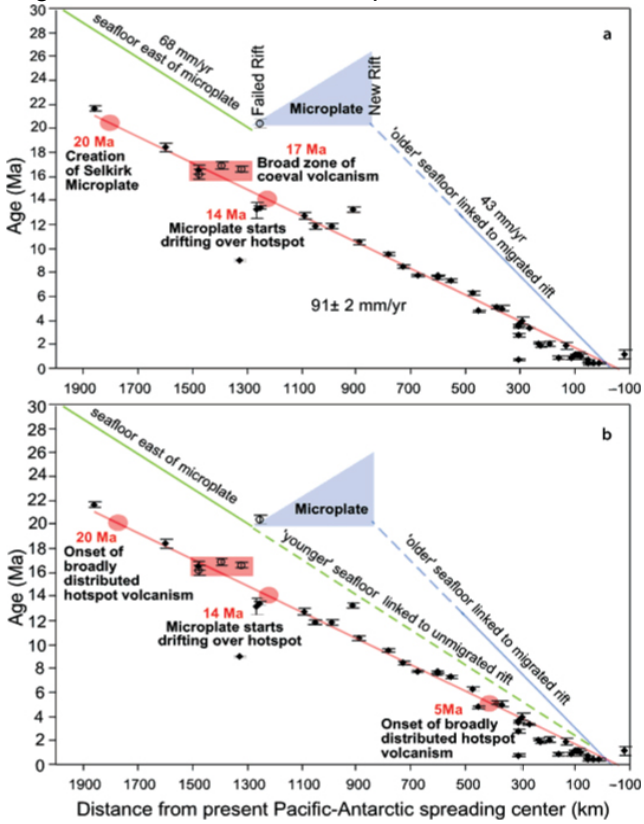

Fig. 1.4-2: (a) $^{40}Ar/^{39}Ar$ and older/'migrated' sea-floor age as a function of distance from the present Pacific-Antarctic spreading axis. The solid red line is the York-2 linear regression fit representing an average rate for the migration of volcanism along the chain of 91 ±2 mm yr–1. As the Selkirk Microplate reached the active hotspot region at about 14 Ma, much older seafloor (≥6 Myr) began to cap the Foundation melting anomaly. This 'older'/'migrated' seafloor placed a sufficiently thick lid over most of the region impacted by the melting anomaly (pulsed plume?) to prevent the migration of hotspot melts to the seafloor during the interval ~14 Ma to ~11 Ma, resulting in the transition from broad zones of hotspot volcanism to a narrow chain of seamounts. Blue solid lines denote 'older' seafloor, unbroken blue lines indicate known sea-floor ages (Mammerickx 1992; Lonsdale 1994), and dashed blue lines indicate extrapolated sea-floor ages. The red swath indicates the broad zone of scattered coeval hotspot volcanism (open spheres) created by the proposed 17 Ma pulse of the Foundation plume crosscutting the narrow Foundation Chain. Analytical error bars are ±2σ. (b) Younger/ 'unmigrated' sea-floor age as a function of distance from the present Pacific-Antarctic spreading center – other details are the same as in Part a. The long green dashed line indicates younger/'unmigrated' sea floor created by the spreading center north of the 'Failed Rift'. The spreading center north of the 'Failed Rift' probably continued spreading normally so that 'younger' (≤6 Ma) seafloor could move over the northern flank of the Foundation hotspot. This younger/'unmigrated' seafloor drifting by the northern flank of the Foundation melting anomaly was thin enough to allow the passage of melts along a narrow strip leading to the creation of a correspondingly narrow chain of Foundation Seamounts.

About ~450 km west of the present Pacific-Antarctic spreading axis, the chain switches from a narrow line of individual or clustered seamounts to a much broader region of en échelon Volcanic Elongate Ridges (VERs) (Fig. 1.4-3). The chemical and isotopic compositions of the young Foundation Chain intraplate basalts reveal a growing influence of the spreading ridge on the off-axis hotspot (plume?) magmatism (Maia et al., 2001). The pattern is coherent with mixing between two sources where two melting zones merge and overlap (Maia et al., 2001). But whether the mantle source for the Foundation hotspot (and hotspots in general) is a mantle plume originating from deep in the mantle is unknown and a topic of controversial debate.

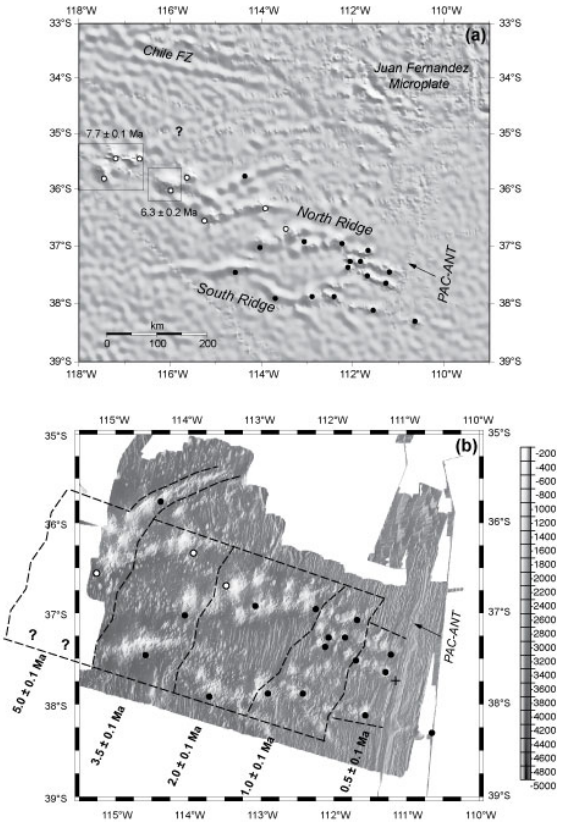

Fig. 1.4-3: (a) Predicted topography of the Foundation Chain region (Smith and Sandwell 1997). Solid circles show locations of 'SO100' or 'L'Atalante (Maia et al., 2001) cruise dredge sites for which $^{40}Ar/^{39}Ar$ ages have been determined. 'North' and 'South' lines indicate the apparent bifurcation of the Foundation Chain. Box labeled 7.7 Ma shows a cluster of coeval seamounts that might be linked to the development of the oldest Pacific- Antarctic Foundation VER (indicated by a question mark). PAC-ANT = Pacific-Antarctic spreading center. (b) Shaded multibeam bathymetry of the Foundation Chain VERs (Maia et al. 2000, 2001). Dashed lines outline inferred en échelon NE-SW elongate 'zones' of coevally erupted VER volcanism. The weighted average of all ages measured for samples recovered from within each 'zone' is shown. Plus symbol denotes point on Pacific-Antarctic spreading center (37°45' S, 111°7.5' W) from which sample site distances along the Foundation Chain have been calculated (see Fig. 1.4-4).

Although VER development was controlled in part by local plate factors (e.g., age/strength of the lithosphere, location of nearest spreading center segment, lithospheric stress), long-lived attributes of the Foundation hotspot melting anomaly (e.g., size, orientation, periodicity) appear to have played also a significant role. The key to testing this notion is the fact that the Foundation Chain represents a rare, possibly unique case of a hotspot trail crossing a fossil microplate. Prior to encountering the Selkirk Microplate, the Foundation Chain formed as broad zones of scattered, synchronous Foundation volcanism – similar to those identified west of the present Pacific-Antarctic spreading center. However, once the significantly older microplate lithosphere began capping the hotspot about 14 Myr ago (O'Connor et al. 2002),

the chain narrowed abruptly into a line of discrete seamounts, only to broaden again about 5 Myr ago when sufficiently young lithosphere once again drifted over the hotspot (Fig. 1.4-3). Foundation hotspot volcanism can therefore be prevented across elongate hotspot zones, if the capping tectonic plate is too thick for melts to penetrate to the surface (O'Connor et al. 1998, 2002). We infer from this information that the Foundation Chain development was controlled primarily by tectonic plate migration over broad hotspot zones of fundamentally constant size and orientation created with an apparent ~1 Myr periodicity (O'Connor et al., 2002).

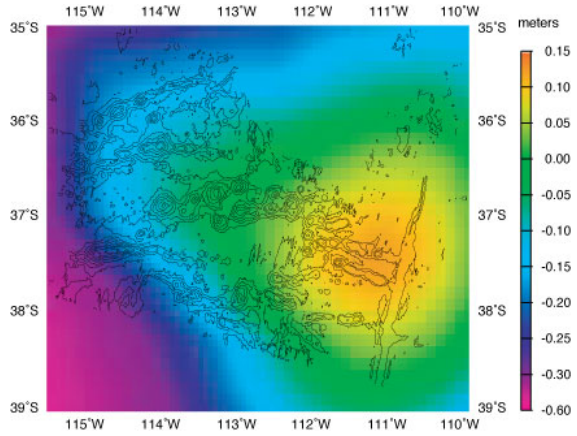

Fig. 1.4-4: Altimetric geoid derived from Geosat, TOPEX/Poseidon, and ERS-1 data, filtered in the 500–2000-km wave band, and showing the clear 0.15-m anomaly centered over the North Ridge-South Ridge group. Scale is in meters. The VERs are distributed along sub-parallel northern and southern lines (Maia et al., 2001). The northern line is an extension of the older seamount chain and is marked by a geoid high located very near the Pacific-Antarctic Ridge axis that possibly marks the location of the Foundation hot spot (Maia et al., 2001). Both the geoid anomaly and the morphology of the edifices show that the north line is the main locus of the hotspot volcanism. Figure from Maia et al. (2001).

The chemical and isotopic compositions of the young Foundation Chain intraplate basalts reveal a growing influence of the PAR on the off-axis hotspot magmatism (Maia et al., 2001). An earlier geochemical model for hotspot-spreading ridge interaction presumes that there is simple binary mixing between 'enriched' hotspot material from the lower mantle (i.e., plume source) with 'depleted' material in the upper MORB mantle (Schilling, 1973; Schilling, 1985; Schilling, 1991). Newer models are suggesting, however, that the upper mantle might have evolved from progressive melting of enriched 'plume' material (Phipps Morgan et al., 1995; Niu et al., 1996; Phipps Morgan and Morgan, 1999). Identifying the depth of contributing mantle sources can only be answered in the case of the Foundation-PAR system once we know the composition of local MORB (i.e., upper mantle). Complete sampling of the PAR east of the Foundation Chain is necessary therefore in order to reconstruct the flow of hotspot mantle to the PAR and establish the mixing behavior of deep (plume?) and shallow mantle sources.

Cruise SO157 of the FS SONNE to the Pacific-Antarctic Ridge (PAR) adjacent to its intersection with the Foundation Seamount Chain in 2001 (Stoffers et al., 2001, 2002) followed earlier visits to the Foundation Seamounts by FS SONNE (1995) and NO L'Atalante (1997), which had discovered silica-rich lavas and indications of widespread hydrothermal activity along this part of the PAR crest and further pin-pointing the present day position of the Foundation hotspot (mantle plume?) as 35 km west of the PAR crest near 37° 25' S (Fig. 1.4-4) inferred from the geoid anomaly and the morphology of the edifices showing that the north line is the main locus of the hotspot volcanism (Maia et al., 2001).

One consequence of hotspot-ridge interactions is the presence of an additional hotspot-derived magma flux at the spreading-axis, which may enhance the development of a long-term robust magma chamber beneath the ridge crest. Such magma chambers permit processing and differentiation of primitive basaltic melts into more evolved andesitic and

dacitic magmas. Elsewhere, highly differentiated lavas have erupted only at central volcanoes where the magma flux is the highest (e.g. Iceland). One cruise objective was to examine whether the silica-rich PAR lavas were restricted to the center of ridge segments (analogous to Iceland central volcanoes) (Stoffers et al., 2001, 2002). Combined with the results from earlier FS SONNE and NO L'ATALANTE cruises, silica-rich lavas have now been recovered from the PAR crest over a distance of 290 km. Unfortunately, the relative proportion of silica-rich to MORB-like lava in the key area from 38.5 -39.5 remains to be established (Fig. 1.4-5).

Objectives

- Map and sample in-situ volcanic and other magmatic rocks from seamounts and volcanic ridges extending diagonally from the northern (Westerly Seamounts) and southern (Diagonal Ridges) sides of the Foundation Chain towards the Pacific-Antarctic spreading axis (PAR) (Figs. 1.4-5 and 1.4-6).
- Sample fresh volcanic glass from the active PAR in order to fill crucial sampling gaps (Figs. 1.4-5 and 1.4-6).

Geological, volcanological, petrological, geochemical and geochronological analyses subsequent to the cruise aim to provide, in combination with the existing published data, to help our understanding of how hotspots interact with spreading ridges and if hotspots originate from shallow plate processes or from mantle plumes upwelling from deep in the mantle.

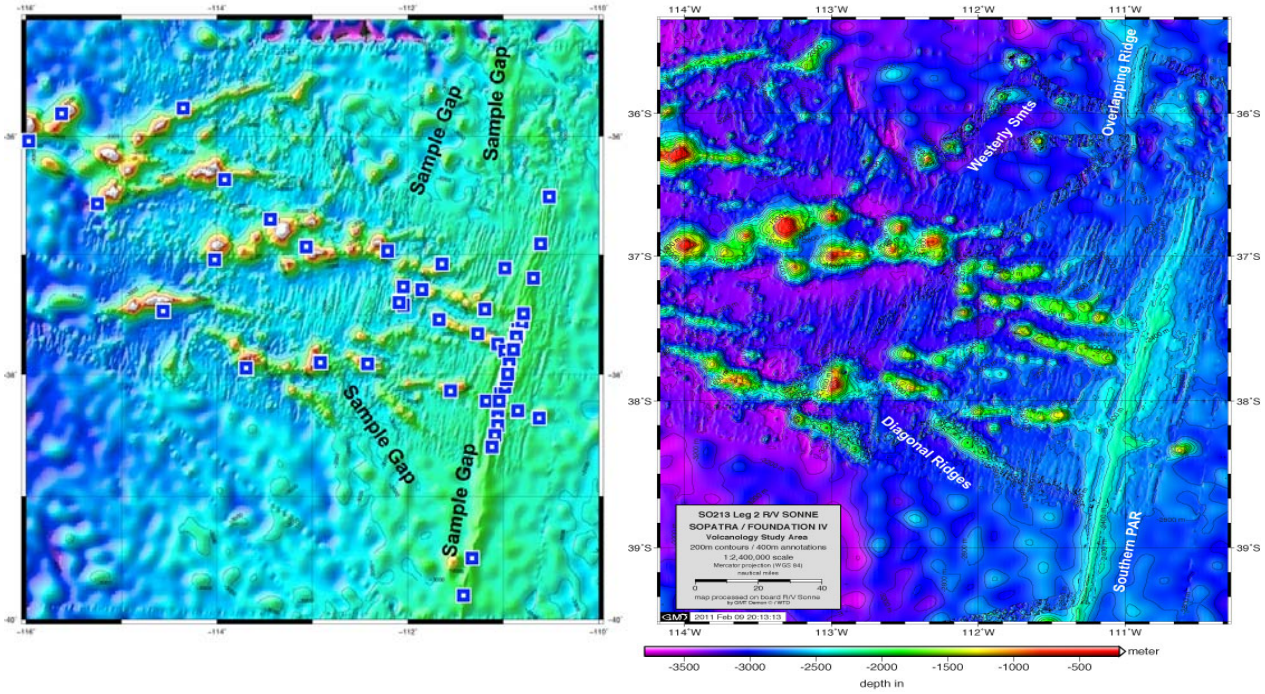

Fig. 1.4-5 (left): GEBCO 8 map of the interstection region of the Foundation Chain and the PAR show existing dredge samples and sampling gaps that are the focus of the SO213 volcanology project.

Fig. 1.4-6 (right): Overview map of the SO213 volcanology study area showing the sampled areas of interest. Map is mixed grid made by WTD on board RV Sonne using EM120 multibeam data and GEBCO 8.

Specific questions and objectives include:

- Is hotspot mantle flow to the PAR uniform and how has it changed during the past 5 Myr?
- How broad is the present Foundation hotspot how has it changed during the past 5 Myr?
- Does the young Foundation hotspot chain form as broad elongate zones of coeval hotspot volcanism?
- Do these ‘zones’ develop at intervals of ~1 Myr while maintaining a steady state size (~250 km by ~150 km) and orientation (NE-SW)?
- Are VERs age-progressive or do they form synchronously?
- Is the Foundation Chain development controlled primarily by plate migration over a broad hotspot of fundamentally constant size?
- Has the Foundation hotspot source pulsed during the past 5 Myr?
- Does the Foundation hotspot mantle originate from a shallow or a deep (i.e., plume) source?
- Do mantle plumes really exist?

2. PARTICIPANTS

2.1. SHIP'S OFFICERS AND CREW

Leg 1

Mallon, Lutz	Master	Tiemann, Frank	Chief Cook
Aden, Nils	Chief Mate/1. Officer	Garnitz, Andre	2nd Cook
Göbel, Jens	2. Officer	Pohl, Andreas	Chief Steward
Hoffsommer, Lars	2. Officer	Royo, Luis	2nd Steward
Walther, Anke	Surgeon	Mucke, Peter	Boatswain
Leppin, Jörg	Electronic Engineer	Kraft, Jürgen	A.B.
Grossmann, Matthias	Sysman	Fricke, Ingo	A.B.
Borchert, Wolfgang	Sysman	Dolief, Joachim	A.B.
Guzman Navarrete, Werner	Chief Engineer	Bierstedt, Torsten	A.B.
Klinder, Klaus	2. Engineer	Weinhold, Rolf	A.B.
Thomsen, Sascha	2. Engineer	Freiwald, Petra	A.B.
Rieper, Uwe	Electrician	Peplow, Michael	S.M./Apprentice
Rosemeyer, Rainer	Fitter	Eidam, Oliver	S.M./Apprentice
Zeitz, Holger	Motorman	Alterdorf, Denis	S.M./Apprentice
Bolik, Torsten	Motorman	Ide, Steven	S.M./Apprentice

Leg 2

Meyer, Oliver	Master	Zeitz, Holger	Motorman
Korte, Detlef	Chief Mate/1. Officer	Bolik, Torsten	Motorman
Buechele, Heinz-Ulrich	2. Officer	Tiemann, Frank	Chief Cook
Hoffsommer, Lars	2. Officer	Garnitz, Andre	2nd Cook
Walther, Anke	Surgeon	Pohl, Andreas	Chief Steward
Grossmann, Matthias	Sysman	Royo, Luis	2nd Steward
Ehmer, Andreas	Sysman	Mucke, Peter	Boatswain
Borchert, Wolfgang	Sysman	Ross, Reno	A.B.
Guzman Navarrete, Werner	Chief Engineer	Mohrdiek, Finn	A.B.
Klinder, Klaus	2. Engineer	Schröder, Christopher	A.B.
Hermesmeyer, Dieter	2. Engineer	Bierstedt, Torsten	A.B.
Rieper, Uwe	Electrician	Weinhold, Rolf	A.B.
Rosemeyer, Rainer	Fitter	Freiwald, Petra	A.B.
Krawczak, Ryszard	Motorman	Peplow, Michael	S.M./Apprentice

2.2. PRINCIPAL INVESTIGATORS

Head project:	Ralf Tiedemann	Alfred-Wegener-Institute for Polar and Marine Research, Bremerhaven
Sub-project 1:	Gabriele Uenzelmann-Neben	Alfred-Wegener-Institute for Polar and Marine Research, Bremerhaven
Sub-project 2:	Dirk Nürnberg	IFM-GEOMAR, Leibniz-Institute for Marine Research, Universität Kiel
Sub-project 3:	Martin Frank	IFM-GEOMAR, Leibniz-Institute for Marine Research, University Kiel
Sub-project 4:	Karsten Haase	GeoCenter Nordbayern University Erlangen-Nürnberg

2.3. SHIPBOARD SCIENTIFIC PARTY

Leg 1

Tiedemann, Ralf	Chief Scientist	AWI, Brhv.
Max, Lars	Sedimentology, Parasound	AWI, Brhv.
Lensch, Norbert	Technical Operation	AWI, Brhv.
Arevalo, Marcelo	Technical Operation	AWI, Brhv.
Ronge, Thomas	Sedimentology	AWI, Brhv.
Benz, Verena	Sedimentology	AWI, Brhv.
Glückselig, Birgit	Sedimentology, Micropal.	AWI, Brhv.
Ullermann, Johannes	Sedimentology	AWI, Brhv.
Molina Kescher, Mario	Hydrography, Sedimentology	IFM-GEOMAR, Kiel
Tapia Arroyo, Raul	Sedimentology	IFM-GEOMAR, Kiel
Poggemann, David	Technical Operation	IFM-GEOMAR, Kiel
Hayward, Bruce	Stratigraphy	Geomarine Res., Auckland
Menze, Sebastian	Sedimentology	AWI, Brhv.
Esper, Oliver	Hydrography, Micropal.	AWI, Brhv.
Gottschalk, Julia	Sedimentology, Parasound	AWI, Brhv.
Romahn, Sarah	Sedimentology	AWI, Brhv.
Dufek, Tanja	Bathymetry	AWI, Brhv.
Maier, Edith	Sedimentology	AWI, Brhv.
Naafs, David	Sedimentology	AWI, Brhv.
Bazhenova, Evgenia	Sedimentology	AWI, Brhv.
Nürnberg, Dirk	Head Sedimentology	IFM-GEOMAR, Kiel
Garlichs, Torsten	Sedimentology	IFM-GEOMAR, Kiel
Steph, Silke	Sedimentology, Phys. Props.	MARUM, Bremen
Kloss, Anna	Sedimentology	MARUM

Leg 2

Tiedemann, Ralf	Chief Scientist	AWI, Brhv.
Max, Lars	Sedimentology, Parasound	AWI, Brhv.
Lensch, Norbert	Technical Operation	AWI, Brhv.
Arevalo, Marcelo	Technical Operation	AWI, Brhv.
Ronge, Thomas	Sedimentology	AWI, Brhv.
Glückselig, Birgit	Sedimentology, Micropal.	AWI, Brhv.
Benz, Verena	Sedimentology	AWI, Brhv.
Ullermann, Johannes	Sedimentology	AWI, Brhv.
Molina Kescher, Mario	Hydrography, Sedimentology	IFM-GEOMAR, Kiel
Tapia Arroyo, Raul	Sedimentology	IFM-GEOMAR, Kiel
Poggemann, David	Technical Operation	IFM-GEOMAR, Kiel
Lamy, Frank	Head Sedimentology	AWI, Brhv.
Sze Ling, Ho	Sedimentology, Parasound	AWI, Brhv.
Weigelt, Estella	Geophysics	AWI, Brhv.
Grützner, Jens	Geophysics	AWI, Brhv.
Penshorn, Dietmar	Technical Operation	AWI, Brhv.
Pulm, Pia	Geophysics	AWI, Brhv.
Busssweiler, Yannik	Geophysics	AWI, Brhv.
Wagner, Christoph	Geophysics	AWI, Brhv.
Eggers, Thorsten	Geophysics	Optimare
O'Connor, John	Vulkanologie	AWI, Brhv./Uni Erlangen
Schmidt, Heike	Vulkanologie	Uni Erlangen
Keith, Manuel	Vulkanologie	Uni Erlangen
Saavedra, Mariem	Stratigraphie	Univ. Salamanca/Marum

Scientists SO213 Leg 1

Scientists SO213 Leg 2

3. CRUISE NARRATIVE

Our SOPATRA expedition SO213-1 started on December 27, 2010 in Valparaiso (Chile) with 24 scientists onboard of RV SONNE. SONNE left pier at 13:00 and headed west to the first working area along the Challenger Fracture Zone (36°-38°S, 85°-110°W). The transit was used to set up our laboratories, measuring systems and devices for sampling the water column and the sea floor.

The first station was reached on December 31, at 6:00 am above a seamount that rises from 5000 m to 2500 m water depth. After mapping the seafloor topography (Simrad) and the distribution of sediment layers below the ocean floor (Parasound), we successfully sampled the sediment surface with the multi-corer (MUC) and retrieved a 13.6 m sediment record with the piston corer (PC) from 2800 m water depth. Nearby, we deployed the CTD with rosette and fluorometer and measured the variability in temperature, salinity, density and chlorophyll concentrations as well as collecting water samples between 4000 m water depth and the sea surface. In addition, we collected plankton using the multinet and the plankton net devices. From December 31, 2010 to January 3, 2011, we successfully performed 5 stations (SO213-1 – SO213-8) with MUC and PC/GC deployments. Although we retrieved a “banana” (a bent pipe) at station SO213-6, we could secure the sediment record. Three other stations marked Parasound-surveys to identify potential coring locations. This was a difficult undertaking. The rugged ocean floor topography, changing very quickly over even short distances, provided too many side echoing from the adjacent peaks and valleys, which in turn had a negative effect on the “screening” of the sediment sequences. Even lowering our ship’s speed to 2 knots did not provide an improvement. Only when the ship stopped was the Parasound system able to deliver interpretable data – a time-consuming procedure.

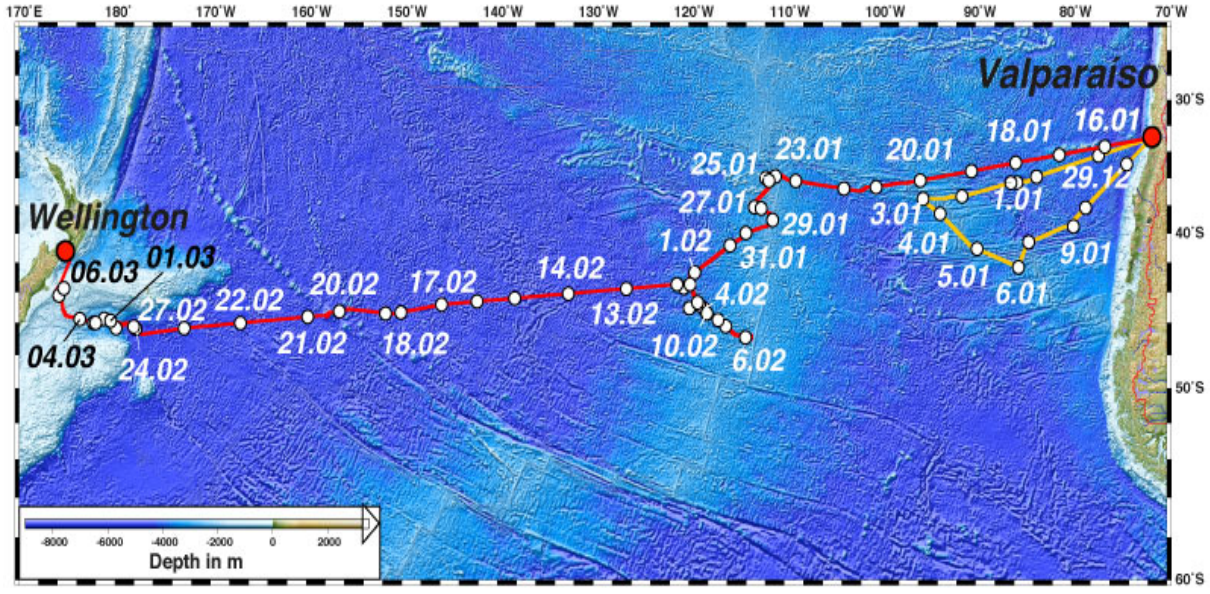

Fig. 3-1: SO213 cruise track of Leg 1 (yellow line) and 2 (red line) and datum

On January 4, 2011, we headed south to recover a latitudinal as well as a deep-water transect of sediment records along the Chile Rise between the Challenger and the Valdivia Fracture Zones (38°-42°S, 79°-94°W). North of the Valdivia Fracture Zone, we discovered a submarine chain of volcanoes unknown to-date. This chain most likely marks a hot spot track. At station SO213-14, we found a deep-sea region covered with manganese nodules. When the MUC was hauled back from a water depth of 4200 m, the sediment surfaces of the MUC-tubes were covered with manganese nodules, comprising about 70% of the recovered ocean floor surface. The detection of suitable coring locations via Parasound was again difficult. Parasound provided interpretable data only when the ship stopped. In total, we

conduct 7 stations with MUC and PC/GC deployments. In this area, it was difficult to retrieve long sediment records, due to relatively stiff sediments (sandy foraminiferal oozes) and the reduced Pleistocene sediment cover. Most of the sediment records already contained Miocene sediments at their base. As a result, two piston core deployments came up with bent pipes. At 3 stations (SO213-09-2; -12-4; -22-2), we collected plankton (multi- and plankton net deployments) and seawater samples (Rosette) and measured the vertical distribution of oxygen, salinity and temperature with the CTD. The latter one was performed in the deep Chile basin on our transit back to Valparaiso.

In the early morning hours of January 12, SONNE moored at the pier in Valparaiso. Thirteen scientists disembarked. Eleven paleoceanographers stayed onboard and thirteen new scientists, mainly geophysicists and volcanologists completed the scientific team of Leg 2. Most of the scientific equipment was already on board, except that of the geophysical team. We loaded one additional container with geophysical equipment and had to install the large seismic winch on the afterdeck.

Cruise SO213-2 started on January 15, 2011 in Valparaiso and SONNE steamed towards the research area at the East Pacific Rise, which stretches from 35°S to 55°S. Leg 2 (SO213-2) was multidisciplinary and pursued scientific targets that are related to the origin and development of the Foundation seamount chain and to the paleoceanographic history of the South Pacific. A common goal of the geophysicists and paleoceanographers was to detect several hundred meters thick sediment sequences by using reflection seismic, thereby conducting pre-site surveys to define potential future IODP drilling locations and to support our IODP proposal CESOP (Cenozoic Southern Ocean Pacific). During the long transit to the East Pacific Rise we performed 2 stations on January 21 and 23, which expanded our east-west traverse of sediment records of the first leg further westward. There, we successfully deployed the MUC and recovered two 3 m long gravity cores.

At 01:00 in the early morning of January 24, we crossed the East Pacific Rise and started the volcanology program. Mapping the axial-high that marks the most active part of a spreading ridge, we transited south and, using a ‘rock corer’, recovered fresh volcanic glass at four stations along a 50 km section of the ‘Overlapping’ section of the PAR. Sampling began at 22:00 and finished at 08.30 on January 25. Next, we steamed to the Westerly Seamounts and, after mapping and finding a suitable dredge site, started dredging operations at about 15:00 on the volcano at northern end of the Westerly Seamount Chain. The first dredge station was unsuccessful but our second attempt recovered rock and glass material. We then steamed south while mapping and successfully dredge-sampling three more seamounts in the 110 km long Westerly Seamount Chain. Leaving the Westerly Seamount Chain at 21:30 on January 26 we transited to a large seamount located about 35 km to the west. On completing our final mapping and dredge station in the Westerly Seamounts at 20:00 hours, we returned to the PAR and finished our fifth rock coring station at 11:00 on January 27 to complete our sampling of a 70 km long section of the ‘Overlapping’ section of the PAR.

Following a 300 km SE transit across the Foundation Chain and hotspot we began dredging operations on the Diagonal Ridges #1 at 05:30 hours on January 28. Our first dredge station on the volcano at the northern end of Diagonal Ridge #1 was unsuccessful. Following additional mapping we found a different station location and concluded successful dredging operations at 13:00 hours on January 28. We then steamed south, mapping Diagonal Ridge #1 and searching for promising dredge sites along the flank that could be dredged in the prevailing weather conditions.

A dredge station on the volcano at the southern end of Diagonal Ridge #1 was unsuccessful. Following further mapping we designated a new location and completed a successful dredge station by 03:00 hours on January 29. After a 50 km transit to the northern end of Diagonal Ridge #2 (80 km east of Diagonal Ridge #1 and closer to the PAR) we completed a successful dredge station at 010:00 hours in the morning of January 29. We then mapped the northern half of the ridge while transiting to the southern end and completing our final dredge station by 15:30 o’ clock on January 29.

Following an 80 km transit to our final sampling area on the PAR south of the Foundation hotspot we started rock coring operations at 23:00 hours on January 29. Mapping and sampling over a distance of 70 km, we completed five successful rock corer stations by 10:30 on January 30, bringing a very successful volcanology program to a close that achieved all the Foundation IV sampling objectives.

After finishing the volcanology program, we left the ridge axis of the East Pacific Rise in southeastward direction. The intention was to detect a large sediment drape on 15-25 Ma old oceanic crust and to perform a seismic pre-site survey to define suitable IODP drilling locations, which could provide a record of Neogene changes in atmospheric and oceanic circulation. During this transit of ca. 500 nm, the increase in sediment thickness was recorded with the Parasound system. During the Parasound survey, we stopped the ship several times in order to sample the ocean floor and the sediment sequences via multi-corer and piston corer/gravity corer.

On February 2, SONNE reached an area comprised of sediment deposits 200 m thick, resting on oceanic crust approx. 20 million years old. During the early morning, the piston corer was deployed and recovered a 9 m long sediment record at station SO213-54. The water column was examined and sampled at station SO213-54 with Rosette, CTD, fluorometer, multinet and plankton net. The air guns and the streamer were deployed and shooting started at 23:30 hours. The seismic transect (322 sm) provided crossing lines at two potential IODP locations and then advanced eastward toward the flank of the East Pacific Rise. When the sediment drape started thinning out all instruments were retrieved at 22:30 hours on February 5. Another goal in this region was to recover a deep-water transect of sediment records. During the seismic transit, deep-water coring locations were already defined via Parasound. We continued the survey line with Parasound profiling to a mountaineous region in the vicinity of the ridge axis of the East Pacific Rise and defined coring locations at shallower water depths. This profile ended at 07:00 hours on February 6. During the following days, from February 6 – 12, eight coring stations with Multi-corer and pisten/gravity core deployments were performed in water depths ranging from 1190 m to 3920 m. All deployments were successful, except those in shallow water depth (stations SO213-57, -58), where no sediment records could be retrieved. The sampling of the sediment surface with the Multi-corer brought about pure foraminiferal sands, which are technically hard to core with the equipment we had available. However, we were able to obtain 6 cores with our gravity-corer at the other stations. Within the sediment cores, changes in color and density show chronologically corresponding patterns. These 6 sediment cores were obtained under rough weather conditions. From the early morning hours of February 8th, the “Roaring 40’” lived up to their name. Winds increased to wind speeds of 9 bft within a short time, and the swell increased continuously to about 8 m. We had to abort our operations. The following days did not bring about an improvement in weather conditions. Despite of bad weather conditions, we were able to retrieve these sediment cores with our gravity corer. However, we had to forego the use of our piston corer, with which the retrieval of larger sediment cores could have been possible.

On February 12, we had to make a hard decision. We abandoned our initial plan of going farther south. The weather forecasts for the next 7 days made it impossible for us to get any work done on 50°S or even further south. Since we anticipated such a situation, we left this region and headed to our alternative research area– the Bounty Trough off the coast of New Zealand.

After having been about 1400 sea miles in transit, the weather finally improved for a short period of time on February 19, right before we reached the “Louisville” seamount chain in the South Pacific basin. We took advantage of the weather to further investigate urgent scientific questions of this area, focusing around the topic of dust flux from Australia via New Zealand to the East Pacific, as well as the origin of the Louisville Seamount chain. Shortly before reaching the seamount chain, we implemented a deep-water station at a depth of 5000 m in the early morning hours. First, we performed a continuous recording of temperature, salinity content and chlorophyll concentration with the CTD probe and sampling of the water column

with our Multi Water Sampler in various water depths. Plankton samples were taken with the Multi-net and the plankton net. Finally, we employed the piston corer and were able to retrieve a sediment core of 12,3 m in length. During the journey across the seamount chain, the marine geologists detected large sediment deposits, located on the top of a plateau and at the flanks of a guyot. We tried to retrieve sediment records from shallow water depths at 690 m and 1990 m. We were able to recover a 5 m long sediment record by piston coring from the deeper station (SO213-68) but failed to retrieve a record at the shallow station (SO213-69). In the evening of February 20, dredge sampling at the “157°W Guyot” provided small boulders with excellent potential for dating and geochemistry studies. After successfully completing the dredging operations on February 21, SONNE steamed westward to the Bounty Trough off the coast of New Zealand.

A typhoon named “Atu” was heading towards our transit route to New Zealand, accompanied by wind speeds of up to 135 mph. “Atu” was to be taken seriously, since a wind force of 12 starts at 65 mph. It was now our primary goal to cross Atu’s southeastern path just before the arrival of the storm in order to reach the New Zealand coastal area without losing working time. So we moved onward toward New Zealand with a speed of 13 kn. Strong tailwinds and a perfect current supported our journey. Since typhoon Atu did not increase its strength during the following days, we were even able to perform a deep-sea station on the morning of February 23. With our piston corer, we retrieved a core 18 m in length from a water depth of 5100 m, which contained the past 400.000 years of climatic and oceanic history.

On February 24th at 03:00 in the morning, we finally reached our new working area off New Zealand, the “Bounty Trough”, which borders by the Chatham Ridge to the north, the Campbell Plateau to the south, and the coast of New Zealand to the west. It was our goal to perform a seismic as well as paleoceanographic program during the remaining time. This region is marked by a high sediment input from glaciated high mountains, the New Zealand Alps. Today, eight river systems transport their sediment load into the Bounty Trough. During glacial periods, the sediment flux was increased multifold since large parts of the southern island were covered by an ice cap, and the sea level was more than 100 m lower. Hence, the river system deposited directly into the Bounty Trough. A northward flowing deep-sea current dispersed the sediment masses once they had reached the end of the Trough. Through this process, so-called “sediment drifts” were created which can reach a thickness of up to 1500 m. Based on the temporal changes in the geometry of these drift bodies, we intend to reconstruct the direction and strength of the current, with the aid of seismic records. At the beginning of the seismic profiling, we passed the location of a deep-sea drill site (ODP-Site 1122) from which a sediment core 600 m in length exists. This record provides the necessary stratigraphy in order to date the various seismic structures. In the late afternoon of February 27, we successfully completed the seismic profiling, in total 308 nm. At times, we had to temporarily turn off the air guns, whenever curious whales visited us.

From February 27 to March 5, we performed an extensive paleoceanographic program at 9 stations with seven piston core and six gravity core deployments. In total, we recovered 13 sediment records, which vary in length from 2.6 m to 18 m. The stormy weather repeatedly forced us to interrupt our station activities for 12 hours on March 4 and for 7 hours on March 5. The last station work of the ship was to perform a Parasound profile across a pockmark field that was first recorded during Polarstern cruise ANT-26-2/ in January 2010. When this work was done on March 6, we left for Wellington, where we arrived on March 7 at 09:00 hours.

4. OPERATIONS AND PRELIMINARY RESULTS

4.1. CTD-PROFILING AND ROSETTE

In order to collect water samples and to obtain vertical water column profiles of oxygen, salinity and temperature, we employed a CTD-rosette system (with Seabird 911 CTD-profiler). During the first leg, we run four stations: at the Challenger Fracture Zone (SO213-02-1), the Chile Rise (SO213-09-2), the Valdivia Fracture Zone (SO213-12-4) and in the Chile Basin (SO213-22-2). During the second leg, three additional stations were accomplished, two of them on the western side of the South Pacific Ridge (SO213-50-1 and SO213-54-2) and one in the deep SW Pacific basin (SO213-66-1). The Seabird 911 CTD was used to analyze the water column from the sea surface to the sea floor. During SO-213, the standard Seabird 911 CTD of RV Sonne was equipped with an ECO fluorometer to measure fluorescence (reflecting chlorophyll-*a* concentrations) in the upper 1000 meters of the water column. The CTD data were used to identify the physical signature of surface-, intermediate- and deep-water masses as well as for locating the position of the chlorophyll-*a* maximum in the water column. The temperature, salinity, oxygen and fluorometer data, immediately available on the ship, were also used to determine the sampling depths of the different watercolumn-based projects (chapter 4.1.2.).

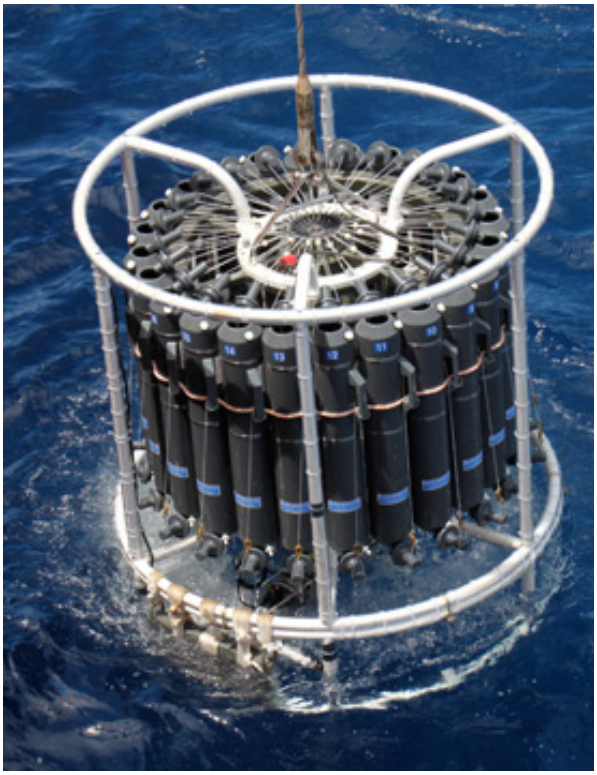

Fig. 4.1-1: Water sampler device (Rosette) equipped with CTD and Fluorometer.

4.1.1. Preliminary results of hydrographic measurements

The CTD profiles of the first leg provide some subtle differences according to their location north and south of the subtropical front (STF). Stations SO213-09-2 and SO213-12-4 are located south of the STF and display a relatively simple vertical water column structure (Fig. 4.1.1-1). Temperature data indicate a strong vertical temperature gradient (~3-4°C/100 m) within the upper 250 m of the water column (seasonal thermocline). Below, within the permanent thermocline (250 – 1000 m water depth), the vertical temperature gradient drops to less than 0.5°C/100 m. At water depths >1000 m, the vertical temperature gradient is very small.

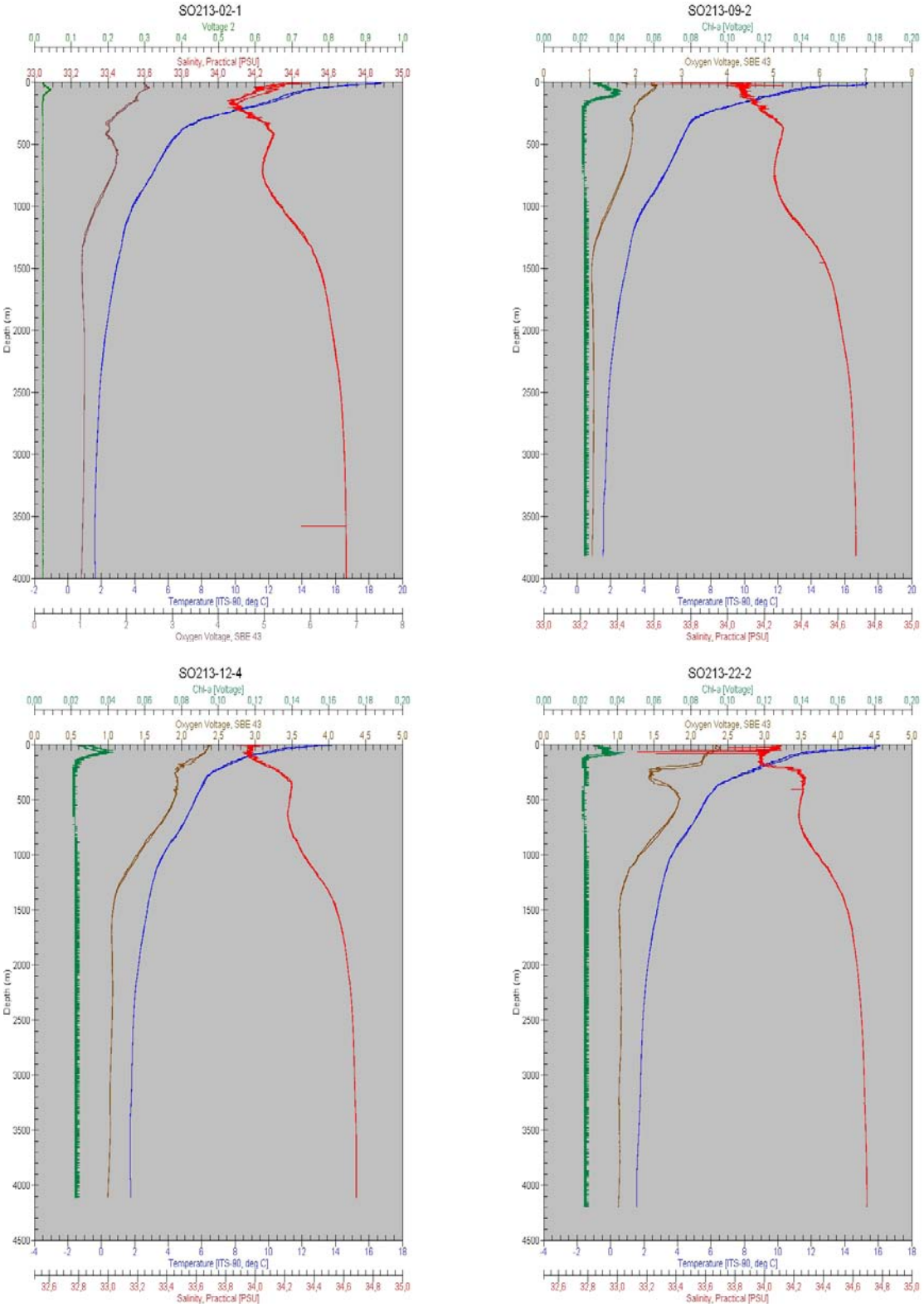

Fig. 4.1.1-1: Distribution of temperature (blue), salinity (red), oxygen (brown) and chlorophyll-a (green) with increasing water depth at stations SO213-2, -9, -12 and -22.

The relatively warm surface waters in the uppermost 10 m of the water column (16.5°C at SO213-09-2 and 14°C at SO213-12-4) are characterized by low salinity (34.0 to 34.1 psu) and high oxygen concentrations. The chlorophyll maximum is located at ~90 m water depth.

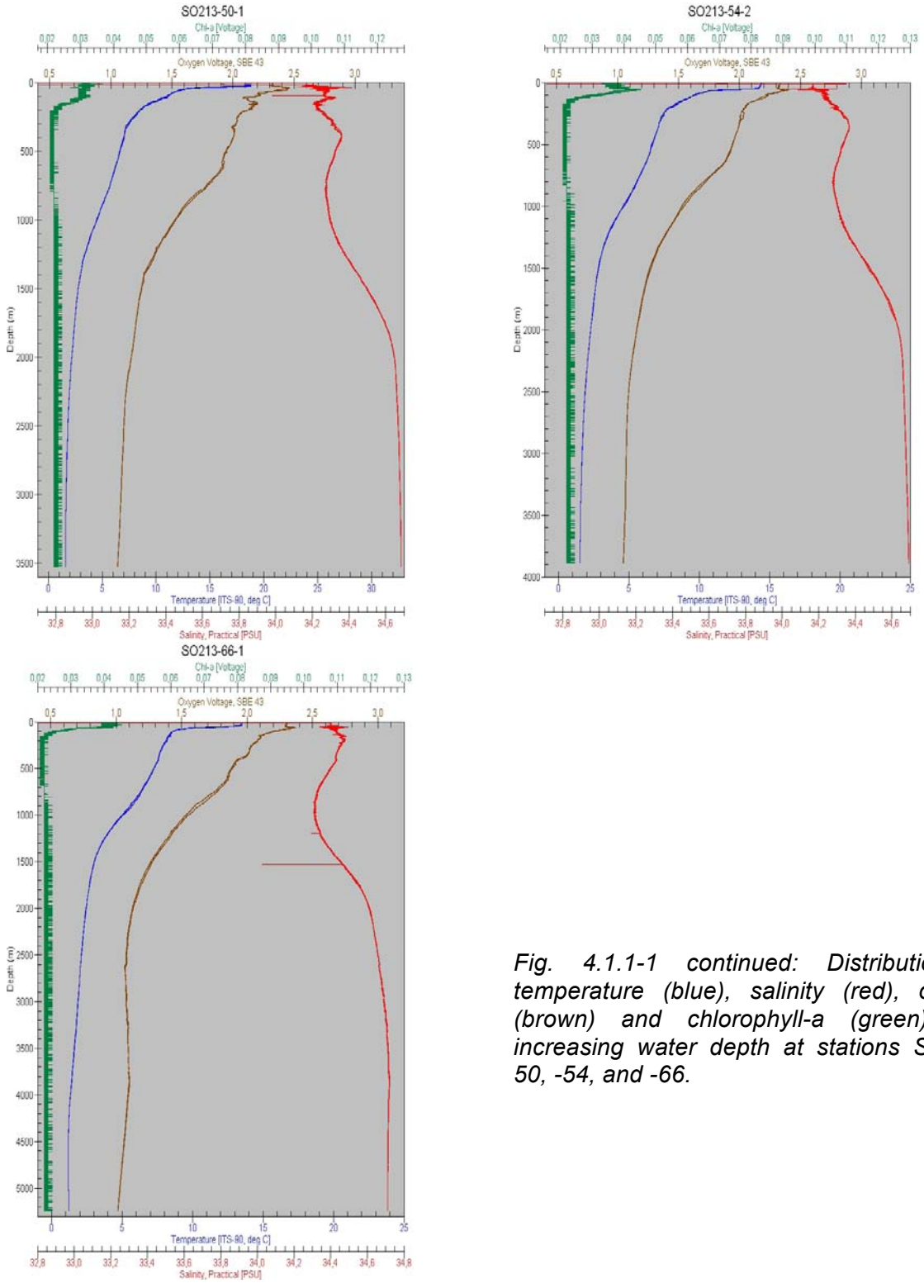

Fig. 4.1.1-1 continued: Distribution of temperature (blue), salinity (red), oxygen (brown) and chlorophyll-a (green) with increasing water depth at stations SO213-50, -54, and -66.

The CTD data indicate a weak subsurface oxygen minimum at the upper end of the permanent thermocline (between 200 and 300 m water depth). Below the sea surface, salinity increases gradually, reaching a maximum at ~400 m water depth. The relatively high salinity is most likely related to the downward mixing of high salinity surface water within the subtropical gyre. Below 400 m water depth, a salinity decrease marks the presence of Antarctic Intermediate Water (AAIW). Below that layer, oxygen concentrations decrease, reaching lowest values at ~1400-1500 m. This deep oxygen minimum is most likely related to

oxygen-poor, southward flowing Pacific Central Water (PCW). However, the boundary between PCW and underlying Circumpolar Deep Water (CDW) is not well defined.

The northern CTD profiles (SO213-02-1, SO213-22-2) are similar to those recorded at stations south of the STF, except for the uppermost 300 m. SST at the northernmost station SO213-02-1 is relatively high (18.5°C), whereas SST at the STF station SO213-22-2 is similar to the SST measured at SO213-09-2 south of the STF (16.5°C). In contrast to the stations south of the STF, sea surface salinity at SO213-02-1 and SO213-22-2 is relatively high compared to the underlying low-salinity water, indicating the influence of high-salinity surface waters derived from the subtropical gyre. At the northern stations SO213-02-1 and SO213-22-2, the oxygen minimum at 200-300 m water depth is developed more distinctly than at stations SO213-09-2 and SO213-12-4 south of the STF. This may result from the oxygen minimum zone (OMZ), which stretches from the continental margin westward into the open ocean.

The CTD profiles from the second leg (SO213-50-1, SO213-54-2, SO213-66-1) provide a similar structure of the water column within the upper 1000 m. Salinity increases with depth, reaching a maximum at 200-300 m. Further below, salinity decreases as a consequence of the presence of AAIW. The core depth of the AAIW between 800 m and 1000 m is characterized by a salinity minimum. SSTs are similar at stations SO213-54-2 and SO213-66-1 (14.4°C and 13.5°C respectively). Low and relatively stable oxygen values mark the water column from 2400 to 3900 m water depth. In a depth of 4000 m to 5200 m, the water column is characterized by decreasing oxygen contents, thereby reflecting the influence of AABW (SO213-66-1).

4.1.2. Water column sampling

The CTD/Rosette device consists of a 24-bottle water collector. Each of the 24 10-liter Niskin bottles of the rosette can be closed separately via the data wire of the winch cable. Before deployment, all the bottles have to be opened; the closing mechanism of each bottle has to be connected with the release-switches of the central controlling device. When triggered via computer command from the board unit, a magnetic switch releases strong rubber bands, which close the selected bottle immediately. When all bottles are closed/filled and the device is back on deck, small vents on top and bottom of each bottle allow for an easy access to the collected water.

Water samples were bottled for a variety of planned analyses: chlorophyll-*a*, dissolved nutrient concentrations (nitrate, phosphate, silicon), stable isotopes ($\delta^{13}C$, $\delta^{18}O$), phytoplankton and neodymium isotopes (Table 4.1.2-1).

Nutrients and chlorophyll-a

The distribution of chlorophyll-a concentrations within the water column was measured with a fluorometer to assess changes in biological productivity. These measurements were accompanied by simultaneous water sampling to determine chlorophyll-*a* and dissolved nutrient concentrations (nitrate, phosphate, silicon). In order to measure the nutrient concentrations of different water masses, 50 ml water samples were taken at 4 stations along specific depth profiles (Table 4.1.2-1), treated with $HgCl_2$ solution to conserve the samples and stored at 4°C. In addition, 7 water samples were taken from selected depths of each CTD/Rosette deployment to calibrate measurements of the fluorometer attached to the CTD probe. The samples were filtered with 25 mm glass microfibre filters (GF/F) and used to directly determine the chlorophyll-a concentration (chapter 4.2.).

Bottle	SO213-02-1*	SO213-09-2*	SO213-12-4*	SO213-22-2
1	[3950] A, B, C	[3771] A, B, C	[4058] A, B, C	[4144] A, B, C
2	[3950] A, B, C	[3771] F	[4058] A, B, C	[4144] F
3	[3500] A, B, C	[3771] F	[3500] A, B, C	[4144] F
4	[3000] A, B, C	[2800] A, B, C, F	[3150] A, B, C	[3500] A, B, C
5	[2500] A, B, C	[2800] F	[3150] – failed -	[2600] – failed -
6	[2000] A, B, C	[2800] - failed -	[3280] A, B, C	[2600] A, B, C, F
7	[1400] A, B, C	[2200] A, B, C, F	[2200] A, B, C	[2600] – failed -
8	[1400] A, B, C	[2200]F	[1600] A, B, C	[1500] A, B, C, F
9	[1000] A, B, C	[2200] - failed -	[1600] A, B, C	[1500] F
10	[700] A, B, C	[1500] A, B, C	[1000] A, B, C	[650] A, B, C
11	[700] A, B, C	[1500]F	[650] A, B, C	[650] F
12	[420] A, B, C	[1500]F	[650] A, B, C	[650] F
13	[420] A, B, C	[750] A, B, C	[500] A, B, C	[500] A, B, C
14	[330] A, B, C	[750]F	[500] A, B, C	[300] A, B, C, F
15	[330] A, B, C	[750]F	[350] A, B, C	[300] F
16	[200] A, B, C	[500] A, B, C	[250] A, B, C	[200] A, B, C, D, E
17	[200] A, B, C, D, E	[400] A, B, C	[200] A, B, C, D, E	[150] A, B, C, D, E
18	[150] A, B, C, D, E	[200] A, B, C, D, E	[150] A, B, C, D, E	[150] F
19	[90] A, B, C, D, E	[150] A, B, C, D, E	[90] A, B, C, D, E	[150] F
20	[70] A, B, C, D, E	[90] A, B, C, D, E	[70] A, B, C, D, E	[90] A, B, C, D, E
21	[50] A, B, C, D, E	[70] A, B, C, D, E	[50] A, B, C, D, E	[70] A, B, C, D, E
22	[50] A, B, C, D, E	[50] A, B, C, D, E	[50] A, B, C, D, E	[50] A, B, C, D, E
23	[30] A, B, C, D, E	[30] A, B, C, D, E	[30] A, B, C, D, E	[30] A, B, C, D, E
24	[10] A, B, C, D, E	[10] A, B, C, D, E	[10] A, B, C, D, E	[10] A, B, C, D, E

Table 4.1.2-1: Water column sampling at CTD stations: Type and water depth [m], A: $d^{18}O$; B: $d^{13}C$; C: nutrients, D: Chlorophyll, E: Nannoplankton; F: Neodymium

SO213-50-1*	SO213-54-2*	SO213-66-1*
[3483] - failed -	[3844] F	[5157] F
[3483] F	[3844] F	[5157] F
[3483] A, B, C, F	[3844] A, B, C	[5157] A, B, C
[3380] A, B, C, F	[3400] A, B, C	[4500] A, B, C, F
[3380] F	[2400] F	[4500] F
[3000] A, B, C	[2400] F	[3800] F
[2300] A, B, C	[2400] A, B, C	[3800] F
[1800] F	[1900] F	[3800] A, B, C
[1800] F	[1900] F	[3000] A, B, C, F
[1800] A, B, C	[1900] A, B, C	[3000] F
[770] F	[1600] A, B, C	[2575] A, B, C
[770] F	[800] F	[2200] A, B, C, F
[770] A, B, C	[800] F	[2200] F
[650] A, B, C	[800] A, B, C	[1400] A, B, C
[380] A, B, C, F	[675] A, B, C	[950] A, B, C, F
[380] F	[350] F	[950] - failed -
[220] A, B, C, D, E	[350] F	[410] A, B, C
[150] A, B, C, F	[350] A, B, C	[175] A, B, C, D, E
[150] F	[200] A, B, C, D, E	[175] F
[110] C, D, E	[175] A, B, C, D, E	[175] F
[90] D, E	[90] A, B, C, D, E	[90] A, B, C, D, E
[50] A, B, C, D, E	[70] A, B, C, D, E	[70] A, B, C, D, E
[30] A, D, E	[50] A, B, C, D, E	[50] A, B, C, D, E
[10] A, B, C, D, E	[10] A, B, C, D, E	[10] A, B, C, D, E

Table 4.1.2-1: continued

Water sampling for stable isotope analyses ($\delta^{13}C$, $\delta^{18}O$)
Seawater samples for stable isotope measurements were taken from different water depths at 4 stations along the cruise track. The sampling depths were chosen individually at each station, depending on depth-related changes in salinity, oxygen and temperature provided by the CTD probe in order to sample the main surface- intermediate and deep-water masses (Table 4.1.2-1). The samples were taken from the 10L Niskin bottles of the CTD rosette. Water samples for the use of carbon isotope analysis ($\delta^{13}C$ of dissolved inorganic carbon ($\delta^{13}C_{DIC}$)) were slowly filled into 50 ml glass bottles, and 150 µl $HgCl_2$ were added to stop any biological activity. Water samples for oxygen isotope analyses ($\delta^{18}O$) were slowly filled into 100 ml glass bottles. Subsequently, all sample bottles were sealed with bees wax in order to avoid fractionation processes and stored at a temperature of 4ºC.

Phytoplankton
For the study of coccolithophore assemblages in the upper water column, seven 2-liter samples from the upper 200 m of the water column were taken at 7 stations along the cruise, which were then filtered through cellulose membranes with 0.45 µm pore size (Table 5.1.2-1). The filters were subsequently dried in the oven at 40ºC.

Neodymium
Water samples from five stations were collected for Nd isotope measurements (Table 4.1.2-1). The main goal is to complete the Nd isotope reference dataset for the South Pacific. Lateron, these data will also be used to compare them with Nd isotope records from sediment surfaces collected at the same stations. Sampling depths were adapted to the vertical structure of the water column to ensure coverage of the major hydrographic features (surface layer, thermocline, OMZ, AAIW, PCW, CDW). This sampling program also considered the water depth of sediment samples that were taken within the study area.

To enable Nd isotope measurements, 20 l of water were taken from the CTD/Rosette, filtered and subsequently acidified with HCl in order to avoid interferences of calcareous organisms and other particles with the trace metal analyses. Afterwards, 2 l of water were separated to determine Nd concentrations. NH3 was used to adjust the pH of the remaining 18 l to values between 7.6 and 8.4, and FeCl3 was added in order to precipitate the metals within 48 hours. The precipitate is then transferred to and stored in 2 l bottles.

The objectives of the Neodymium-study are (1) to determine the neodymium isotopic composition ($^{143}Nd/^{144}Nd$, expressed in εNd notation) of South Pacific water masses, (2) to assess the modern contributions of Antarctica, South America and New Zealand to the seawater Nd isotope signal of the South Pacific, and (3) to trace the export of Antarctic Bottom Water (AABW) formed in the Ross Sea into the South Pacific.

4.2 FLUOROMETER

In order to obtain information on the lateral and vertical distribution of phytoplankton in the eastern South Pacific, chlorophyll-a measurements have been carried out with the ECO fluorometer attached to the CTD. To calculate true chlorophyll-*a* concentrations from the raw signal (measured in volt) of the fluorometer, chlorophyll-*a* from the water column was measured with a photospectrometric fluorometer. At seven distinct depths, water samples from the rosette have been taken (Table 4.1.2-1) and were filtered through Whatman GF/F filter circles. The filtered residuals were dissolved in 40 ml aceton (90%), ultrasonicated for at least 1 minute and kept cool over night. The dissolved samples were measured (at 665 nm wave length) with a photospectrometric Turner Designs digital fluorometer to determine the chlorophyll-*a* concentration (Table 4.2-1; 1. value). In addition, we measured the phaeopigment concentration by treating the samples with 1N HCl and measuring them a second time (Table 4.2-1; 2. value).

Depth	SO213-02-1			SO213-09-2			SO213-12-4			SO213-22-2		
[m]	blank	1.	2.	blank	1.	2.	blank	1.	2.	blank	1.	2.
10	0.930	18.50	8.85	0.750	11.80	6.21	0.660	34.10	16.50	0.412	14.90	7.66
30	0.930	28.20	14.00	0.721	18.10	9.70	0.670	28.80	14.80	0.377	10.80	5.62
50	0.980	40.70	21.60	0.647	24.70	13.20	0.606	43.60	22.90	0.370	28.60	15.30
70	1.020	22.40	13.40	0.659	33.70	18.60	0.580	48.00	26.50	0.373	70.60	41.00
90	0.935	40.40	26.5	0.680	38.00	21.80	0.550	44.70	26.00	0.373	29.90	17.60
150	0.920	12.40	8.15	0.740	25.70	17.30	0.544	7.21	4.29	0.382	10.20	5.24
200	0.860	2.86	1.90	0.800	3.76	2.77	0.540	9.40	5.45	0.388	4.15	3.42

Depth	SO213-50-1			SO213-54-2			SO213-66-1		
[m]	blank	1.	2.	blank	1.	2.	blank	1.	2.
10	0.800	5.33	2.89	0.630	17.7	8.88	0.537	18.3	9.20
30	0.840	5.17	2.86	-	-	-	-	-	-
50	0.781	5.83	3.17	0.620	19.3	10.1	0.600	25.3	13.7
70	-	-	-	0.595	18.7	10.6	0.526	14.6	8.45
90	0.745	8.30	4.71	0.535	15.3	9.44	0.526	9.65	6.06
110	0.732	8.62	5.25	-	-	-	0.555	1.90	1.26
175	-	-	-	0.517	3.01	1.97	-	-	-
200	-	-	-	0.525	4.07	2.50	-	-	-
220	0.704	5.02	3.42	-	-	-	-	-	-

Table 4.2-1. Results of the fluorometer measurements (raw data)

4.3. MULTINET

The multinet was deployed at 7 stations (Table 5.2.) to obtain plankton samples from different water depth profiles between 1000 m and the sea surface. Samples were taken at the following water depth intervals: 1000-500 m, 500-300 m, 300-150 m, 150.50 m and 50-0 m. The multinet consisted of a steel box with 5 net hoses, each with a mesh size of 55 μm.

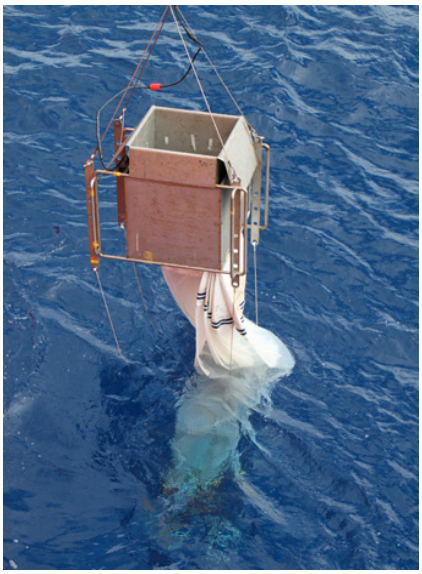

Fig. 4.3-1: Multinet

On the lower end of the multinet, a frame with 5 net beakers (1 liter each) was attached. In order to collect larger plankton fractions such as zooplankton (radiolarians, foraminifera, dinoflagellates), the net beakers had been equipped with 41 μm mesh size gaze. The release of the each net occured via data wire of the winch cable. The multinet was lowered

with closed nets down to 1000 m water depth at a maximum speed of 0.5 m/s. A board unit allowed for the opening and closing of the nets at selected water depth intervals, according to the information transmitted by a pressure sensor installed on the device. The heaving speed was 0.3 m/s. When the multinet was back on board, the remaining plankton in the net hoses was washed into the beakers. The plankton and remaining seawater were transferred into 1-liter bottles and fixed with formalin solution (2% end concentration).

MN Haul	Depth 1 [m]	Depth 2 [m]	Depth 3 [m]	Depth 4 [m]	Depth 5 [m]
SO213-02-2	1000-500	500-300	300-150	150-50	50-0
SO213-09-3	1000-500	500-300	300-150	150-50	50-0
SO213-12-5	1000-500	500-300	300-150	150-50	50-0
SO213-22-3	1000-500	500-300	300-150	150-50	50-0
SO213-50-2	1000-500	500-300	300-150	150-50	50-0
SO213-54-3	1000-500	500-300	300-150	150-50	50-0
SO213-66-2	1000-500	-failed-	-failed-	-failed-	-failed-
SO213-66-4	-	500-300	300-150	-failed-	50-0

Table 4.3-1. *Multinet hauls and collected depth intervals at SO213 stations.*

4.4. PLANKTON NET

A plankton net with 10 µm mesh size was used at 6 stations along the cruise to collect plankton samples from the upper 100 m of the water column. The net was lowered and heaved at a winch speed of 0.3 m/s. The samples were stored in 500 ml bottles and fixed with formalin (2% end concentration).

MN Haul	Depth 1 [m]
SO213-02-3	100-0
SO213-09-1	100-0
SO213-12-3	100-0
SO213-22-1	100-0
SO213-54-1	100-0
SO213-66-1	100-0

Table 5.3. Plankton net hauls and collected depth intervals at SO213 stations.

4.5. HYDROACOUSTIC MEASUREMENTS

4.5.1 SIMRAD EM120 swath bathymetry - data acquisition and data processing

The seafloor topography was continuously mapped during the cruise. The multibeam echo sounder Simrad EM120 from Kongsberg has been permanently installed on RV Sonne. This system transmits 191 beams per ping as narrow as 1°, with an operating frequency of 12 kHz. The angular coverage sector can be set up to 150°, thus enabling to achieve a maximum swath width of 5.5 times the water depth. The EM120 was operated using the standard settings for deep-sea mapping.

The system was monitored during data acquisition in order to obtain high quality data. The opening angle of the fan was manually set from 100° to 130° according to topography and water depth. The bathymetric data was used to provide precise depth information and bathymetric charts of the research areas to the scientists on board. SIMRAD EM120 calculated the water depth by runtime measurement of the acoustic signal, which was

transmitted and then again received by the transducer mounted underneath the vessel. Information about the water sound velocity in the water column is very important in order to obtain highly accurate bathymetric data. Profiles of water sound velocity were generated from CDT data, which were measured at different sites during the cruise. The global bathymetric dataset GEBCO (The general Bathymetric Chart of the Ocean 2008) with a bin size of 30 arc seconds was used to generate charts with the open-source software GMT (Generic Mapping Tool) and Fledermaus 7.2 (IVS3D) was implemented to plan the details of the cruise.

Parts of the acquired data were processed on board. The raw data (.all) was imported into the software CARIS SIPS & HIPS 6.1 to detect any errors in navigation and depth measurements. After data cleaning, it was exported in ASCII format and downloaded into Fledermaus 7.2 for the purpose of visualization, as well as chart generation with GMT.

4.5.2 SIMRAD EM120 swath bathymetry - Preliminary results

During the cruise, new seamounts were discovered and mapped, including a chain of four volcanoes, which are shown in Figs. 4.5.2-1, -2, -3. They extend in E-W direction over 55 km, 2 are about 20 to 15 km long and up to 1 km high (between stations SO213-19 and -20; Fig. 4.5.2-5).

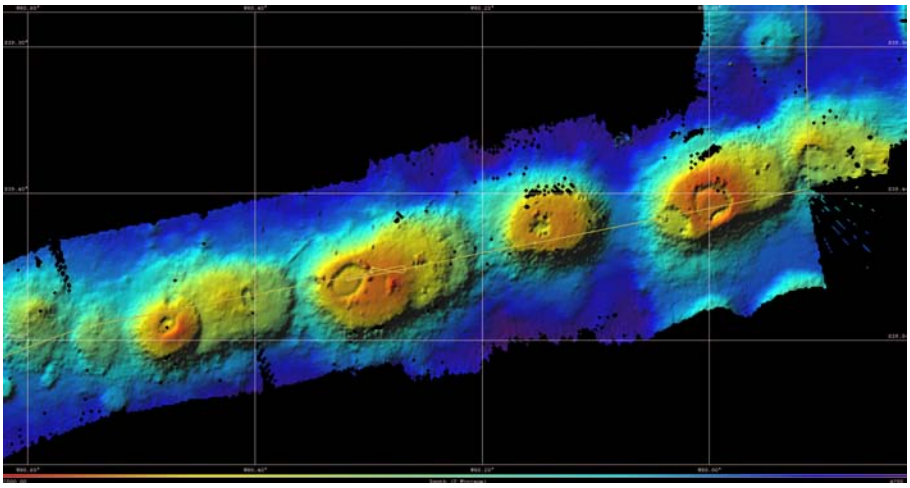

Fig. 4.5.2-1: Seamount chain visualized by SIS (operating software) during data acquisition

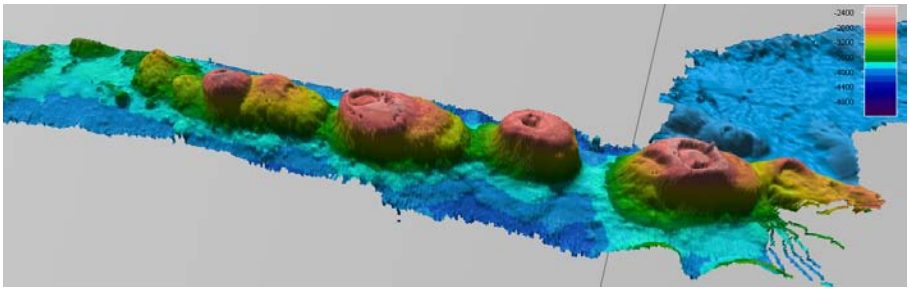

Fig. 4.5.2-2: Seamount chain in Fledermaus 7.2 (unprocessed data)

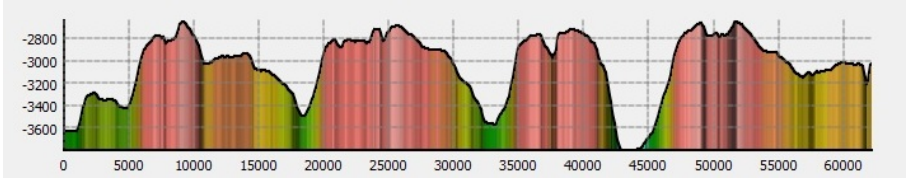

Fig. 4.5.2-3: Profile in E-W directions across the seamount chain

The area shown in Fig. 4.5.2-4 was systematically mapped through 45 km of N-S profiles and 15 km of E-W profiles. The water depths varied from 2100 to 4700 m. Visible are N-S trending elements, which are aligned parallel to the Chile Rise. The E-W trending structures belong to the corresponding fracture zone. This multibeam data from this systematically mapped area will be used for a further backscatter analysis to determine grain sizes of the surface sediments, as part of a master thesis. In the survey area, three probes of bottom sediments were taken successfully in different locations using a Multicorer. In the northern part of this area (Fig. 4.5.2-4, -5), we had obviously discovered another deep-sea area with manganese nodules (Fig. 4.5.2-6), as the sediment surfaces of the MUC tubes were covered with manganese nodules, comprising about 70% of the recovered ocean floor surface.

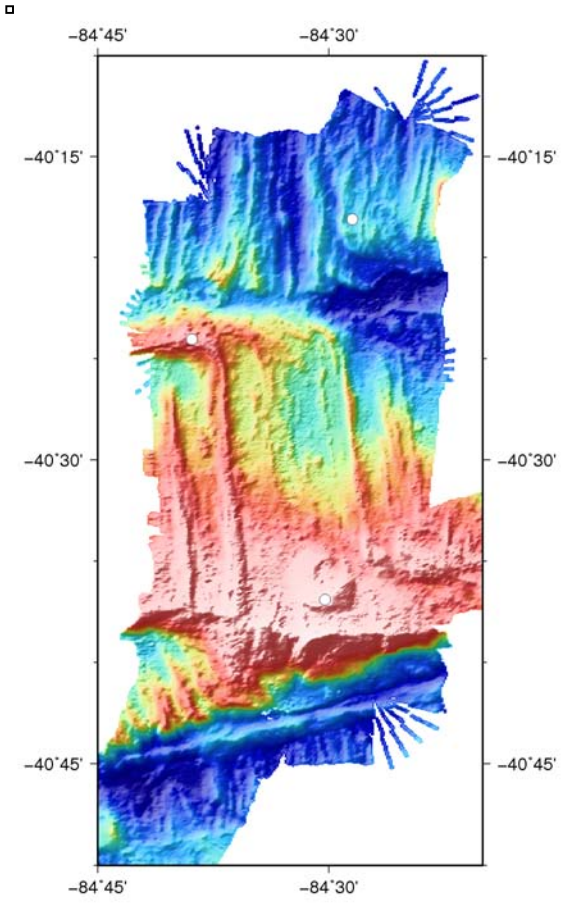

Fig. 4.5.2-4: Systematically mapped area (processed data). White dots indicate coring locations.

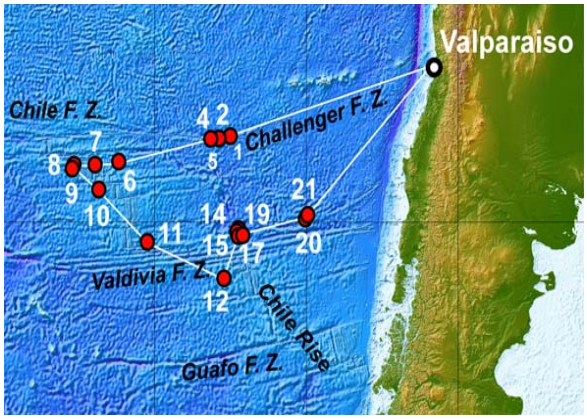

Fig. 4.5.2-5: Location of systematically mapped area: stations SO213-14 to -19.

Fig. 4.5.2-6: Manganese nodules from the surface of one MUC tube (station SO213-14)

4.5.3. Sedimentacoustics: ATLAS PARASOUND

The ATLAS PARASOUND sub-bottom profiler acts as a low-frequency sediment echo sounder and as high-frequency narrow-beam sounder to determine the water depth. It uses the parametric effect, which produces additional frequencies through nonlinear acoustic interaction of finite amplitude waves. If two sound waves of similar frequencies (e.g., 18 kHz and 22 kHz) are emitted simultaneously, a frequency signal of the difference (e.g., 4 kHz) is generated for sufficiently high primary amplitudes. The new component is traveling within the emission cone of the original high frequency waves, which are limited to an angle of only 4.5°. The resulting footprint of 7 % of the water depth is much smaller than for conventional systems and both vertical and lateral resolutions are significantly improved (Fig. 4.5.3-1).

The ATLAS PARASOUND system has been permanently installed on RV SONNE. The hull-mounted transducer array has 128 elements within an area of 1 m^2. It requires up to 70 kW of electric power due to the due to the low parametric efficiency.

The PARASOUND sub-bottom profiler on RV SONNE is equipped with digital data acquisition software from ATLAS Hydrographic, which is subdivided into ATLAS Parastore and ATLAS Hydromap Control. ATLAS Parastore allows the buffering, transfer and storage as well as the visualization of the digital echograms at very high repetition rates. ATLAS Hydromap Control is responsible for user-defined modifications of the system (e.g., pulse rate or interval) and also supports the operator in running the system properly.

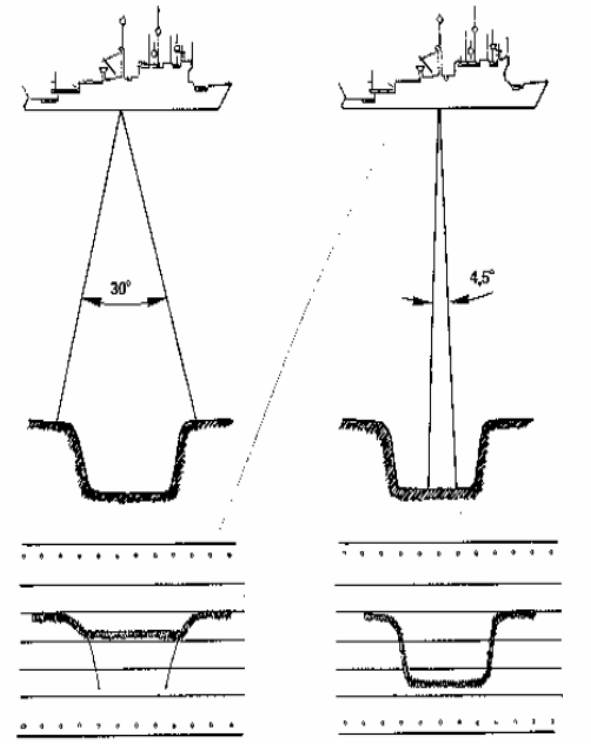

Fig. 4.5.3-1: The extremely narrowed beam of 4.5° of the ATLAS PARASOUND compared to a conventional echosounder system with an angle of 30°. The ATLAS PARASOUND even resolves small-scale bottom structures and offers a deeper penetration into the seafloor (ATLAS Hydrographic).

4.5.4. Sedimentacoustics – Preliminary results

The PARASOUND system was the major tool to recover sediment archives and to detect suitable core locations during RV SONNE cruise SO213. In total, 3358 nautical miles were profiled during this expedition. Figures 4.5.4-1 to -5 provide a summary of backscatter profiles with selected core locations from different working areas.

Challenger Fracture Zone (CFZ) (36-38°S; 85-110°W)
Fig. 4.5.4-1a-c shows the core locations within the area of the Challenger Fracture Zone *(CFZ)*. Sediment deposits were detected mostly on top of ridge structures and adjacent depressions (Fig. 4.5.4-1a-b). The most promising coring site was within the *CFZ* (Fig. 4.5.4-1c), which indicates huge sediment packages of well-stratified sediments up to 150m in thickness.

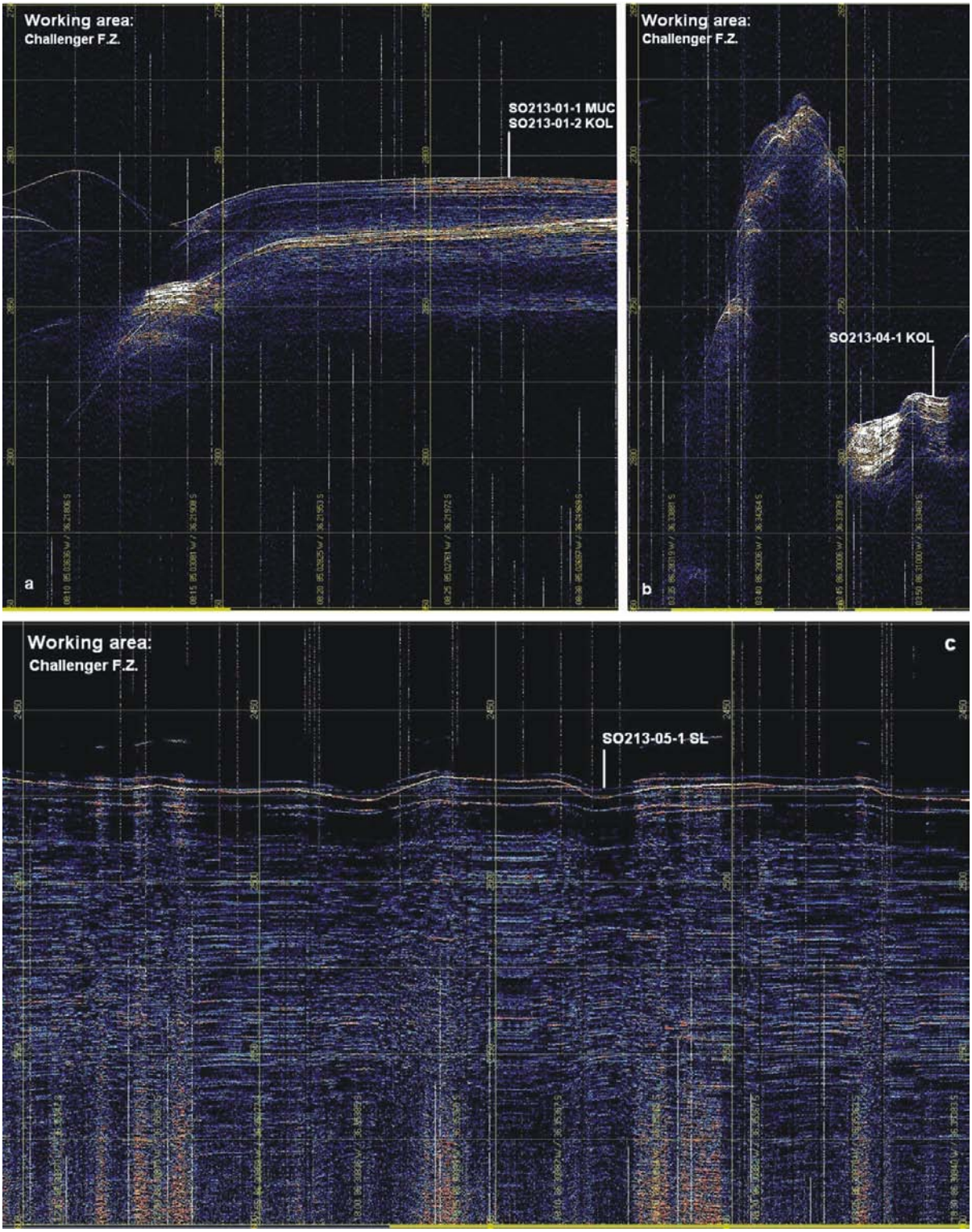

Fig. 4.5.4-1a-c: Challenger Fracture Zone. Summary of PARASOUND profiles at the CFZ and associated coring sites (vertical white bars). Note the deep sediment penetration (~150m) at core locations SO213-5 on top of the ridge structure.

Chile Rise including Valdivia Fracture Zone (ChiRi) (38-43°S; 79-94°W)

The area of the Chile Rise including the Valdivia Fracture Zone *(ChiRi)* shows a pattern of pronounced differences in sediment deposition and preservation (Fig. 4.5.4-2a-e). The PARASOUND profiles indicate rough seafloor topography, and suitable core sites were again only found on top of ridges or in small-scale depressions filled with sediments. The

sediment deposits varied from several meters to tens of meters in sediment thickness. At the Valdivia Fracture Zone, a seamount chain and several ridges were mapped during the cruise (Fig. 4.5.4-2c-e). Some parts of the ridge structures offered vast areas of well-defined sediment layers with a sediment thickness of several tens of meters (Fig. 4.5.4-2d). In contrast, within the area of the seamount chain (Fig. 4.5.4-2e), little to no sediment archives could be identified, probably due to rough bottom topography and flanks too steep to be recorded by the ATLAS PARASOUND system.

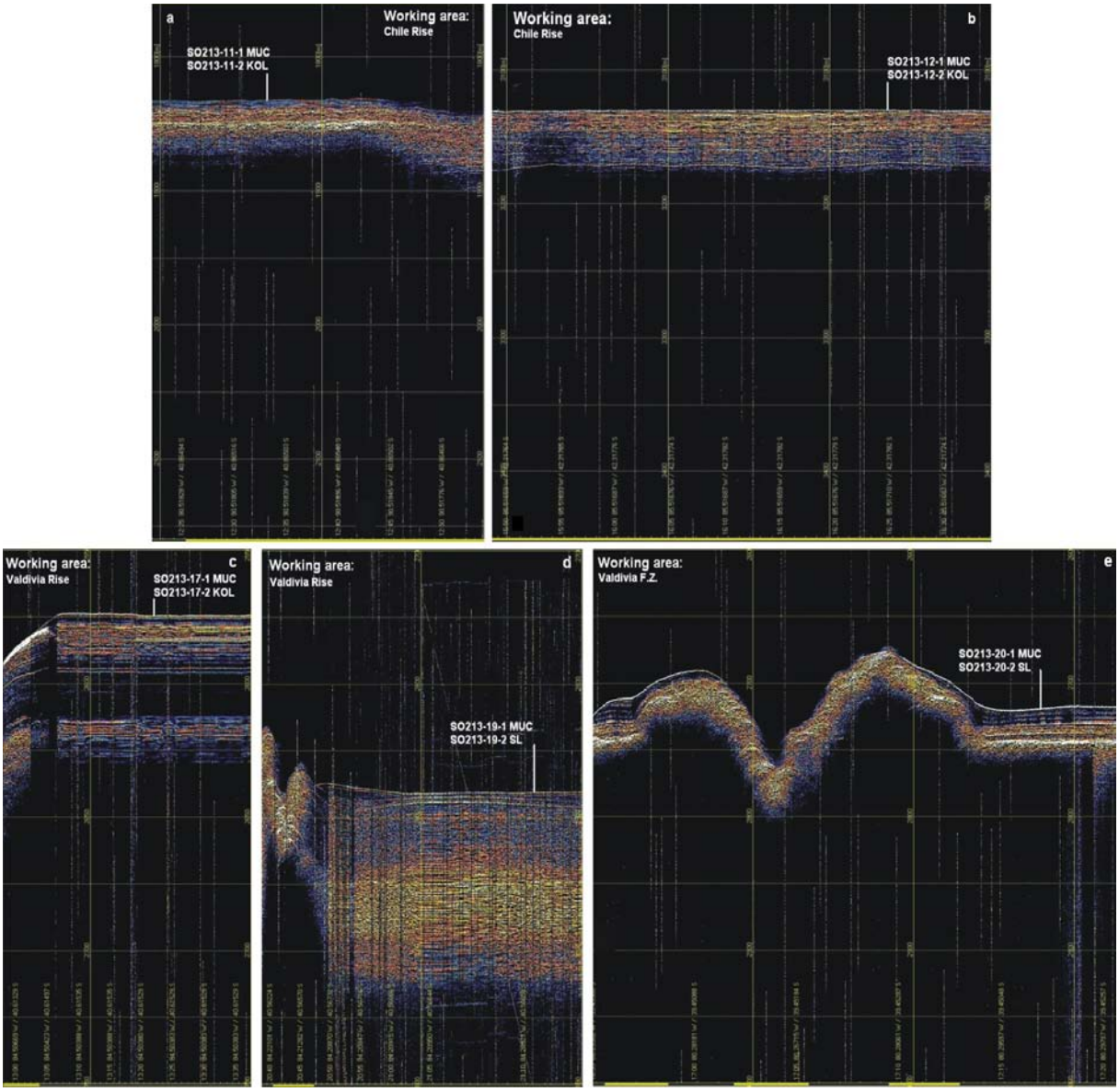

Fig. 4.5.4-2a-e: Summary from selected PARASOUND profiles with coring sites (vertical white bars) at the Chile Rise including Valdivia Fracture Zone. Fig.xx e shows part of a profile recorded on top of a seamount, at the associated seamount chain of the Valdivia Fracture Zone.

East Pacific Ridge (EPR) (40-47°S; 114-121°W)

At the East Pacific Ridge *(EPR),* several hydro-acoustic profiles were taken along and perpendicular to the ridge axis (Fig. 4.5.4-3a-d). Due to the position of the ridge in the central South Pacific, the sediments are clearly dominated by open pelagic deposition. Recovered sediments span Pleistocene to Early Miocene in age and indicate low sedimentation rates. The sediment thickness increases with distance to the ridge axis and varies from tens of meters (Fig. 4.5.4-3a and c) up to 100m. This is due to the fact that the age of the crust becomes older with increasing distance to the ridge axis, which means

sediments had more time to accumulate. One of the goals of the SOPATRA expedition was the detection of suitable drilling sites for the Integrated Ocean Drilling Program “IODP”. In Fig. 4.5.4-3b, one potential drilling site location (IODP1B) is shown. Please note the huge, well-defined sediment horizons. The entire sediment body exceeded the maximum penetration (about 150m) of the PARASOUND system.

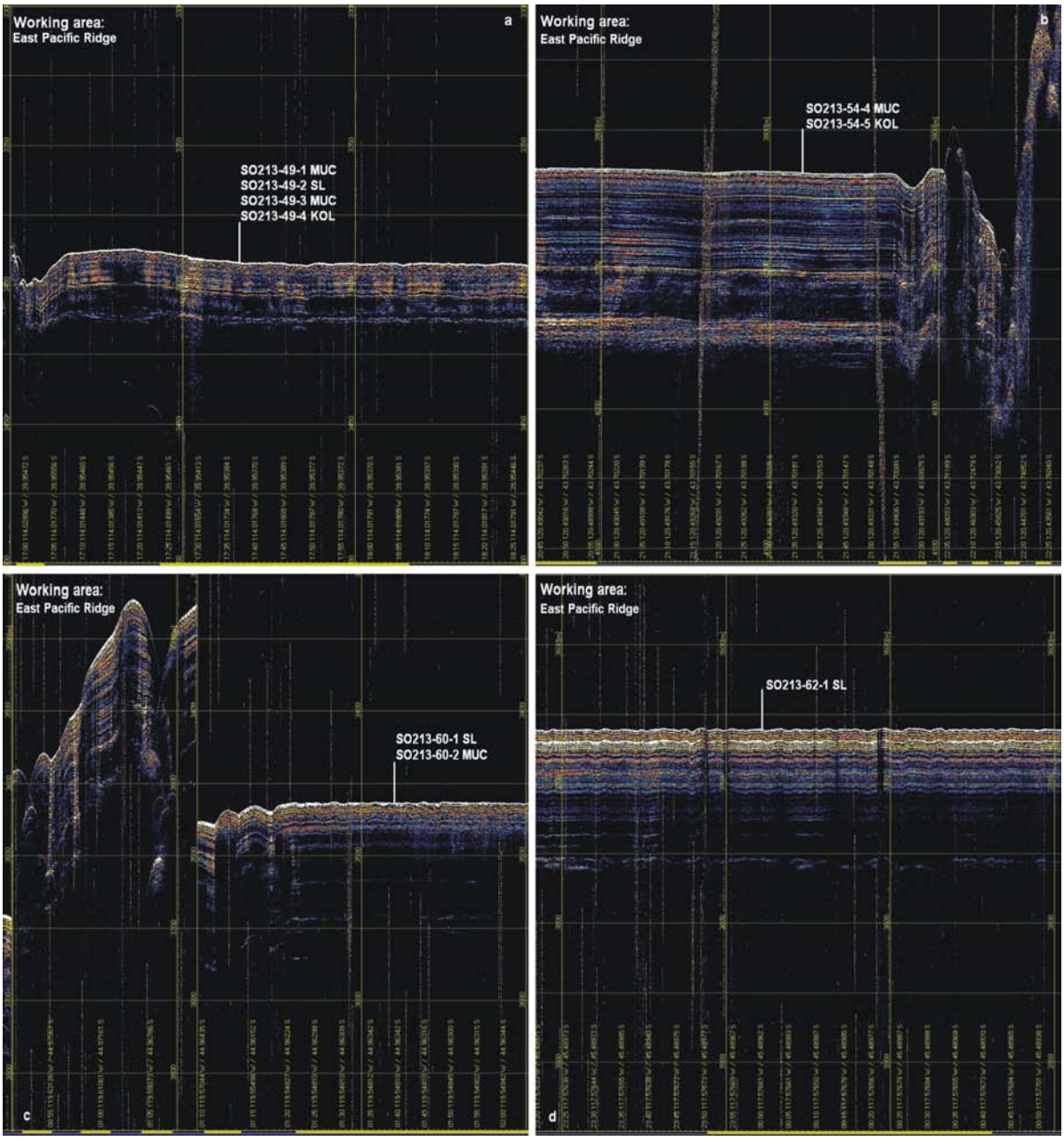

Fig. 4.5.4-3a-d: Summary of selected PARASOUND profiles with coring sites (vertical white bars) at the East Pacific Rise. Fig. 4.5.4-3b shows a potential IODP drilling site, together with core site SO 213-54-5 KOL (vertical white bar, 3828m water depth). Please note the deep penetration (>150m) at this location.

SW Pacific Basin including Louisville Seamounts (SWB) (45-47°S; 151-173°W)

After leaving the East Pacific Ridge, the next working area was located at the Louisville Seamounts, where large sediment deposits were detected on top of a seamount. Unfortunately, the piston corer failed and we were only able to recover surface sediments with the Multicorer (MUC). Fig. 4.5.4-4a-b indicates core locations at the deep SW Pacific Basin, where well-stratified sediments were detected through PARASOUND.

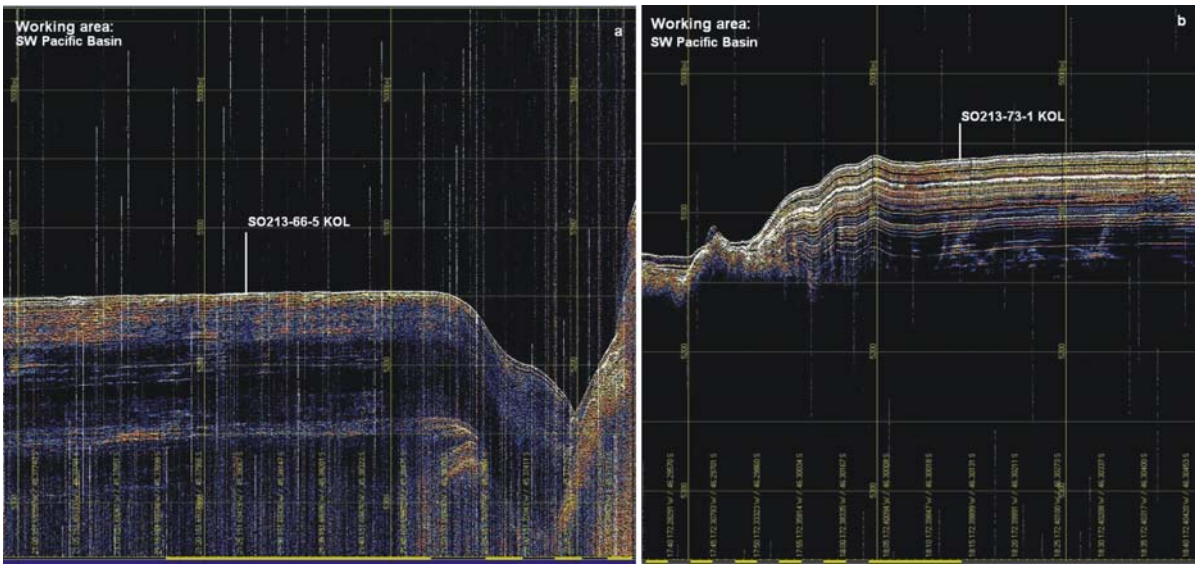

Fig. 4.5.4-4a-b: Summary of selected PARASOUND profiles with coring sites (vertical white bars) in the SW Pacific Basin

New Zealand Margin between Chatham Rise and Campbell Plateau (NZM) (45-47°S; 178°W-174°E)

The last working area in front of New Zealand was covered by huge sediment packages (Fig. 4.5.4-5a-b), which were well recorded by the PARASOUND. A suite of long and high-resolution sediment cores from several depths were recovered successfully between the Chatham Rise in the north and Campbell Plateau in the south within the Bounty Trough.

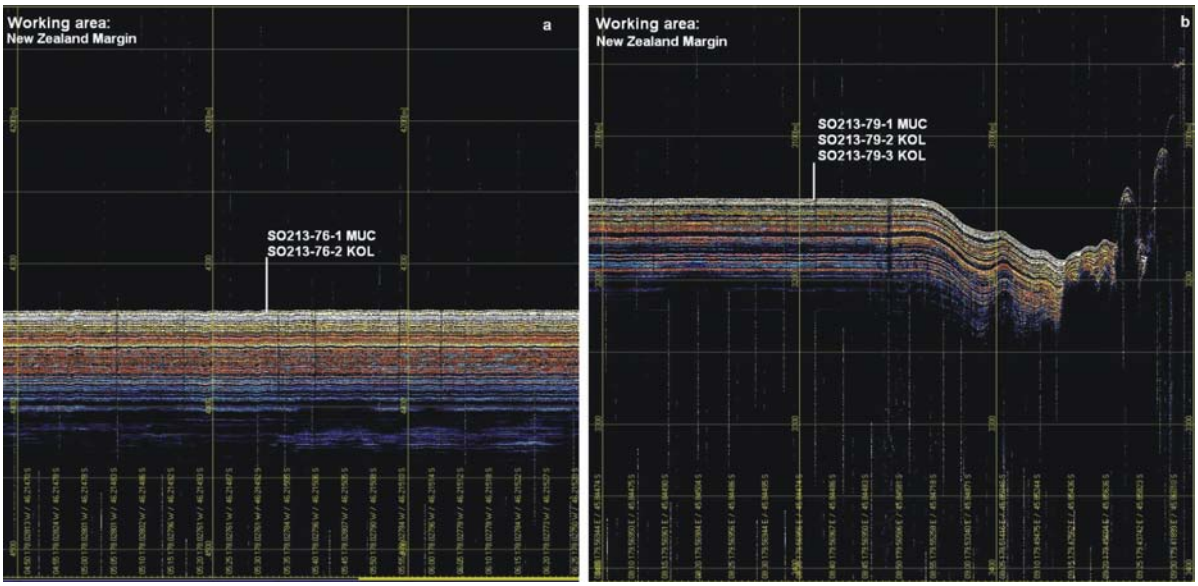

Fig. 4.5.4-5a-b: Summary of selected PARASOUND profiles with coring sites (vertical white bars) at the New Zealand Margin. Please note the well-defined sediment horizons.

4.6 SEDIMENTS: SAMPLING, LOGGING, FACIES

We retrieved sediment cores and surface sediment samples in the South Pacific from five working areas (Fig. 4.6.-1A, B).

- ***Working area 1 (CFZ)*** along the Challenger Fracture Zone (~36-38°S; ~85°-110°W) was primarlily sampled during SO-213 Leg 1 and extended during Leg 2. It comprises a latitudinal coring transect from the Chile Basin westward to the eastern flanks of the East Pacific Ridge.
- ***Working area 2 (ChiRi)*** includes sediment cores at the Chile Rise (~41°S), including the Valdivia Fracture Zone (east to ~80°S), and was completed during Leg 1.
- ***Working area 3 (EPR)*** was located on the western flank of the East Pacific Ridge. Sediment cores were recovered between ~40°S and 47°S during Leg 2. A detailed depth transect extending from the EPR crest northwestward covers water depths from ~3100-4000 m and is located between ~44° and 46°S. This working area extends the Polarstern expedition ANT26-2 EPR transect (~54-58°S) northward.

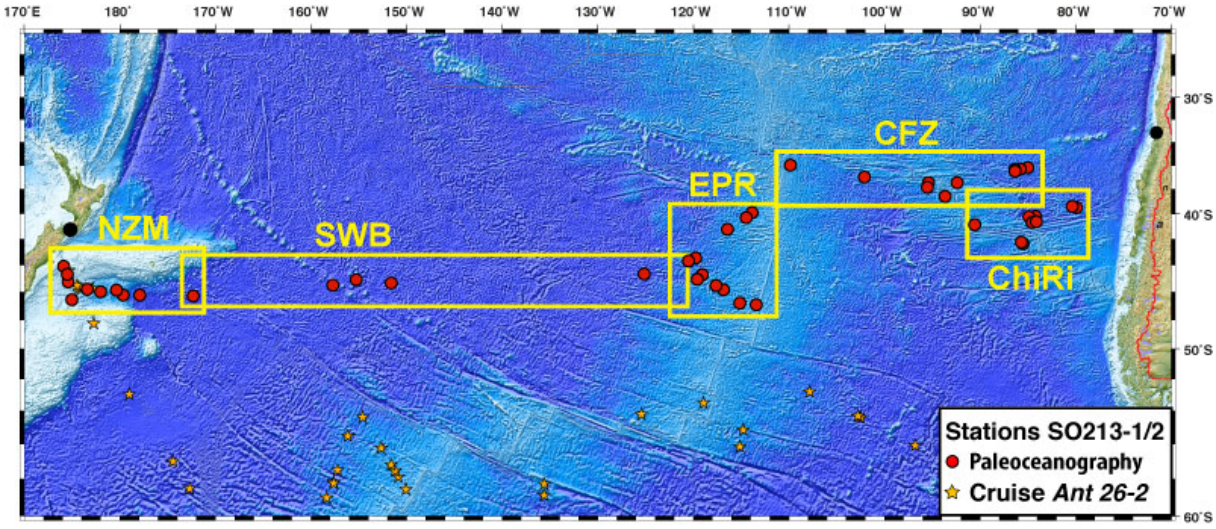

Fig. 4.6-1A: Overview map with working areas and coring stations during Sonne expedition SO213 (red dots) and Polarstern expedition ANT26-2 (yellow stars).

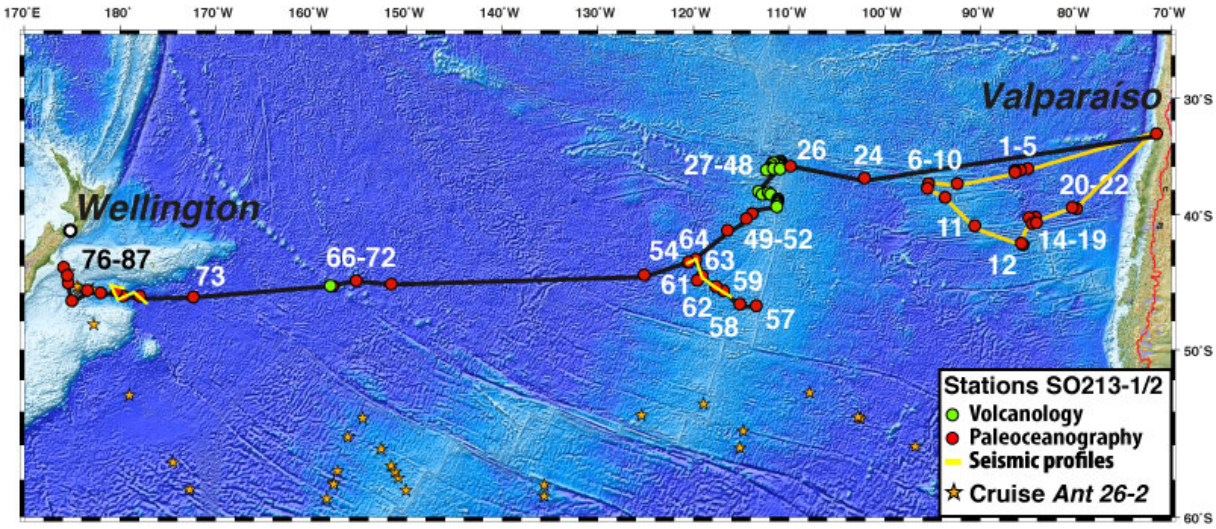

Fig. 4.6-1B: Cruise track with all station stations during Sonne expedition SO213. Paleoceanographic stations are marked by red dots.

- ***Working area 4 (SWB)*** covers the SW Pacific basin and extends from the western flank of the EPR westwards across the Louisville Seamount chain (Leg 2) to the outermost reaches of the Bounty fan.
- ***Working area 5 (NZM)*** is located on the New Zealand continental margin directly south of the Chatham Rise. It comprises a detailed depth transect of sediment cores that starts a ~4400 m water depths at the outer Bounty Trough (~46°S; ~178°W) and ends landwards at the uppermost continental slope, close to the shelf break off New Zealand´s South Island (at ~44°S; 174°E), at ~560 m water depth (Leg 2)

Information on core length and recovery is given in Table 4.6.2-1 and Fig. 4.6.2-2. The coring locations are shown in Fig. 4.6-1. An overview of the major lithologies, including a preliminary interpretation of these data. Consideration of the physical properties and color scans is provided in chapter 4.6.4 (Sediment facies).

4.6.1. Multicorer

Deployment

The multicorer was deployed 35 times in total during SO213 Leg 1 and 2. After several improvements to the device, a successful series of core recovery yielded almost 12 full tubes of sediment. The multicorer was lowered with an average speed of 1 m/s to a depth of about ~30-40 m above seafloor, where it was stopped for ~2-3 minutes. It was then again lowered with a speed of 1 m/s until bottom contact. Contact with the seafloor was monitored through the cable tension. The multicorer was left on the seafloor for about 1 minute, then pulled out with a speed of 0.3 m/s and finally heaved with a speed of 1 m/s.

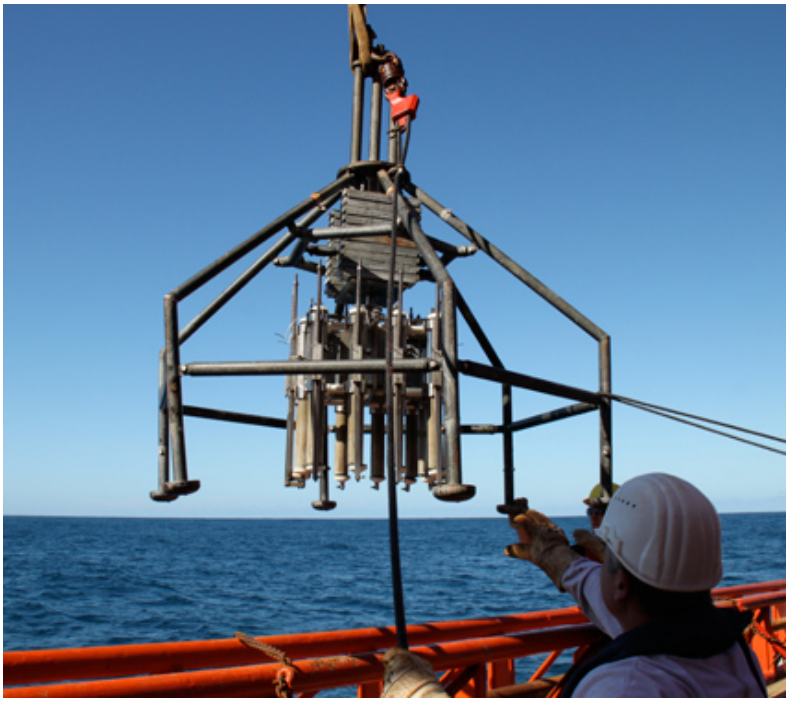

Fig. 4.6.1.-1 AWI multicorer, technical specifications:
Height: approx. 2250 mm
Diameter: approx. 1900 mm
Weight of head: approx. 180 Kg
Weight of framework: approx. 465 Kg
Number of tubes: 12
Diameter of tubes: 100 mm

Sampling

Sediment recovery of each of the 12 tubes was recorded, seawater was siphoned off (for bottom water analyses) and the sediment was briefly described. Core tops (1 cm thick) were either preserved in Rose Bengal and alcohol, or put into plastic bags. All tubes were completely cut into 1 cm thick slices and put into plastic bags (Whirlpack). Sediment samples were distributed among various working groups at the Alfred-Wegener-Institute (AWI, Bremerhaven), the IFM-GEOMAR Kiel, and the Geomarine Research Institute (St Johns, Auckland, New Zealand).

Tube	**1**	**2**	**3**	**4**	**5**	**6**	**7**	**8**	**9**	**10**	**11**	**12**	
Station						**[cm in tube]**							**Station [total cm]**
SO 213-1-1	12	10	15	10	12	10	10	25	25	7	10	-	146
SO 213-6-1	17	11	5	1	9	10	-	-	-	-	-	-	53
SO 213-7-1	26	25	25	12	24	23	24	20	23	24	25	26	277
SO 213-8-1	10	-	1	-	-	-	-	-	-	-	-	-	11
SO 213-8-3	4	6	19	-	-	-	-	-	-	-	-	-	29
SO 213-10-1	28	18	21	27	16	28	27	4	16	-	26	16	227
SO 213-11-1	13	-	-	-	11	-	-	-	-	-	-	-	24
SO 213-12-1	27	28	27	27	19	21	27	27	28	21	23	26	301
SO 213-14-1	31	31	32	31	30	30	26	31	29	28	26	32	357
SO 213-15-1	14	11	2	19	5	18	19	-	13	10	13	15	139
SO 213-17-1	18	21	14	21	6	16	20	20	13	14	11	21	195
SO 213-19-1	-	15	14	14	16	14	16	-	-	-	5	14	108
SO 213-20-1	6	-	-	-	5	-	-	-	5	-	-	-	16
SO 213-22-4	36	21	38	36	30	33	34	32	21	33	34	34	382
SO 213-24-1	8	11	8	11	16	27	26	11	27	7	25	11	188
SO 213-26-1	31	26	28	21	32	30	29	-	32	31	-	31	291
SO 213-49-1	-	-	-	-	-	-	-	-	-	-	-	-	0
SO 213-49-3	31	26	31	33	32	30	26	32	30	31	31	32	365
SO 213-54-4	29	28	29	27	29	29	29	29	29	26	21	28	333
SO 213-57-1	4	-	-	-	-	-	-	6	-	-	-	1	11
SO 213-58-1	3	1	-	4	-	-	-	-	-	-	-	-	8
SO 213-59-1	2	2	16	2	15	15	-	15	-	2	16	2	87
SO 213-60-2	26	25	26	25	23	24	24	25	27	22	26	28	301
SO 213-61-1	21	28	23	28	26	25	28	27	28	26	26	26	312
SO 213-63-1	43	42	40	44	46	31	44	40	31	46	44	46	497
SO 213-64-2	30	30	26	26	30	29	29	30	31	30	30	28	349
SO 213-68-1	20	19	-	18	-	-	-	-	20	-	-	18	95
SO 213-71-2	9	24	-	-	-	-	-	-	-	-	-	-	33
SO 213-76-1	31	31	32	32	31	31	32	26	26	31	30	31	364
SO 213-78-1	31	31	31	30	30	32	31	31	31	31	30	31	370
SO 213-79-1	18	22	16	16	15	20	16	18	17	20	16	15	209
SO 213-81-1	21	23	24	14	26	26	25	24	19	26	23	24	275
SO 213-84-2	24	26	21	21	28	28	26	25	25	24	23	23	294
SO 213-85-1	7	-	-	-	-	-	-	-	-	6	6	?6	19
SO 213-87-7	26	27	29	24	26	25	24	?24	24	24	25	26	280
SO 213 Total													6946

Tab. 4.6.1.-1: List of multi-corer recovery during SO-213, Leg 1 and 2.

4.6.2. Gravity corer and piston corer

Deployment

During expedition SO213, 20 piston corers with core barrel lengths between 15 and 20 m (KOL) and 24 gravity corers with length between 5 and 15 m (SL) were deployed. 40 successful deployments resulted in a total core recovery of 348.5 m including 10.44 m core length recovered by the pilot corer (TC), triggering the KOL (Figs. 4.6.2-1, -2). At 4 stations, all located on top of shallow seamounts, we did not recover any sediment.

The gear types and length of the coring devices were chosen based on acoustic sediment profiles done with the PARASOUND echosounding system, considering acoustic patterns such as the strength of characteristic reflectors, their spacing, and the total sub-bottom penetration (Chapter 4.5.4). Core recoveries and barrel lengths in the individual working areas (Fig. 4.6-1A, Tab. 4.6.2-1) were as follows:

- ***Working area 1 (CFZ):*** 4 KOL deployments (barrel lengths 15-20 m) recovered sediment cores ranging from 11.02 to 12.52 m. In addition, we recovered 3 rather short SL (0.9 to 3.54 m), using barrel lengths of 5 and 10 m.
- ***Working area 2 (ChiRi):*** 3 KOL (barrel lengths 15 m) recovered core lengths of 1 to 5.43 m and 4 SL (barrel lengths 8-15 m) resulted in core lengths of 0.55-9.58 m.
- ***Working area 3 (EPR):*** 3 KOL deployments (barrel lengths 15 m) recovered 8.86-11.92 m long sediment records. In addition, we deployed the SL 9 times (barrel lengths 10 m) and obtained 7 sediment cores ranging from 2.11 to 7.08 m. The KOL could not be deployed because of bad weather conditions.
- ***Working area 4 (SWB):*** At two deepwater stations (>5000 m water depth), we obtained two long (12.36 and 17.93 m) sediment cores using 15 and 20 m barrel lengths. Two attempts with the gravity corer on top of a seamount in 660 m water depth were unsuccessful. A further KOL deployment (15 m barrel length) at a deeper seamount (2000 m water depth) with good Parasound penetration unfortunately resulted a bent core and 4.50 m of strongly disturbed sediment.
- ***Working area 5 (NZM)*****:** Coring at the New Zealand margin was very successful with 7 KOL deployments (barrel lengths 20 m) that recovered long sediment records ranging from 16.64 to 17.92 m. Due to bad weather conditions, we unfortunately had to switch to the gravity corer (barrel lengths 10-15 m), which recovered 6 sediment cores with lengths ranging from 2.88 to 7.71 m. In order to obtain additional sediment material for the envisaged diverse post-cruise studies, we took double cores at stations SO213-79, SO213-82, and SO213-87. Furthermore, we prolonged an earlier Polarstern record (station PS75/104-1; core length 12.39 m) to 17.43 m length (SO213-85-2).

The piston corer with split piston developed by Fa. Marinetechnik Kawohl (marinetech.-kawohl@tonline.de) can be fitted with a core barrel up to 30 m in length (in 5 m increments). The core diameter is 9 cm. On RV Sonne, the piston corer was deployed with an 18 mm steel cable attached to the ship´s deep-sea winch (max. speed: 2 m/s for up to 70 kN or max. speed: 1 m/s for up to 140 kN). The piston corer was lowered with an average speed of 1.0 m/s to ~50 m above seafloor, where it was stopped for ~5 minutes. It was then lowered with a speed of 0.3 m/s until the pilot trigger core hit the seafloor. Contact with the seafloor was monitored through the cable tension. When the pilot core reached the seafloor, the piston corer was released, free falling by ~5 m before reaching the seafloor, and penetrating into the sediments. The device remained at the seafloor for about 30 seconds after piston release in order to allow for deep penetration, then pulled out with a speed of 0.3 m/s. Once out of the sediment, it was heaved up with a speed of 1.0 m/s. Two types of gravity corers were run, one with a core diameter of 12 cm and a barrel of ~1.5 tons, the second and more successful device with a core diameter of 9 cm and a barrel of ~2.0 tons. Both devices were lowered with 1 m/s to the seafloor. The devices remained on the seafloor for about 20 seconds in order to allow for deep penetration, and was then pulled out with a speed of 0.2 m/s. Heave velocity was 1.0 m/s.

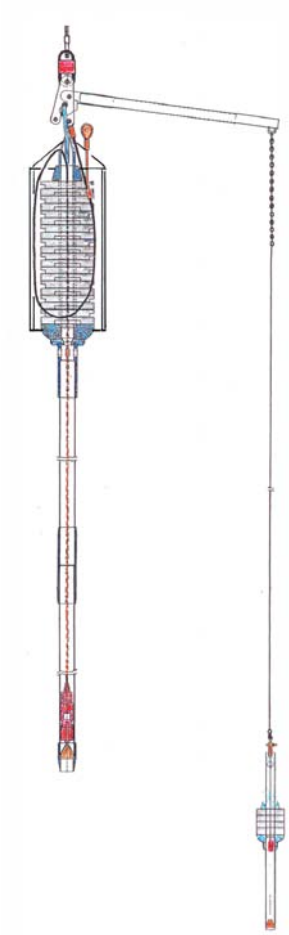

Fig. 4.6.2-1. Operation of a 15 m piston corer during SO213-1 (right) and schematic diagram of the split-piston corer from Fa. Marinetechnik Kawohl, deployed during SO-213-1

Core handling

The core liners of the piston and gravity cores were orientated, then labeled (Fig. 4.6.2-3), and commonly cut into 1 m sections. Before closing the core segments with plastic caps, smear slides were taken from the top of each segment for biostratigraphic analyses and initial carbonate content determinations, which were performed using 15%-hydrochloric acid. After the measurement of physical properties with the multi-sensor core loggers (see chapter 4.6.3), cores not opened on-board R/V Sonne were stored in a reefer container at a temperature of 4° C and transported to Bremerhaven. Based on initial biostratigraphic analyses and physical property data, most cores were selected for opening and on-board sampling (Tab. 4.6.2-1). Each section was split into working and archive halves. The sediment surface was cleaned and smoothed before core photos were taken, and lithological description started. Color reflectance measurements were taken of the archive half. The archive halves were usually packed into plastic D-tubes and stored at ~4°C in the reefer. The working halves were completely used up, providing sample material for the various working groups (Fig. 4.6.2-4). The sediment from core catchers was packed whenever possible, and stored at ~4°C. The trigger cores were likewise logged, and afterwards split into halves. The archive half of the trigger core was visually described and color scanned.

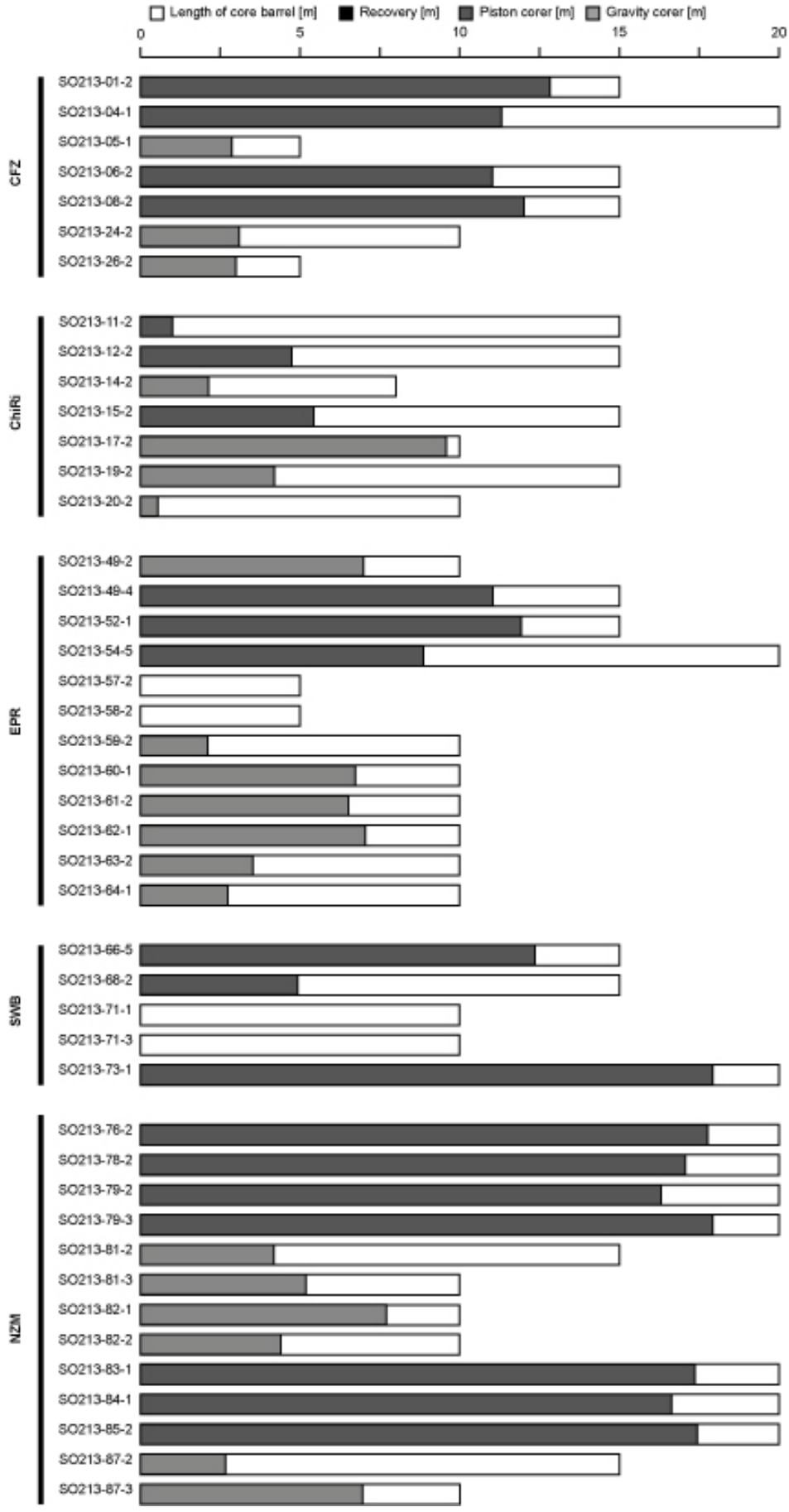

Fig. 4.6.2-2. Length of core barrel and core recovery of piston and gravity corers

Station	Sediment recovery [cm] of sediment cores	Sediment records opened (X)	Sediment records fully sampled (archive half)
SO 213-1-2	1321	X	
SO 213-4-1	1193	X	X
SO 213-5-1	287	X	
SO 213-6-2	1163	X	X
SO 213-8-2	1201	X	X
SO 213-11-2	100	X	
SO 213-12-2	558	X	
SO 213-14-2	214	X	
SO 213-15-2	604	X	
SO 213-17-2	985	X	
SO 213-19-2	420	X	
SO 213-20-2	55	X	
SO 213-24-2	309	X	
SO 213-26-2	300	X	
SO 213-49-2	699	X	
SO 213-49-4	1188		
SO 213-52-1	1269	X	X
SO 213-54-5	971		few cm between 9th and 8th section
SO 213-57-2	0		
SO 213-58-2	0		
SO 213-59-2	211	X	X
SO 213-60-1	673	X	X
SO 213-61-2	652	X	X
SO 213-62-1	705	X	X
SO 213-63-2	353	X	X
SO 213-64-1	274	X	
SO 213-66-5	1349	X	X
SO 213-68-2	493		0- 5 cm
SO 213-71-1	0		
SO 213-71-3	0		
SO 213-73-1	1859	X	
SO 213-76-2	1834	X	
SO 213-78-2	1782	X	
SO 213-79-2	1690	X	0-1 cm
SO 213-79-3	1862		
SO 213-81-2	418		
SO 213-81-3	518	X	
SO 213-82-1	771	X	
SO 213-82-2	439		
SO 213-83-1	1781		
SO 213-84-1	1724		0- 4 cm
SO 213-85-2	1760		
SO 213-87-2	266		
SO 213-87-3	695		
Total	**34946**		

Tab. 4.6.2-1: Sediment recovery of piston and gravity cores

Labelling of core liners and D-tubes

Liners and D-Tube caps contain the following information (Fig. 4.6.2-3):

- Core number (e.g., SO213-02-1 KOL)
- "A" for archive half, "W" for working half
- Arrow pointing to base with depths of section top and base
- Top and base of each section is marked with "Top" and "Base/Bottom", respectively, and the continuous depth alongside the core

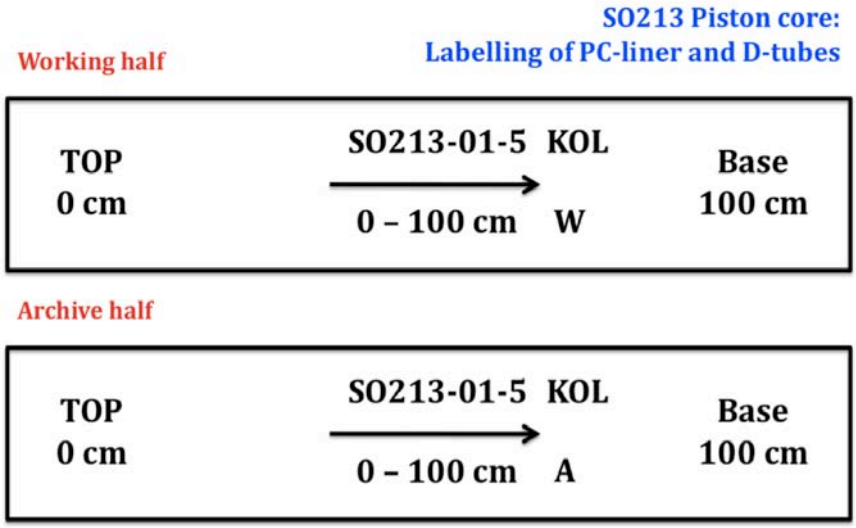

Fig. 4.6.2-3 Labelling of core liners and D-tubes

Visual core description and core photography

The sediment core descriptions (see Appendix D) summarize data obtained during the onboard visual inspection of each core. All descriptions were documented with the software package APPLECORE, using a lithology custom file containing patterns following the standard IODP/ODP sediment classification scheme, a modified version of the lithologic classification of Mazzullo et al., (1988). Sediments were named on the basis of composition and texture, using a principal name together with major and minor modifiers. Sediment core descriptions were performed on the archive halves and were complemented by microscopic analyses of sediment smear slides from selected lithologies found in the individual cores. Due to time and man-power restrictions, we were not able to perform systematic smear slide analyses of all major lithologies onboard. The lithological classification followed the scheme suggested by Mazzullo et al., (1988). According to this classification, sediments encountered during SO-213 are granular sediments consisting of pelagic and, subordinately, siliciclastic particles. Pelagic particles are defined as bioclastic grains composed of the skeletal remains of open-marine calcareous and siliceous microfauna and microflora, derived from foraminifers, nannofossils, diatoms, and radiolarians as well as minor amounts of sponge spicules and silicoflagellates. The siliciclastic components encountered during SO213 consist of terrigenous and volcanogenic mineral and rock fragments, primarily including silt and clay-sized minerals (we defined the sum of both as “mud”).

Sediment names consist of a principal name related to the major biogenic component and the degree of compaction. During expediton SO213, we only encountered unconsolidated calcareous and/or siliceous biogenic sediments (generally “ooze”, and if dominated by foraminifera, “sand”). For siliciclastic sediments, the principal name describes the texture (gravel, sand, mud (silt+clay)) based on the Udden-Wentworth grain-size scale (Wentworth, 1922). The principal name of biogenic and siliciclastic sediments is preceded by major modifiers and followed by minor modifiers that may refer to mixed biogenic, siliciclastic, and volcaniclastic components:

1. 25%–50%: components in this range modify the principal name.
2. 10%–24%: components in this range are added with the suffix “-bearing” (e.g., foraminifer-bearing).
3. 0%–9%: components with these abundances are not named, unless they are of significant importance for the interpretation.

Additional information in the core description logs includes the location and nature of sedimentary structures, the occurrence of ichnofossils, the degree of bioturbation, and accessories (such as pyrite, iron sulfides, laminae, shell fragments, etc.) The symbols used to designate structures found in each core are shown in Appendix D (core description). Sediment colors were determined using a “Munsell Soil Color Chart“. But as the color measurements taken with the Minolta spectrophotometer are more reliable, we included the L*-records into the lithology logs. Furthermore, the core description logs also include the magnetic susceptibility data of each core. Core sections were photographed using a digital camera (Olympus E-10). The single images were arranged for each core and are presented accordingly (see Appendix E).

Sampling scheme of sediment cores

The 1m-long working half segments of selected sediment cores (4.6.2-4) were sampled for shore-based analyses according to the following scheme, repeating every 2 cm:

0-1 cm	org. geochemistry (AWI) / foram. geochemistry (IFM-GEOMAR)
1-2 cm	bulk sample (AWI) / Nd-isotope geochemistry (IFM-GEOMAR)

In addition, the following samples were taken for onboard studies (Table 4.6.1):

Every ~30 cm	1 tooth pick for lithological classification
Every ~100 cm	1 syringe for foraminferal biostratigraphy at the base of each core segment
Every ~100 cm	1 tooth pick for nannofossil biostratigraphy at the base of each core segment

Samples were taken in whole slices from the working half and were placed in plastic bags (Whirl-Packs). Every ~30 cm, a syringe with defined volume was taken for physical property analyses by AWI and IFM-GEOMAR. The working halves were completely sampled following the scheme below.

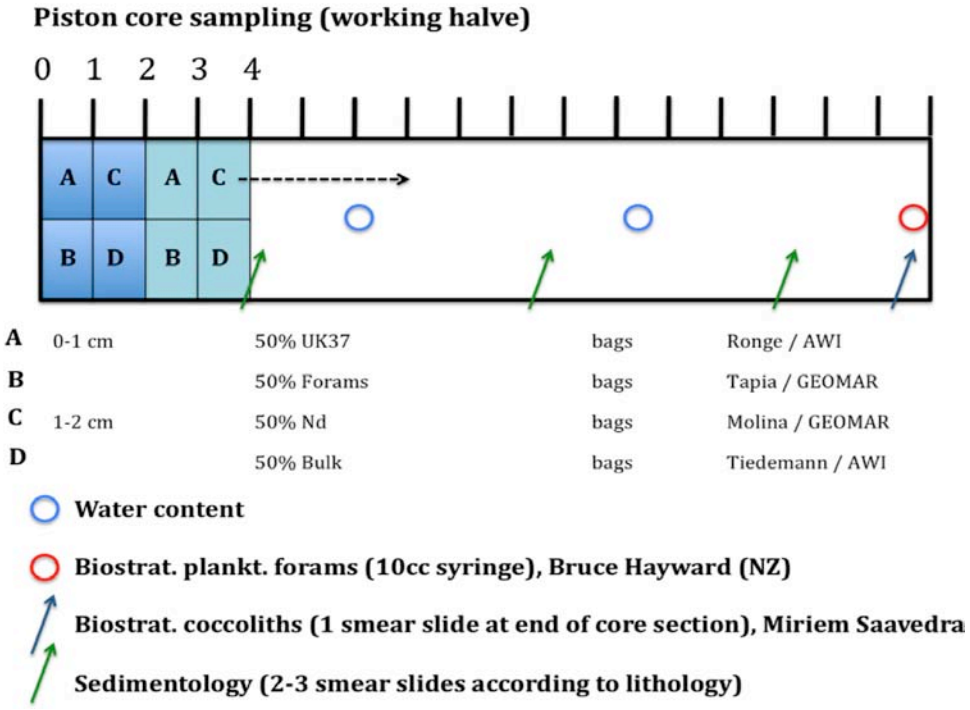

Fig. 4.6.2-4. Sampling scheme applied for sediment cores recovered during SO213-1.

4.6.3. Shipboard core logging

4.6.3.1 Physical properties and magnetic susceptibility

Methods

Physical properties of the sediment cores were measured aboard RV SONNE using the GEOTEK Multi Sensor Core Logger (MSCL). This device enables the determination of P-wave velocity, Gamma Ray Attenuation (GRA)-density and magnetic susceptibility in whole, unsplit cores.

In order to obtain a constant room temperature, the sediment core segments were stored in the air-conditioned Magnetics and Gravimetry Laboratory for at least 24 h after core retrieval. Afterwards, the core sections were logged with the MSCL one after another at 1 cm increments by placing them on the rails of a conveyor system, aligned at the start position (the length of each segment had to be adjusted manually). At the beginning of each sediment core, a 52 cm long PVC core liner filled with de-mineralized water was measured. At the end of each core, a 103 cm long PVC core liner filled with de-mineralized water was used to push the last core segment through all sensors. We used the GEOTEK MSCL 6.2 program and the GEOTEK Utilities 6.1 software for measurements and data processing.

P-wave velocity of the core was measured by an ultrasonic P-wave system mounted on the center sensor stand. The P-wave plate transducers (PWTs) produce a short P-wave pulse (frequency: 500 kHz, pulse repetition rate: 1 kHz), which propagates through the core and is detected by the receiver. Pulse time circuitry is used to measure the travel time of the pulse with a resolution of 50 ns. The distance traveled by the P-waves is measured as outside core diameter (accuracy: 0.1 mm). Additional temperature measurements needed for the accurate determination of P-wave velocities were carried out with a standard platinum resistance thermometer (PRT). Prior to logging, core thickness and temperature calibrations were carried out using liners with known length and water values at known temperatures (measured with the Hg-thermometer).

The GRA-density was measured using a Caesium-137 source (activity: 356 MBq; energy: 0.662 MeV) emitting a narrow gamma ray beam (5.0 mm), and a gamma ray detector (Gammasearch2, Model SD302D, Serial number 3047, John Caunt Scientific Ltd.) mounted on the sensor stand. The density of the core material is determined by measuring the number of gamma photons that pass through the core without attenuation (count time: 10 s). For later data processing and for the conversion of gamma counts into density, a water-filled PVC core liner containing an aluminum pyramid was measured in 2 mm steps before logging each sediment core.

The magnetic susceptibility of the sediment cores was determined using a Bartington M.S.2 susceptibility meter and a loop sensor (MS2C) with a diameter of 140 mm (#208). An oscillator circuit in the sensor produces a low-intensity (80 A/m RMS) non-saturating alternating magnetic field (0.565 kHz). Magnetic susceptibility of the sediments causes a change in the oscillator frequency that is electronically converted into (artificial) magnetic susceptibility values (SI). The sampling time was set to 10 s.

Subsequent processing of the physical property data included the conversion of gamma counts into density (using the equation type Ax2+Bx+C; whereas A, B and C were determined with calibration core measurements), the calculation of P-wave velocities (calibrated with water core of known temperature and theoretical sound velocity), sub-bottom depth corrections, as well as corrections of the magnetic susceptibility at the top and bottom of each core. Whenever necessary, the magnetic susceptibility was drift-corrected using measurements on the water-filled PVC liners, which were logged at the beginning and at the end of each core. Faulty P-wave and GRA-density values measured at section breaks were eliminated.

Interpretation
Of the physical property data, particularly magnetic susceptibility and GRA-density data were very useful to distinguish the major lithologies found in the sediment cores. GRA-density records have been partly helpful for core correlation (see figures in chapter 4.6.4) and will further be used for the determination of dry bulk density, which is needed for the calculation of accumulation rates.

Sediments recovered during SO-213 were primarily composed of calcareous microfossils and generally minor amounts of siliciclastic material, and are thus characterized by low magnetic susceptibilities and high densities. A few cores recovered from below the carbonate compensation depth in the deep SW Pacific basin contained a significant siliceous (low GRA-densities and magnetic susceptibilities) and siliciclastic component (high density, high magnetic susceptibility). Furthermore, sediments from the New Zealand margin contain higher amounts of terrigenous material. This terrigenous component is reflected in magnetic susceptibility of sediment records that is generally linked to Fe-bearing minerals. In the pelagic South Pacific, potential sources of such particles are either wind-delivered dust or local (sub)marine volcanism. These records are thus very useful to record changes in eolian dust supply. Furthermore, the short-term variations in magnetic susceptibility can be used to develop a preliminary stratigraphic framework. At the New Zealand margin, magnetic susceptibility is generally much higher and mainly reflects hemipelagic terrigenous sediment supply. Furthermore, the distal sediment cores from the Bounty Trough revealed numerous peaks of high magnetic susceptibility and GRA-density that are either linked to redeposition events (turbidites) or volcanic ash layers. Further details of the physical property data of the individual cores are discussed in the sediment facies chapter (4.6.4.). Magnetic susceptibility logs are displayed in the working area plots (Figs. 4.6.4-1, -2, -3, -4, -5) and in the core description sheets (Appendix D).

4.6.3.2. Color-scan

Methods
During the SO213 expedition, the hand-held Minolta spectrophotometer type CM-2002 was used to color scan sediment surfaces from open core segments by measuring the light reflectance. For the measurements, the device was directly placed on the sediment surface that was covered by clear clear plastic wrap. The spectrum of the reflected light was measured by a multi-segment light sensor, and the spectral reflection was measured at a 20nm pitch for wavelengths of 400 to 700 nm. The variation in the illumination from the CM-2002 pulsed xenon arc lamp was automatically compensated by a double-beam feedback system. Before the measurements of each core-segment were taken, the spectrophotometer was calibrated for white color reflections as well as for black colors using “zero-calibration”. The color calibration is essential to avoid any variation in color measurements due to the laboratory environment (temperature, humidity, background light) and instrument variations. Measurements were taken at intervals of 1 cm. The data were processed by the program Minolta SpectaMagic v.2.11 (release 1998), running on a Toshiba Satellite 2060 DS laptop computer.

Interpretation
The reflection data, and the standard color-values X, Y, Z are automatically calculated by SpectraMagic, and are displayed in the L*, a* and b* CIELAB color coordinates. Most useful for the interpretation of our sediments were the L*- and b*-values. The L*-value represents brightness and can be directly correlated to gray value measurements. The b*-value reflects green colors and, hence, is indicative of changes in biogenic silica production in our sediment records. The L* values of the individual cores are displayed in the core description sheets (Appendix D) and discussed in the sediment facies chapter (4.6.4).

4.6.4 Sediment facies and results

Preliminary interpretations of the sediment facies are based on sedimentological and physical properties, as well as color-scan data, and include shipboard biostratigraphic analyses. The graphical core descriptions (lithology) and photographs can be found in Appendix D and E.

4.6.4.1. Challenger Fracture Zone (CFZ)

Sediments from our cores at the approximately east-west oriented CFZ core transect are entirely calcareous. Most sediment cores are dominated by foraminiferal “sand” that only partly contains larger amounts of nannofossils (foraminifera-nannofossil ooze or nannofossil-foraminiferal ooze). Shipboard biostratigraphy based on foraminifera and nannofossils (chapter 4.7) suggests that the calcareous oozes are deposited with very low sedimentation rates (Chapter 4.7) of less than 0.5 cm/kyr.

The GRA-density of the CFZ sediment cores mostly varies between 1.5 and 1.9 g/cm2 and generally increases with progressing age and compaction (Fig. 4.6.4-1). The fine-scale down-core variability in GRA-density probably reflects changes in the sediment composition, particularly in the ratio between calcareous nannoplankton and foraminifera (higher GRA-density values seemingly correlate with higher amounts of calcareous nannoplankton). Although these findings need to be verified post-cruise by additional sedimentological and chemical analyses, they indicate that the GRA-density records can be of potential use for stratigraphic correlations. GRA-density records will further be used for the determination of dry bulk density, which is needed for the calculation of accumulation rates.

The siliciclastic content is generally very low and only reaches slightly higher levels in core SO213-26-2 (mud bearing to “muddy” foraminifera nannofossil ooze). In the pelagic Southeast Pacific, potential sources of siliciclastics are either wind-delivered dust or origin from local (sub)marine volcanism. Today, atmospheric dust transport to the Southeast Pacific is mainly linked to the westerlies, with distal source regions in Australia and New Zealand.

The westward transport of atmospheric dust from more proximal source regions in South America, however, is hindered due to the weak east-to-west component of the wind field in these latitudes. Enhanced transport of South American dust to the coring locations could only have occurred during times when the southeast trade wind system and the wind belt were located significantly further to the south. Therefore, magnetic susceptibility values in the sediment cores recovered in the CFZ working area are low ($<10^5$ SI units) compared to other oceanic regions with stronger input of terrigenous material. Nevertheless, the magnetic susceptibility records exhibit significant long- and short-term down-core variability. One striking feature is an increase in magnetic susceptibility in concordance with the intensification of Northern Hemisphere Glaciation (ca. 3–2.4 Ma). This long-term change is most prominent in the magnetic susceptibility records of cores SO213-01-2, SO213-04-2, and SO213-24-2 (Fig. 4.6.4-1).

4.6.4.2. Chile Rise including Valdivia Fracture Zone (ChiRi)

The sediment records recoverd from the ChiRi region are mainly composed of calcareous material. More specifically, the calcareous material is dominated by foraminiferal “sand” that partly contains larger amounts of nannofossils (foraminifera-nannofossil ooze or nannofossil-foraminiferal ooze). The siliciclastic content is very low as indicated by low magnetic susceptibility values (Fig. 4.6.4-2). Thus, the sediments from ChiRi and CFZ are very similar in composition and marked by low sedimentation rates. The sediment records from ChiRi span the time interval of the last ca. 15 Ma. This time interval seems to be most complete and best preserved at core SO213-17. The color L* record from core SO213-17 points to a

Middle to Late Miocene carbonate maximum (maximum in L* values), which is marked by very homogeneous nannofossil ooze as indicated by very low amplitudes in L*. The sediment records from cores SO213-15, -19 and -20 are marked by a large hiatus from 0 – ca. 11 Ma and provide a more detailed view into the time interval from 11 – 15 Ma, which comprises a large part of the carbonate maximum.

4.6.4.3. East Pacific Ridge (EPR)

The working area at EPR is marked by carbonate-rich sediment deposition. The sediment composition varies between foraminiferal and nannofossil oozes. The cores (SO213/59-2 to SO213/63-2) provide a depth transect at the western flank of the EPR from ca. 3160 m to 3963 m water depth. Especially magnetic suceptibillity and Color L* records from these cores can be correlated in detail (Fig. 4.6.4-3). Preliminary dates based on nannofossils suggest that the cores clearly resolve glacial-interglacial cycles and cover up to ca. 900 ka. The sedimentation rates are relatively low (0.5 – 2 cm/ka) but higher than in working area ChiRi.

4.6.4.4. Southwest Pacific Basin (SWB)

Cores were retrieved at the westernmost flank of the EPR from water depths of ca. 3400 m (SO213/49-4 and SO213/52-1). Sediments are primarily foraminifera or foraminifera-nannofossil oozes that are only partly slighty mud-bearing. The cores cover the past ca. 4-5 Ma and are thus very condensed records with low sedimentation-rates.

Core SO213/66-5 has been recovered from the deep SWB (5150 m water depth) and is dominated by diatom-rich sediments that generally contain clay (clay-bearing diatom ooze or diatom clay). The GRA density and and the magnetic susceptibility records display a distinct trend towards higher values from ca. 11 to 4.5 m core depth (Fig. 4.6.4-4). Cyclic variations on dm-scale occur throughout the core particularly in the GRA-density record. Unfortunately, there are no preliminary ages for this core yet. However, the location of the core below the carbonate compensation depth far away from any terrigenous sources suggests very low sedimentation-rates. This implies that the “short-term” GRA-density fluctuations could represent glacial-interglacial cycles and the “long-term” increasing trend possibly a strengthening of eolian sediment input over the Plio-Pleistocene.

Core SO213/68-2 has been retrieved from the Louisville Seamount chain from a water depth of ca. 2000 m. It has not been opened as the core recovered from a bent tube is strongly disturbed. Lithological information from core breaks reveals foraminifera “sand” with few nannofossils that suggest that sediments are relatively young and may resolve glacial-interglacial cycles (Fig. 4.6.4-4). Parasound surveys suggest that the seamount chain is partly sediment covered and may allow for relatively shallow water depth sediment records in the future. Due to bad weather and time constrains, we could unfortunately not spend more effort to recover cores from this region.

Core SO213/68-2 has been recovered from the deep basin (ca. 5050 m water depth), west of the Louisville Seamount chain. Sediments are again primarily diatom oozes that contain relatively high amounts of clay. There are short intervals that contain poorly preserved nannofossils suggesting a basal age of <0.44 ka (ca. 18 m core length). The core is thus characterized by moderately high sedimentation rates of up to 5 cm/ka. It is likely that the core location is reached by terrigenous sediment input from the NZM.

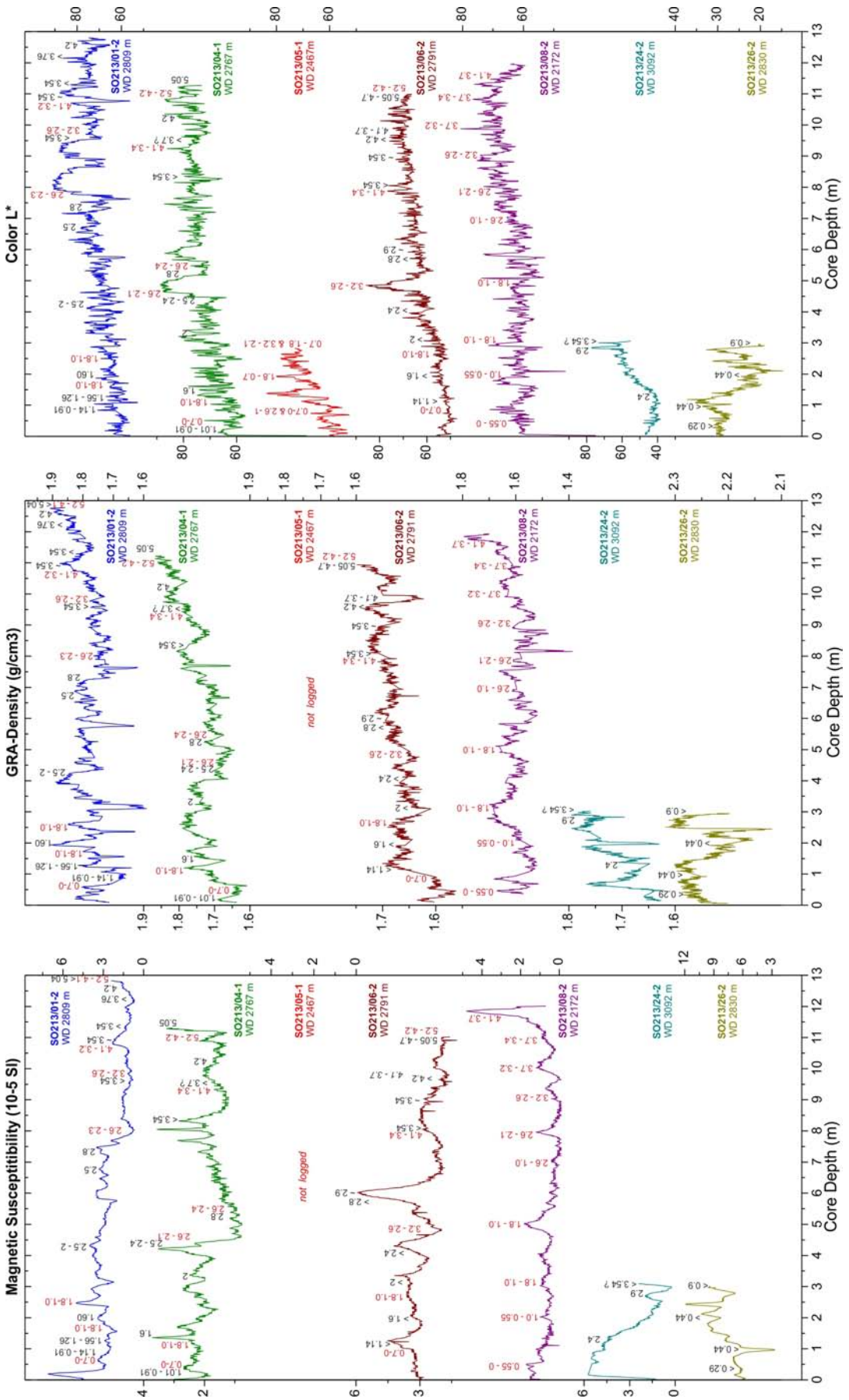

4.6.4-1. Magnetic susceptibility, GRA-density, and L records from the CFZ (working area 1) with biostratigraphic time markers (red: foraminifera; black: calcareous nannofossils; number are estimated ages in Ma).*

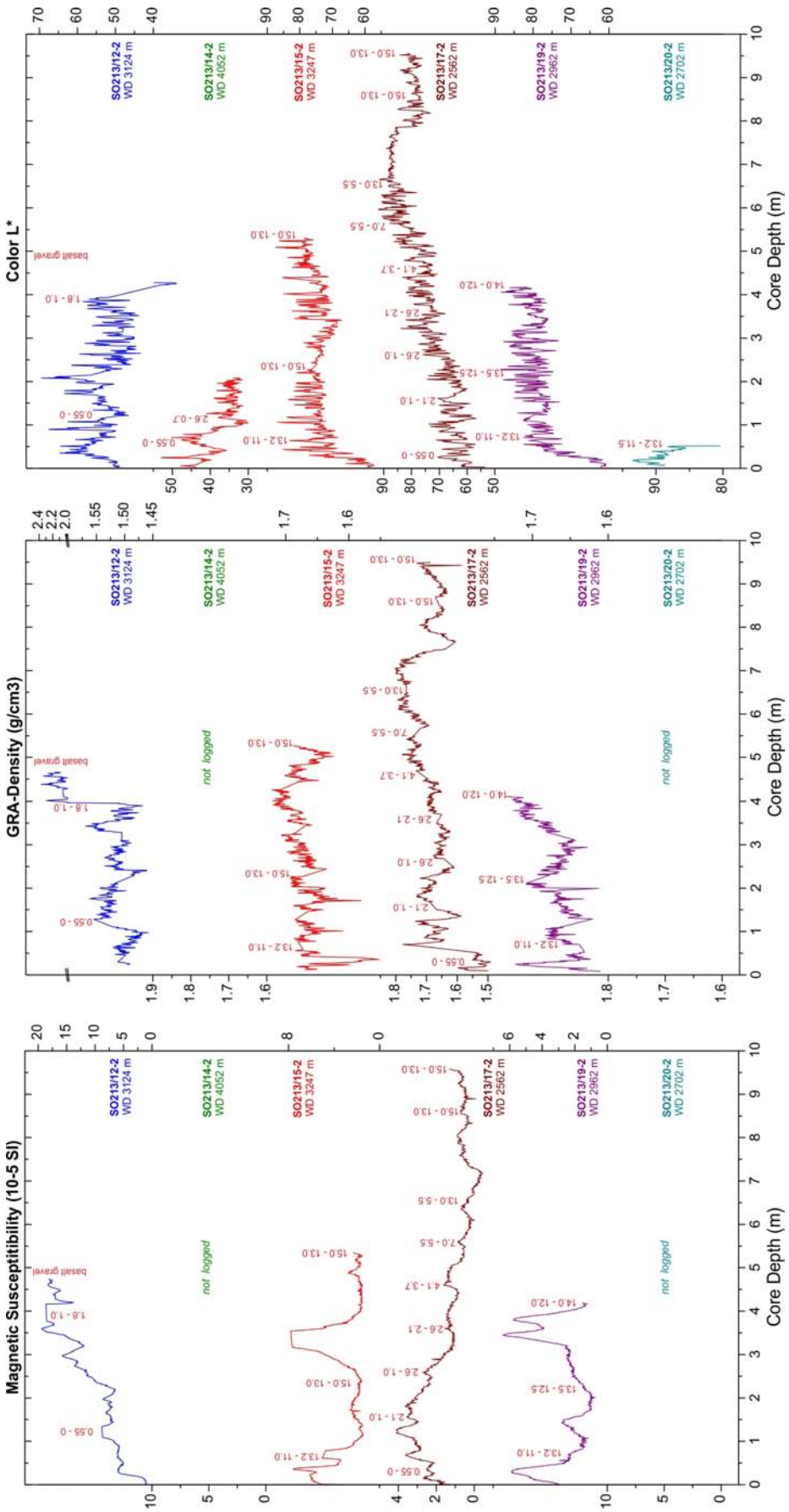

4.6.4-2. Magnetic susceptibility, GRA-density, and L records from the ChiRi (working area 2) with biostratigraphic time markers (red: foraminifera; black: calcareous nannofossils; number are estimated ages in Ma).*

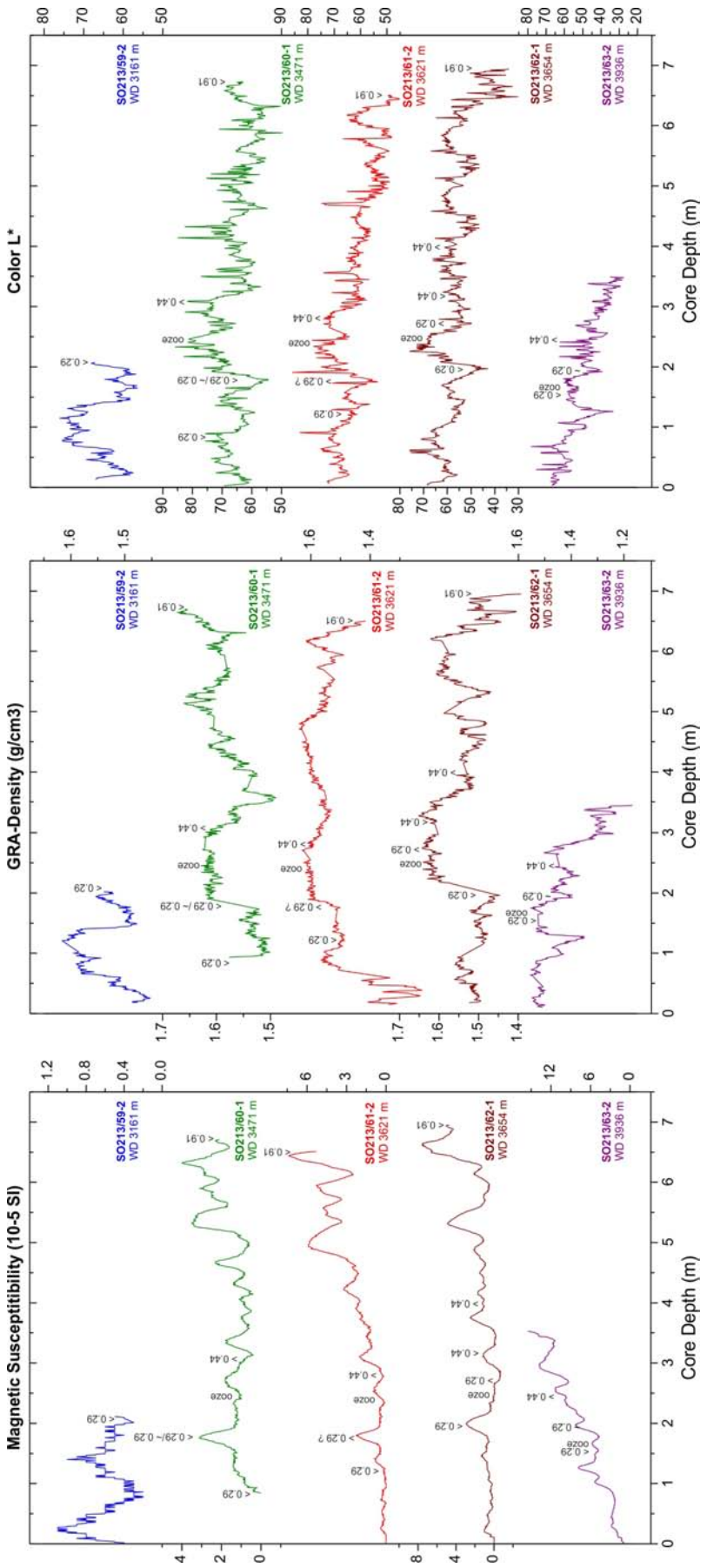

4.6.4-3. Magnetic susceptibility, GRA-density, and L records from the EPR (working area 3) with biostratigraphic time markers based on calcareous nannofossils (number are estimated ages in Ma).*

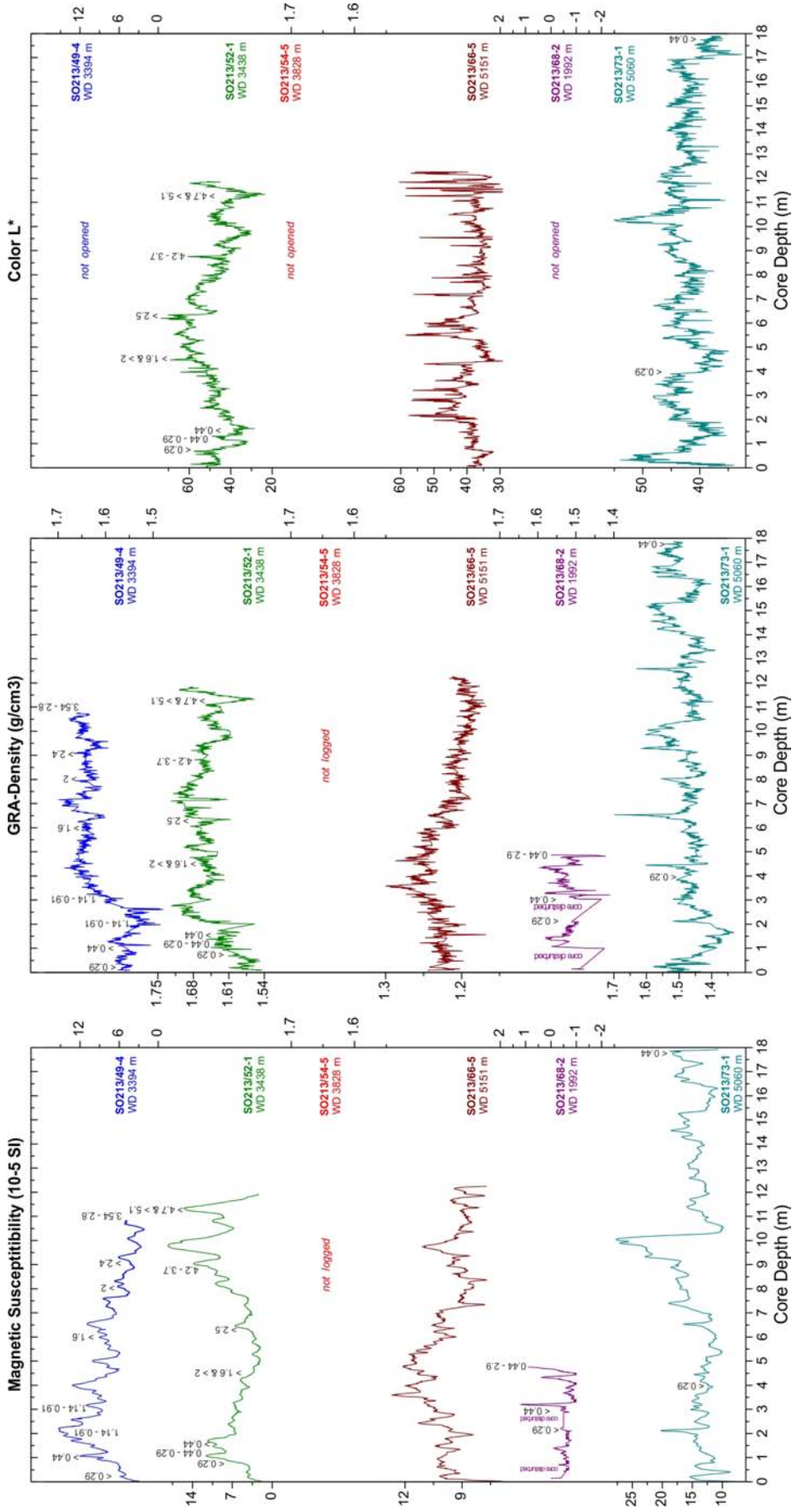

4.6.4-4. Magnetic susceptibility, GRA-density, and L records from the SWB (working area 4) with biostratigraphic time markers (red: foraminifera; black: calcareous nannofossils; number are estimated ages in Ma).*

4.6.4.5. New Zealand Margin (NZM)

Sediment cores at the NZM were retrieved along an east-west and further upslope southeast-northwest oriented depth transect starting in the outer Bounty Trough at ca. 4300 m water depth and ending at the upper continental slope south of the Champbell Plateau at ca. 500 m water depth (Fig. 4.6.4-5). Sediments along this transect are primarily mud-bearing to muddy nannofossil and muddy foraminifera-nannofossil oozes. Physical property records (e.g., magnetic susceptibility; Fig. 4.6.4-6) allow for detailed correlations of sediment cores along the transect. We tentatively assigned magnetic susceptibility maxima (i.e., more terrigenous sediments) to cold marine isotope stages as suggested by previous studies in the area (e.g., Carter et al., 2000; Pahnke et al., 2003). Conversely, low magnetic susceptibility intervals indicate more carbonate-rich sediments.

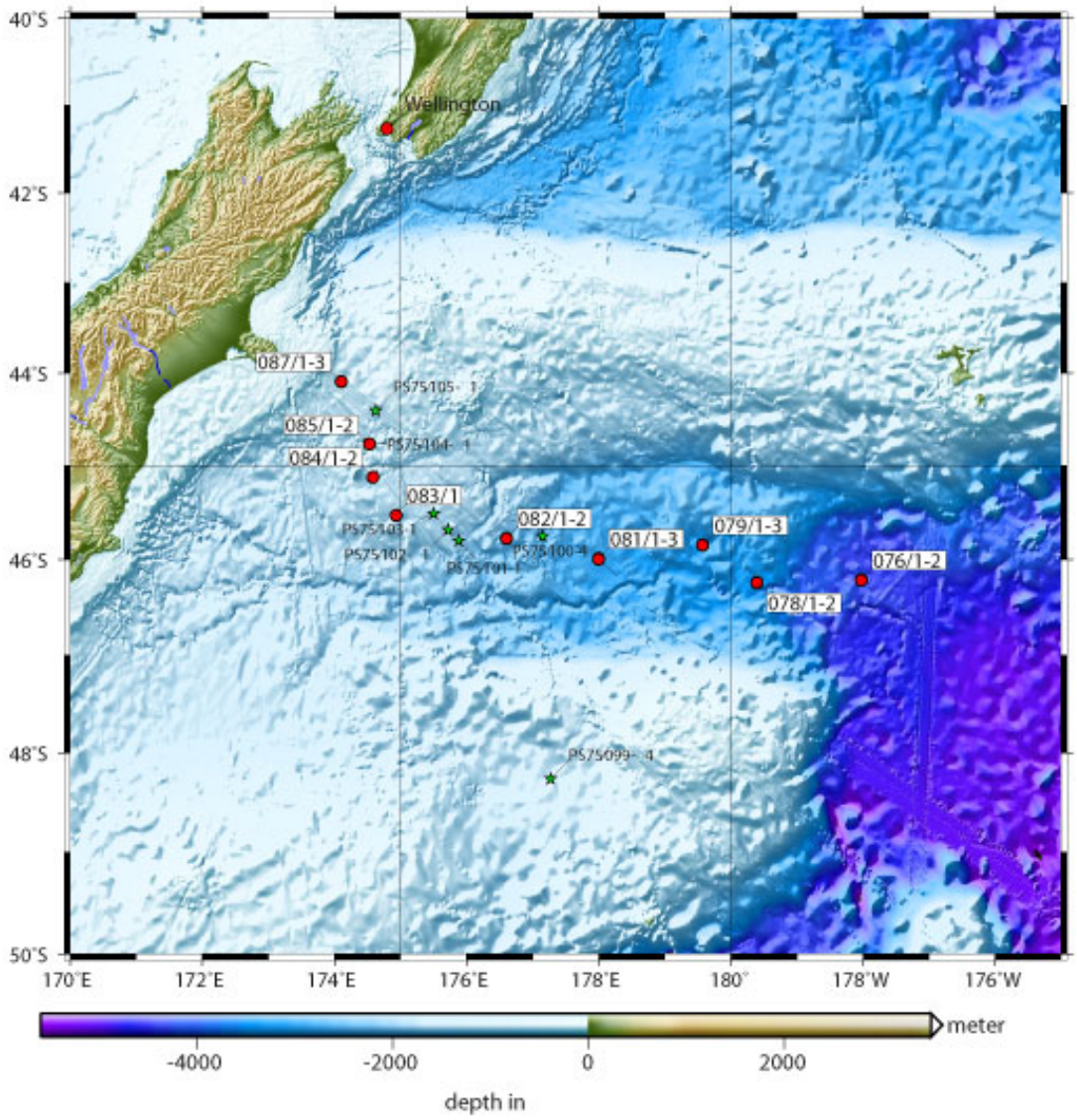

4.6.4-5. Bathymetric map of the NZM working area 4 with core locations along a depth transect. Green stars mark sediment cores recovered during RV Polarstern cruise Ant26-2.

The tentative correlation of the magnetic susceptibility records reveals remarkably similar pattern (Fig. 4.6.4-6). The deepest cores (SO213/76-2, SO213/78-2, and SO213/79-3) provide very high resolution records with decreasing sedimentation-rates from ca. 4300 m to 3150 m water depth. These distal sediment cores from the Bounty Trough reveal numerous

peaks of high magnetic susceptibility and GRA-density that are either linked to redeposition events (distal turbidites) or volcanic ash layers. Further upslope sedimentation-rates significantly decrease and sediments are characterised by mud-bearing foraminifera nannofossil oozes up to a water depth of ca. 1600 m. The more proximal sediment cores from the upper continental slope, are again characterised by more frequent terrigenous lithologies and consequently higher sedimentation-rates. The shallowest sediment core SO213/87-3 probably only covers parts of the Holocene.
Taken together, our coring transect from the NZM provides unique possibilities to reconstruct the water mass structure in exceptionally easy correlatable sediment cores. These records cover the complete depth range from Antarctic Bottom water across the Antarctic Intermediate to shallow Antarctic Mode Water.

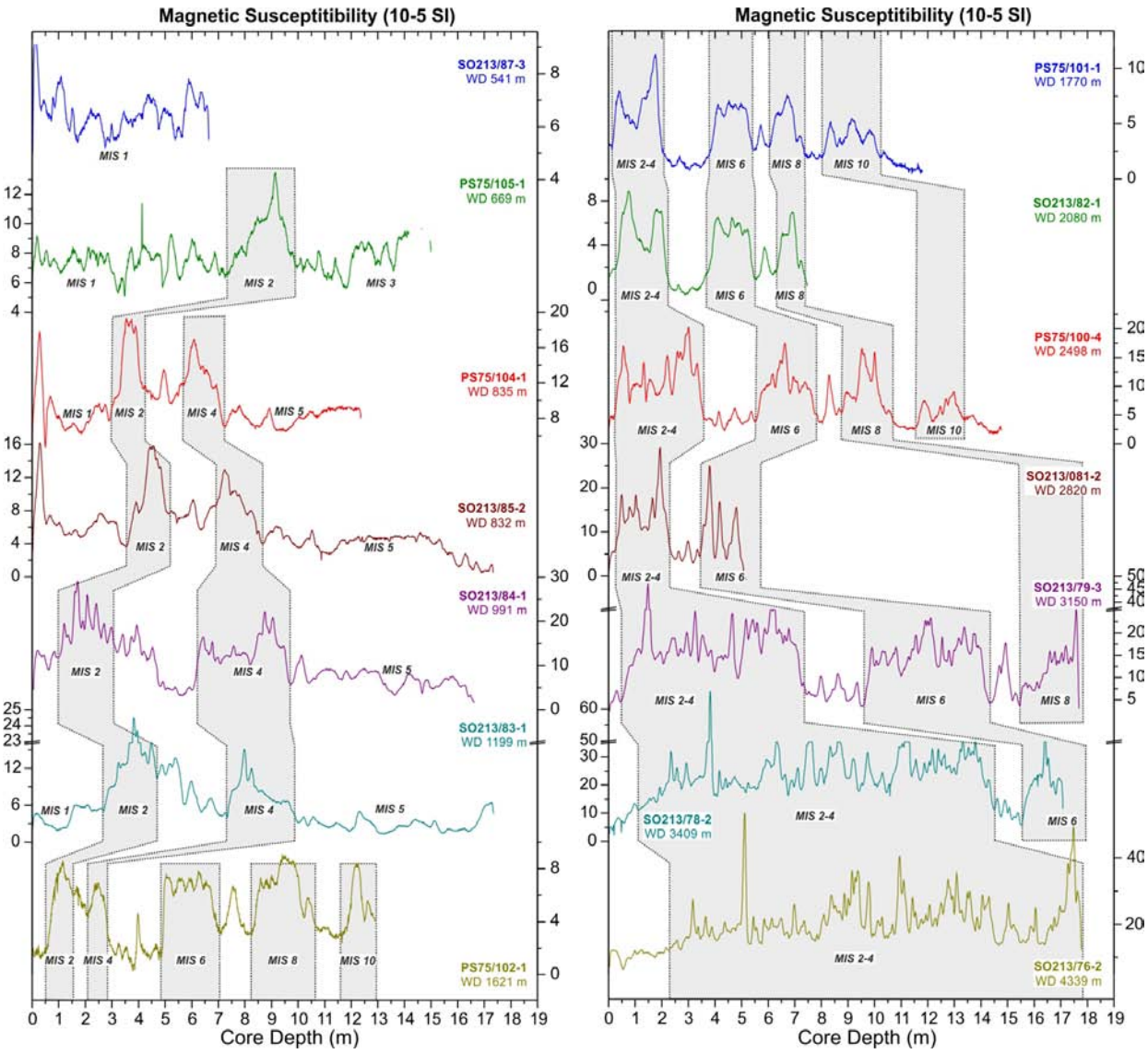

4.6.4-6. Magnetic susceptibility records from the NZM depth transects (working area 5) with tentative stratigraphic correlations. The figure includes data from RV Polarstern cruise Ant26-2 (Gersonde et al., 2012). MIS=marine isotope stage.

4.7. BIOSTRATIGRAPHY AND PRELIMINARY RESULTS

4.7.1. Planktic and benthic foraminifers – Samples and dating rationale

Introduction

Samples from SO213 Leg 1 (stations 1-22) were processed and dated onboard the Sonne, with some additional infill samples later dated onshore. Samples from Leg 2 (stations 24-85) were taken on the ship and provided to the author on its arrival in New Zealand. These samples were processed and examined onshore and the results presented here. If no ages are provided for a core then no samples were provided.

Species listed in this report are mostly those that are abundant or may be useful in constraining the age. All observations and cited numbers of specimens are based on scanning one tray of >150 um foraminifera on board RV Sonne or back onshore. Planktic % and planktic fragmentation Index (Frag Index) are calculated from a quick count of 100 foraminiferal specimens and fragments.

Dating rationale

The planktic foraminiferal age ranges and datums used are generally the known global ranges as cited by Kennett & Srinivasan (1983), but in some instances updated from detailed work on and offshore (e.g. DSDP 284, 593, ODP 1123) in the Southwest Pacific around New Zealand (e.g. Hornibrook, 1982; Hoskins, 1990; Scott et al., 1990; Crundwell, 2004). In some species there is some uncertainty about the actual timing of a datum, particularly in warm subtropical-temperate waters of the Southern Hemisphere (e.g. LO *Gr. crassaformis*, LO *Gr. puncticulata*, FO *Gr. crassacarina*, timing and extent of zones of dextral coiling of *Gr. crassaformis*). The age range used here for the common Pliocene keeled globorotaliid *Gr. pliozea*, is that established around New Zealand, as it seems to be a southern hemisphere (even South Pacific) species.

Benthic foraminifera are not considered to be good for international biostratigraphy, with the obvious exception of those deep-water cosmopolitan species that became extinct during the PETM event. There is another, only recently well-documented, interval of enhanced extinctions that is a useful indicator of age through the Late Pliocene-Middle Pleistocene. This is the Last Global Extinction, in which several families, 20 genera and ~100 distinctive, deep-water, largely cosmopolitan benthic species became extinct, starting in the Late Pliocene, but mostly during the MPT (1.2-0.6 Ma, Hayward et al., 2007). These species withdrew from deep waters (>3000 m) earlier than in intermediate water depths, although the highest occurrence (often rare) of the families Stilostomellidae, Glandulonodosariidae and Chrysalogoniidae was 0.8-0.57 Ma at every site. Some species disappeared earlier (e.g. *Siphonodosaria subspinosa, Vulvulina pennatula, Amplectoductina multicostata*) than others and several are everywhere the last survivor species (e.g. *Siphonodosaria lepidula, Strictocostella scharbergana, Pleurostomella acuminata*).

Samples

Samples were from three sources: Multicore samples (MUC) were from spare sediment from tubes with little sediment recovery or spare intervals in cores used for staining benthics. Core-catcher samples where the sediment was scraped or washed from inside the core-catcher – usually dated deepest sediment penetrated by core, but sometimes had contamination probably from the sediment surface. Other samples were from 1 cm intervals from inside the open core and sampled with a syringe.

On board the Sonne or back in the laboratory, samples were washed over a >63 um sieve and dried in an oven, then some of the >150 um fraction was examined in a picking tray.

Planktic Foraminiferal datums used in dating Sonne 213 samples

Abbreviations
FO = first occurrence datum
LO = last occurrence datum
FCO, LCO = first or last common occurrence datum
FGO, LGO = first or last global datum (for benthics)
FO NZ, LO NZ = first or last occurrence datum in New Zealand

Ma	Zone	NZ Stage	Foraminiferal event	References
0.45		Wc	LO *Globorotalia crassaformis* in STW (NZ region)	Crundwell et al., 2008
0.55		Wc	*Globorotalia truncatulinoides* dextral to sinistral coiling switch	Scott unpubl.
0.55		Wc	LO *Pleurostomella acuminata* in SW Pacific	Hayward et al., 2007
0.57		Wc	LO Extinction Group benthics in ODP 1125, ODP 1123	Hayward et al., 2007
0.65		Wc	LGO *Strictocostella scharbergana* >2000 m	Hayward et al., 2007
0.7		Wc	FCO *Globorotalia truncatulinoides* (in SW Pacific)	Hornibrook & Jenkins, 1994
~0.7		Wc	LCO *Globorotalia puncticuloides/puncticulata*	Scott et al., 2007
0.75		Wc	LGO *Orthomorphina perversa* >2300 m	Hayward et al., 2007
0.87		Wc	LGO *Chrysalogonium stimuleum* >2300 m	Hayward et al., 2007
1		Wc	LO *Siphonodosaria lepidula* >2000 m (Pacific)	Hayward et al., 2007
~1		Wc	LO *Globorotalia tosaensis* ss morphotypes	Scott et al., 1990
~1		Wc	LCO Extinction Gp >3000 m SW Pacific	Hayward et al., 2007
~1		Wc	LO *S. lepidula* >3000 m SW Pacific	Hayward et al., 2007
1.2		Wc	LO Siph*onodosaria pomuligera* >2300 m	Hayward et al., 2007
~1.8		Wn	FGO *Globorotalia truncatulinoides*	Kennett & Srinivasan, 1983
1.8			**Pliocene/Pleistocene boundary for this report**	
~2		Wn	LO *Zeaglobigerina woodi*	Hornibrook et al, 1989
2.2		Wn	LO *Vulvulina pennatula* (outside Nth Atlantic)	Hayward et al., 2007
2.3		Wn	LGO *Chrysalogonium equisetiformis* >2500m	Hayward et al., 2007
2.4		Wn	FO *Globorotalia crassacarina*	Cooper et al., 2004
2.4		Wn	LGO *Amplectoductina multicostata* >2300 m	Hayward et al., 2007
2.4		Wn	LGO *Siphonodosaria subspinosa* >2500 m	Hayward et al., 2007
2.4		Wm/Wn	FO *Globorotalia crassula*	Cooper et al., 2004
2.45		Wn	LO *Globorotalia crassaformis* (dextral)	Cooper et al., 2004
~3		Wm	LO *Siphonodosaria paucistriata* >2300 m	Hayward et al., 2007
3.1		Wp/Wm	FO *Globorotalia crassaformis* (dextral)	Cooper et al., 2004
3.1		Wp/Wm	LO *Globorotalia crassaconica*	Cooper et al., 2004
3.2		Wp/Wm	FO *Globorotalia tosaensis*	Scott et al., 1990
3.3		Wp	LO *Globorotalia subconomiozea*	Cooper et al., 2004
~3.4		Wp	FO *Globigerina rubescens*	Kennett & Srinivasan, 1983
3.4		Wp	LO *Globorotalia pliozea*	Hornibrook, 1982
3.4	N20	Wp	LO *Sphaeroidinellopsis seminulum*	Kennett & Srinivasan, 1983
3.4	N20	Wp	LO *Sphaeroidinellopsis paenedehiscens*	Kennett & Srinivasan, 1983
3.6		Wo/Wp	LO NZ *Hopkinsina mioindex*	Hornibrook et al., 1989; Boersma, 1986
3.6		Wo/Wp	FO *Globorotalia praehirsuta*	Scott et al., 1990
3.6		Wo/Wp	FO *Globorotalia inflata triangula*	Scott et al., 1990
3.7		u Wp	FO *Globorotalia puncticuloides*	Scott et al., 1990
3.7		u Wp	LCO *Globorotalia pliozea*	Scott et al., 1990
~4		Wo	LO *Stilostomella rugosa*	Hayward et al., 2007
4.1		Wo	FO *Globorotalia inflata*	Scott et al., 2007
4.1		Wo	FO *Globorotalia subconomiozea*	Cooper et al., 2004
4.2		Wo	LO *Zeaglobigerina nepenthes*	Berggren et al., 1996
4.2		Wo	LO *Globorotalia margaritae*	Ogg et al., 1988
4.6		Wo	LO *Globorotalia mons*	Scott et al., 1990
5.2	N18	Tk/Wo	LO *Globorotalia juanai*	Scott et al., 1990
5.3		Tk/Wo	FO *Spheroidinella dehiscens*	Kennett & Srinivasan, 1983
5.3		Tk/Wo	FO *Globorotalia puncticulata* ss	Cooke et al., 2008
5.3			**Miocene/Pliocene boundary**	
5.3		Tk/Wo	LO *Globorotalia sphericomiozea*	Cooper et al., 2004
5.4		Tk	FO *Globorotalia crassaformis*	Cooper et al., 2004

5.4		Tk	FO *Globorotalia margaritae*	Scott et al., 1990
5.4		Tk	FO *Globorotalia pliozea*	Scott et al., 1990
5.5		Tk	FO *Globorotalia sphericomiozea*	Cooke et al., 2008
~5.5	N18	Tk	LO *Globorotalia miotumida* s.l.	Morgans et al., 1996
5.6		Tk	FO *Globorotalia crassaconica*	Scott et al., 1990
5.8		Tk	LO *Globorotalia mons*	Cooper et al., 2004
6.6	N18	Tt/Tk	FO *Globorotalia conomiozea*	Kennett & Srinivasan, 1983
~8		Tt	LO NZ *Rectuvigerina ongleyi*	Boersma, 1986; Hornibrook et al., 1989
8.9	N16	Tt	LO NZ *Globoquadrina dehiscens*	Cooke et al., 2008
10.5	N16	Tt	LO *Globorotalia panda*	Scott et al., 1990; Scott, 1995
10.5		Tt	LO *Globorotalia mayeri*	Cooper et al., 2004
10.5		Tt	LO *Orbulina suturalis*	Cooper et al., 2004
~11		Sw	FO NZ *Globorotalia juanai*	Cooper et al., 2004
~11	N15	Sw	LGO *Globorotalia challengeri*	Kennett and Srinivasan, 1983
~11.5	N15	Sw	LO *Catapsydrax* spp.	Kennett & Srinivasan, 1983
12.7		Sl/Sw	LO *Globorotalia conica*	Morgans et al., 1996; Scott, 1991
12.7	N13	Sl/Sw	FO NZ *Globorotalia miotumida*	Cooper et al., 2004
12.7	N13	Sl?sw	LO NZ Globorotalia *praemenardii*	Cooper et al., 2004
12.7		Sl/Sw	LO *Globorotalia partimlabiata*	Scott unpubl.
13.2		Sl	FO *Paragloborotalia mayeri* ss	Scott, 1991
15	N9	Sl	FO *Globorotalia panda*	Scott et al., 1990
~15	N9	Sl	FGO *Globorotalia challengeri*	Kennett and Srinivasan, 1983
15.1	N9	Sc/Sl	FO *Orbulina suturalis*	Berggren et al., 1995; Morgans et al., 1996
16	N8	Sc	FO *Globorotalia praemenardii*	Cooper et al., 2004

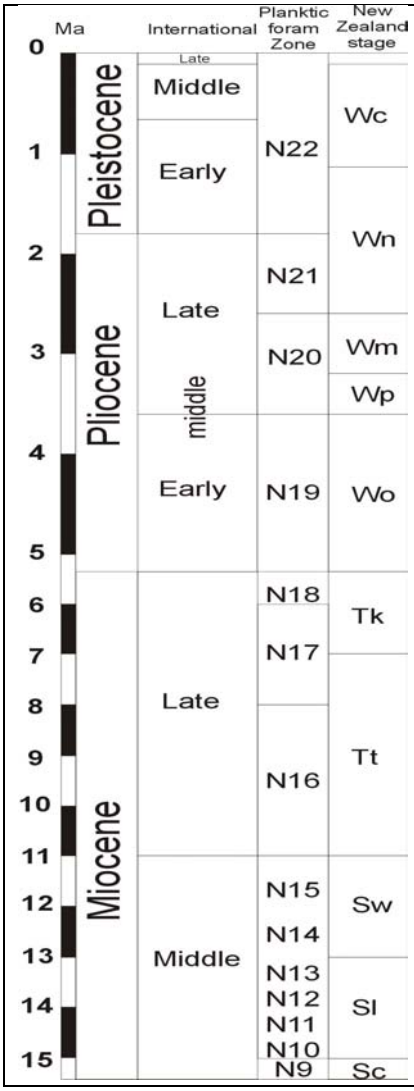

Neogene subdivisions used in this report.
[Note the recommendation that the Pliocene-Pleistocene boundary be shifted from 1.8 to 2.4 Ma is not followed as all literature gives time ranges of foraminiferal taxa according to the old scale].

4.7.2. Results summary of foraminiferal biostratigraphy **(details in Appendix I)**

Challenger Fracture Zone

01-2 Kol (piston core), 2816 m
77-78 cm: Middle Pleist (~0.8-0.6 Ma)
176-177 cm: Early Pleist (12.4-1 Ma)
276-277 cm: Early Pleist (2.4-1 Ma), with reworked Early Plio (5.2-3.4 Ma)
310-311 cm (turbiditic sand): Mixed E Plio (5.2-4.2 Ma) and Late Plio (3.2-2.1 Ma)
480-481 cm: Late Plio (2.4-1 Ma)
799-781 cm (white ooze): Late Plio (~2.4 Ma)
982-983 cm: early Late Plio (~3.4-3.1 Ma)
1081-1083 cm: mid Plio (4.1-3.4 Ma)
Core-catcher >1283 cm: Early Plio (5.3-4.1 Ma)

04-1 Kol (piston core), 2767 m
0-5 cm: Middle Pleist-Rec, probably Holocene. Mean annual SST (MAT) 16.5-17ºC
25-26 cm: Middle-Late Pleist (0.7-0 Ma), with some Late Plio-Early Pleist (2.4-1 Ma)
134-135 cm: Early Pleist (1.8-1 Ma)
237-238 cm: Late Plio-Early Pleist (2.4-1 Ma)
337-378 cm: Late Plio (2.4-1.8 Ma)
437-438 cm (just above white ooze): Late Plio (3.1-2.45 Ma)
537-538 cm: (just below white ooze): Mid Plio (~3.2-3.1 Ma)
637-638 cm: mid Plio (3.7-3.3 Ma)
730-731 cm: Middle-Late Plio (3.7-3.1 Ma)
930-931 cm: mid Plio (4.1-3.4 Ma)
Core-catcher >1131 cm: Early Plio (5.2-4.2 Ma)

05-1 SL (gravity core), 2495 m
86 cm: Middle Pleist-Rec (0.7-0 Ma), mixed with Latest Plio-Early Pleist (2.1-1 Ma)
186 cm: Early Pleist (1.8-0.7 Ma)
Core-catcher >287 cm: Early Pleist (1.8-0.7 Ma) mixed with Late Plio (3.2-2.1 Ma)

06-2 Kol (piston core), 2798 m
99-100 cm: Middle Pleist (0.55-0.4 Ma), with mixed in Late Plio-Early Pleist (2.4-1 Ma)
300-301 cm: ?Early Pleist (?1.8-1 Ma)
400-401 cm: Late Plio-Early Pleist (2.4-1.0 Ma)
500-501 cm (just below white ooze): Late Plio (3.1-2.45 Ma)
599-600 cm: Late Plio (3.1-2.45 Ma)
700-701 cm: mid Plio (4.1-3.4 Ma)
800-801 cm: mid Plio (4.1-3.4 Ma)
1001-1002 cm: mid Plio (4.1-3.7 Ma)
Core-catcher >1102 cm (incl. volc frags): Early Plio (5.3-4.2 Ma)

08-2 Kol (piston core), 2181 m
99-100 cm: Middle-Late Pleist (0.7-0 Ma)
199-200 cm: Middle Pleist (1-0.55 Ma, probably 0.8-0.6 Ma)
300-301 cm: Early Pleist (1.8-0.7 Ma)
500-501 cm: Early Pleist (1.8-1.0 Ma)
700-701 cm: Late Plio-Early Pleist (2.4-1.0 Ma)
798-799 cm: Late Plio (~2.5-2.3 Ma)
899-900 cm: Late Plio (3.1-2.45 Ma)
1000-1001 cm: mid Plio (3.4-3.1 Ma)
1100-1101 cm: mid Plio (4.1-3.4 Ma, possibly 3.7-3.4 Ma)
1200-1201 cm (incl. volc frags): mid Plio (4.1-3.4 Ma)
Core-catcher >1201 cm (incl. volc frags): Early Plio (4.1-3.7 Ma)

Chile Rise, including Valdivia Fracture Zone

11-1 MUC, 11-2 Kol (piston core), 1845 m
Surface sediment: Middle Pleist-Rec (0.55-0 Ma); mean annual SST (MAT) 13.5ºC.
Core-catcher >100 cm (contains fragments of semi-lithified ooze): sediment and lithified ooze.
Planktics: Common sinistral *Gr. truncatulinoides* (<0.55 Ma) and *Gr. inflata.*
Age: Middle Pleist-Rec (0.7-0 Ma, probably 0.55-0 Ma)

12-2 TC, Kol (trigger core & piston core), 3151 m
SST at this site today measured at 13ºC
TC 83-84 cm: Middle Pleist-Rec (0.55-0 Ma)
Kol 140 cm: Middle Pleist-Rec (0.55-0 Ma)
Kol 218-219 cm: Late Plio (~2.4 Ma) ?mixed
Kol 318-319 cm: Late Plio-Early Pleist (2.4-1 Ma)
Kol 393-394 cm (bottom of fine sediment, some basalt): Mixed Middle, Late Plio & Early Pleist (>3.1 Ma, 3.1-2.45 Ma, 1.8-1.0 Ma)
Core-catcher >474 cm (contains basalt gravel in minor matrix): Middle Pleist-Rec (0.55-0 Ma), mixed with Late Plio-Pleist (2.4-0.4 Ma). Probably contamination from surface sediment.

14-1 MUC, 4069 m
SST at this site today measured at 15.5ºC
Surface sediment brown mud with scattered foraminifera: Middle Pleist-Rec (0.55-0 Ma)

14-2 SL (gravity core), 4069 m
65-66 cm: Middle Pleist-Rec (0.55-0 Ma)
113-114 cm (dark clay, very little sand or forams): Late Plio-Early Pleist (2.4-0.7 Ma), possibly ~1 Ma
Core-catcher >214 cm (red-brown clay): NF. No sand sized foraminifera nor biogenics.

15-2 Kol (piston core), 3260 m
59-60 cm: Middle Mio (13-12 Ma)
229-230 cm: Middle Mio (14-12.7 Ma)
Core-catcher >534 cm (white nanno ooze): Middle Mio (14-12.7 Ma)

17-2 SL (gravity core), 2581 m
SST at this site today measured at 15.5ºC
57-58 cm: Middle Pleist-Rec (0.55-0 Ma)
157-158 cm: Latest Plio-Early Pleist (2.4-1.0 Ma)
258-259 cm: Late Plio-Early Pleist (2.4-1.0 Ma)
358-359 cm: Late Plio (3.1-2.45 Ma)
458-459 cm: Latest Mio (5.5-5.3 Ma)
557-558 cm: Latest Mio (6-5.5 Ma)
657-658 cm: Late Mio (9-7 Ma)
757-758 cm: Middle Mio (12.7-~11 Ma)
857-858 cm: Middle Mio (12.7-11 Ma)
Core-catcher >958 cm (white nanno ooze): Middle Mio (13-11.5 Ma), minor Plio-Pleist (? contamination in core catcher).

19-2 SL (gravity core), 2955 m
59-60 cm: Middle Mio (12.7-10.5 Ma)
218-219 cm: Middle Mio (12.7-10.5 Ma)
Core-catcher >420 cm (white nanno ooze): Middle Mio (13.5-12.5 Ma).

20-2 SL (gravity core), 2715 m
~12 cm of brown foram sand with sharp burrowewd contact on white nanno ooze.

Core-catcher >55 cm (white nanno ooze): Middle Mio (13.5-12.7 Ma) and minor Late Pleist-Rec.

22-4 MUC (multicore), 4128 m
Red-brown mud with strong dissolution of forams
31-36 cm: Middle Pleist-Rec (0.55-0 Ma)

Volcano dredges, East Pacific Rise

33-1 (dredge)
Orange brown gritty mud with abundant foraminifera.
Late Plio-Early Pleist (2.4-0.7 Ma)

36 (dredge)
Orange brown gritty matrix in basalt. Common stained and unstained foraminifera.
Mixed Mid Plio (rare ?4-3.4 Ma), Early Pleist (1.8-0.7 Ma) and Middle Pleist-Recent (0.5-0 Ma) ages.

38-1 (dredge)
Thin white marl on two basalt cobbles.
Cobble 1: Mid Plio-Early Pleist (?4-0.7 Ma)
Cobble 2: Late Plio (3.1-2.4 Ma)

East Pacific Rise

49-2SL (gravity core) 3392 m
Core-catcher, ~700 cm: Late Plio (3.1-2.45 Ma).

49-4Kol (piston core) 3394 m
Core-catcher,1105 cm: Late Plio (3.1-2.45 Ma)

52-1Kol (piston core) 3438 m
182-183 cm: Pleist (<1.8 Ma), probably Middle Pleist (<0.55 Ma), with Plio reworking.
392-393 cm: Middle Pleist, probably early Middle Pleist (~0.7 ma), no reworking.
492-493 cm: Late Plio (3.1-2.45 Ma)
592-593 cm: Late Plio (3.1-2.45 Ma)
692-693 cm: Late Plio (3.1-2.45 Ma)
890-891 cm: Mid Plio (4.1-3.4 Ma)
991-992 cm: Early Plio (4.1-3.6 Ma, probably ~ 4.1 Ma)
1030 cm: Early Plio (5.3-4.1 Ma)
1091-1092 cm: Miocene-Plio boundary (5.4-5.2 Ma)
Core-catcher, 1195 cm: Latest Miocene (5.6-5.3 Ma)

54-5Kol (piston-core) 3828 m
Core-catcher, 890 cm: Mixed Miocene, Plio and Pleist.

60-1SL (gravity core) 3471 m
281 cm: Middle-Late Pleist (<0.55 Ma), probably Middle Pleist (0.55-0.45 Ma)
481 cm: Early Pleist (1.0-0.7 Ma)
581 cm: Late Plio-Early Pleist (2.4-0.87 Ma)
Core-catcher, 673 cm: Late Plio-Early Pleist (2.4-~1.2 Ma)

61-2SL (gravity core) 3621 m
160 cm: Middle-Late Pleist (<0.55 Ma)
360 cm: Early-Middle Pleist (~1-0.7 Ma)
459 cm: Late Plio-Early Pleist (2.4-1.0 Ma)
560 cm: Late Plio-Early Pleist (2.4-1.0 Ma)
Core-catcher, 652 cm: Middle-Late Pleist (<0.55 Ma), probably contamination.

62-1SL (gravity core) 3654 m
302 cm: Middle-Late Pleist (<0.55 Ma)
402, 404 cm: Early-Middle Pleist (~1.0-0.7 Ma)
502 cm: Early-Middle Pleist (~1.0-0.7 Ma)
604 cm: Early-Middle Pleist (~1.0-0.7 Ma)
Core-catcher, 705 cm: Early Pleist (~1.0 Ma)

63-2SL (gravity core) 3936 m
150 cm: Middle-Late Pleist (<0.55 Ma)
252 cm: Early Pleisto (1.0-0.7 Ma)
350 cm: Late Plio-Early Pleist (2.4-1.2 Ma), probably Late Plio (~2.4-2.3 Ma)
Core-catcher, 355 cm: Late Plio-Early Pleist (2.4-1.0 Ma)

64-1SL (gravity core) 3925 m
106 cm: Mixed Early-Middle Pleist (1-0.7 Ma) and Mid-Late Pleist (<0.55 Ma)
Core-catcher, 275 cm: Strongly dissolved; Mixed late Miocene (12.7-6.5 Ma) and Pleist (<1.8 Ma)

Louisville Ridge

70-1 (dredge)
Thin white marl on basalt cobble. Very sparse fauna.
Mixed ages: Plio-Middle Pleist (4.1-0.7 Ma) and Middle Pleist-Recent (<0.55 Ma).

Bounty Trough

76-2Kol (piston core) 4339 m
Core-catcher, 1778 cm: Middle-Late Pleist (<0.55 Ma)

78-2Kol (piston core) 3409 m
1698 cm: Middle-Late Pleist (<0.55 Ma)
Core-catcher, 1710 cm: Middle-Late Pleist (<0.55 Ma)

79-2Kol (piston core) 3142 m
930 cm: Middle-Late Pleist (<0.55 Ma)
Core-catcher: Middle-Late Pleist (<0.7 Ma, probably <0.55 Ma)

82-1SL (gravity core) 2066 m
555 cm: Middle Pleist (<0.55 Ma)
Core-catcher, 772 cm: Middle-Late Pleist (<0.8 Ma, possibly 0.8-0.55 Ma)

84-1Kol (piston core) 991 m
Core-catcher, 1665 cm: Middle Pleist (~0.8-0.55 Ma)

85-2Kol (piston core) 832 m
Core-catcher, 1745 cm: Middle-Late Pleist (<0.55 Ma)

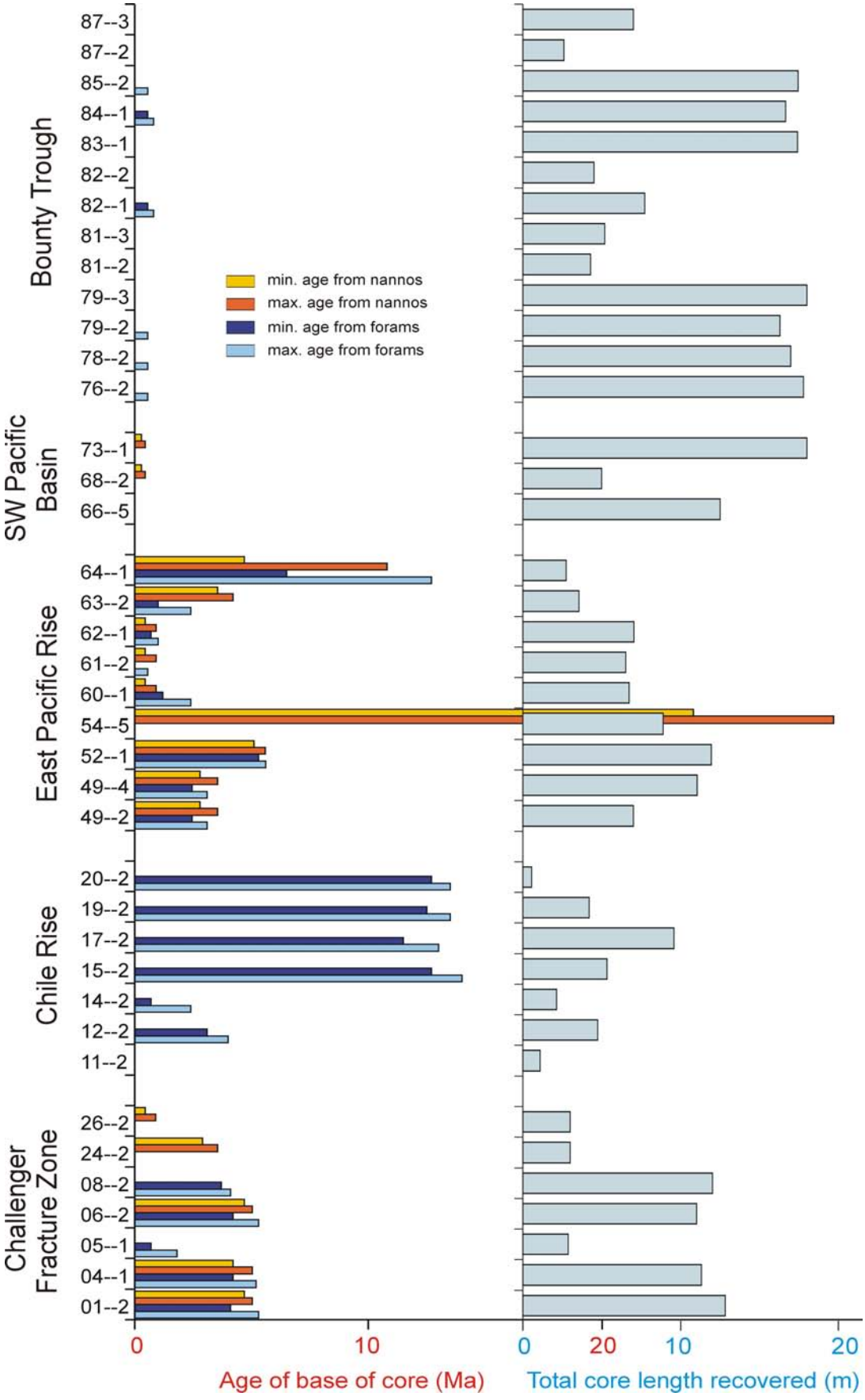

Fig. 4.7.2-1: Summary of sediment recovery and biostratigraphic age of bottom of each core, SO213

Benthic Foraminiferal datums used in dating Sonne 213 samples

The stratigraphic ranges and distributional record of the group of elongate cylindrical benthic foraminifera is poorly known in the South-east Pacific, thus the preliminary record from the Sonne 213 cores adds new useful information.

A total of 48 extinct benthic species have been recorded from the single trays scanned from each sample – further species can be expected with more targeted searching. All species were cosmopolitan in their distribution. The faunal assemblage becomes less diverse through time from mid Pliocene, Early Pliocene and Middle Miocene (23-28 spp.), Late Pliocene (19 spp.), to Early Pleistocene (19 spp.). The Early Pleistocene extinct benthics in this region were dominated by *Siphonodosaria lepidula* and *Strictocostella scharbergana* – a combination that continued in lower numbers back till at least the Middle Miocene. Additional species whose presence characterises older faunas include *Amplectoductina multicostata* (Late Pliocene and earlier); large *Vulvulina pennatula, Siphonodosaria subspinosa,* and *Nodosarella rotundata* (mid Pliocene and earlier); *Siphonodosaria paucistriata, S. pilulata, Stilostomella rugosa,* and *Strictocostella hyugaensis* (Middle Miocene).

Large elongate uniserial specimens visible to the naked eye (>0.5 mm long) are usually *Chrysalogonium equistiformis*, which was present from mid Miocene-Late Pliocene. Fourteen species were relatively abundant and widespread, whereas the record of the other 34 was more sporadic and less reliable. These widespread species were: *Chrysalogonium deceptoria, C. equisetiformis, C. stimuleum, Glandulonodosaria glandigena, Orthomorphina jedlitschkai, O. perversa, Amplectoductina multicostata, Pleurostomella acuminata, P. bolivinoides, P. subnodosa, P. tenuis, Siphonodosaria lepidula, S. subspinosa,* and *Strictocostella scharbergana.*

Extinction Group benthic record (specimens) summarised in time intervals								
	E Pleist	**L Plio**	**M Plio**	**E Plio**	**L Mio**	**M Mio**		**Total**
Ma	**1.8-0.8**	**2.4-1.8**	**3.7-2.4**	**5.3-3.7**	**11-5.3**	**15--11**		
No of samples	24	6	17	15	4	10		76
Chrysalogoniidae								
Chrysalogonium ciperense	.	.	1	.	.	1		2
Chrysalogonium deceptoria	7	3	3	4	.	.		17
Chrysalogonium equisetiformis	.	2	12	7	.	4		25
Chrysalogonium stimuleum	9	3	14	3	.	.		29
Lotostomoides calomorphum	1	.	.	.	.	.		1
Scallopostoma ovicula	.	.	.	1	.	.		1
Glandulonodosariidae								
Glandulonodosaria ambigua	2	.	2	.	.	.		4
Glandulonodosaria glandigena	1	3	9	4	.	4		21
Glandulonodosaria lutzei	.	.	.	.	.	1		1
Orthomorphina jedlitschkai	6	2	3	4	.	1		16
Orthomorphina multicosta	.	.	2	.	.	.		2
Orthomorphina perversa	6	3	5	2	1	3		20
Pleurostomellidae								
Amplectoductina multicostata	.	.	5	2	1	3		11
Ellipsoglandulina labiata	1	2	3	1	.	.		7
Ellipsoidella heronallenia	.	.	1	.	.	.		1
Ellipsoidella pleurostomelloides	.	.	1	1	.	.		2
Ellipsoidina ellipsoides	.	1	.	.	.	.		1
Nodosarella inaequalis	.	.	.	1	.	.		1
Nodosarella rotundata	.	.	2	1	.	.		3
Ossagittia thomasae	1	.	.	.	.	.		1
Obesopleurostomella boltovskoyi	.	.	1	.	.	1		2
O. pleurostomella	.	.	.	.	1	.		1
Pleurostomella acuminata	3	3	5	5	.	1		17
Pleurostomella acuta	2	.	.	.	.	.		1
Pleurostomella alternans	.	.	1	3	.	.		4
Pleurostomella bolivinoides	1	2	3	1	1	1		9
Pleurostomella subnodosa	2	.	3	5	1	1		12
Pleurostomella tenuis	5	2	17	5	.	.		29

Stilostomellidae								
Siphonodosaria cooperensis	8	.	.	1	.	.		9
Siphonodosaria gracillima	.	1	.	.	1	.		2
Siphonodosaria insecta	.	.	8	2	.	.		10
Siphonodosaria jacksonensis	2	.	.	2	.	.		4
Siphonodosaria lepidula	49	16	50	40	8	33		196
Siphonodosaria longispina	.	.	.	.	.	1		1
Siphonodosaria paucistriata	.	1	.	3	1	7		12
Siphonodosaria pilulata	.	.	.	.	.	2		2
Siphonodosaria pomuligera	3	5	.	6	2	1		17
Siphonodosaria subspinosa	.	1	4	17	2	5		29
Stilostomella rugosa	.	.	.	.	.	1		1
Strictocostella hyugaensis	.	1	.	.	.	19		20
Strictocostella matanzana	.	1	.	.	1	.		2
Strictocostella modesta	.	.	.	.	.	1		1
Strictocostella scharbergana	42	12	16	18	1	7		96
Strictocostella spinata	.	.	.	.	.	2		2
Uvigerinidae								
Hopkinsina mioindex?	.	.	6	7	.	.		13
Rectuvigerina striata	.	.	.	1	2	.		3
Rectuvigerina ongleyi	.	.	.	.	.	1		1
Textulariidae								
Vulvulina pennatula			5	2	.	.		7
Number of species per interval	19	19	26	28	13	23		48

4.7.3. Nannoplankton - Samples and dating rationale

Work aboard *Sonne* included collecting sediment cores and establishing an initial age model based on biostratigraphic markers, specifically calcareous nannofossils during Leg 2. Each core was assigned a maximum age based on microfossil assemblages present in the core catcher (cc), and a more detailed stratigraphic analysis was performed on selected cores by dating samples from the top of the core segments. Samples from Multicore (MUC) and from inside the open core (1 cm intervals) were also retrieved to provide further refinement.

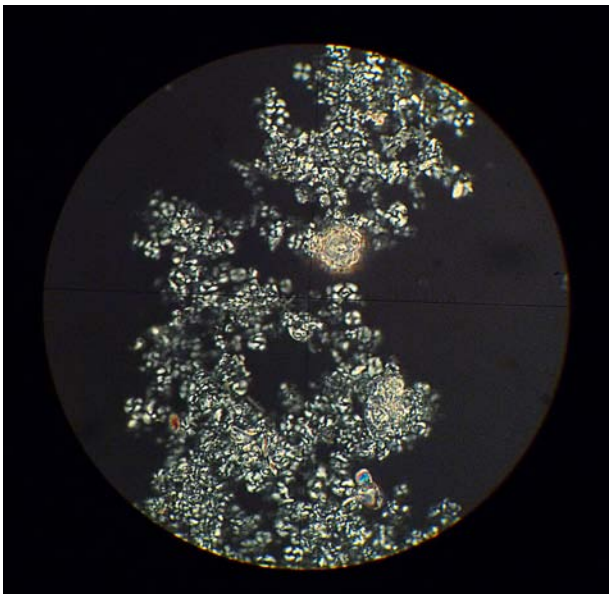

Fig. 4.7.3-1. Example of calcareous nannoplankton assemblage in Light Microscope (polarized light) at 1000X magnification. Picture taken onboard from sample SO213/054-5/786 cm depth

Smear slides were prepared following the Backman and Shackleton (1983) procedure, using Norlan adhesive to fix the glass cover slips. Each collected sample was examined for calcareous nannoplankton assemblages under the light microscope, at a magnification of 1000X in (using normal light and polarized light, see figures 4.7.3-1).

Our calcareous nannofossil biostratigraphic work was based on the works of Perch-Nielsen (1985), Bown and Young (1998), Hine and Weaver (1998), Young (1998) and Lourens *et al.,* (2004). See figures 4.7.3-2 and 4.7.3-3.

Cenozoic Calcareous Nannofossil Datums used in dating Sonne 213 samples

Species Event		Age (Ma)	Zone (base)	Reference
B	*Emiliania huxleyi*	0.29	NN21	Lourens et al., 2004
T	*Pseudoemiliania lacunosa*	0.44	NN20	Lourens et al., 2004
Tc	*Reticulofenestra asanoi*	0.91		Lourens et al., 2004
Br	*Gephyrocapsa (>4µm)*	1.01		Lourens et al., 2004
Bc	*Reticulofenestra asanoi*	1.14		Lourens et al., 2004
T	*Gephyrocapsa (>5.5µm)*	1.26		Lourens et al., 2004
T	*Helicosphaera sellii*	1.34		Lourens et al., 2004
B	*Gephyrocapsa (>5.5µm)*	1.56		Lourens et al., 2004
T	*Calcidiscus macintyrei*	1.61		Lourens et al., 2004
B	*Gephyrocapsa (>4µm)*	1.69		Lourens et al., 2004
Pliocene-Pleistocene boundary		**1.806**		
T	*Discoaster brouweri*	1.93	NN19	Lourens et al., 2004
Bc	*Discaoaster triradiatus*	2.14		Lourens et al., 2004
T	*Discoaster pentaradiatus*	2.39	NN18	Lourens et al., 2004
T	*Discoaster surculus*	2.49	NN17	Lourens et al., 2004
T	*Discoaster tamalis*	2.80		Lourens et al., 2004
T	*Sphenolithus* spp.	3.54		Lourens et al., 2004
T	*Reticulofenestra pseudoumbilica*	3.70	NN16	Lourens et al., 2004
B	*Pseudoemiliania lacunosa*	4.2		Perch-Nielsen, 1985
B	*Discoaster tamalis*	4.2		Perch-Nielsen, 1985
T	*Ceratholithus acutus*	5.04		Lourens et al., 2004
B	*Ceratholithus rugosus*	5.05	NN13	Lourens et al., 2004
T	*Triquetrorhabdulus rugosus*	5.28		Lourens et al., 2004
Miocene-Pliocene boundary		**5.332**		
B	*Ceratholithus larrymayeri*	5.34		Lourens et al., 2004
B	*Ceratholithus acutus*	5.35		Lourens et al., 2004
T	*Discoaster quinqueramus*	5.58	NN12	Lourens et al., 2004
Tc	*Nicklithus amplificus*	5.98		Lourens et al., 2004
X	*Nicklithus amplificus/T. rugosus*	6.79		Lourens et al., 2004
B	*Nicklithus amplificus*	6.91		Lourens et al., 2004
B	*Amaurolithus* spp.	7.33		Lourens et al., 2004
B	*Discoaster bergrenii*	8.29	NN11	Lourens et al., 2004
T	*Catinaster calyculus*	9.67		Lourens et al., 2004
T	*Discoaster hamatus*	9.69	NN10	Lourens et al., 2004
T	*Catinaster coalitus*	9.69		Lourens et al., 2004
B	*Discoaster hamatus*	10.55	NN9	Lourens et al., 2004
B	*Catinaster calyculus*	10.76		Lourens et al., 2004
B	*Catinaster coalitus*	10.89	NN8	Lourens et al., 2004
T	*Coccolithus miopelagicus*	11.02		Lourens et al., 2004
Tc	*Disccoaster kugleri*	11.58		Lourens et al., 2004
Bc	*Discoaster kugleri*	11.86	NN7	Lourens et al., 2004
T	*Coronocyclus nitescens*	12.12		Lourens et al., 2004
T	*Calcidiscus premacintyrei*	12.45		Lourens et al., 2004
Tc	*Cyclicargolithus floridanus*	13.33		Lourens et al., 2004

T	*Sphenolithus heteromorphus*	13.53	NN6	Lourens et al., 2004
T	*Helicosphaera ampliaperta*	14.91	NN5	Lourens et al., 2004
Tc	*Discoaster deflandrei*	15.80		Lourens et al., 2004
Bc	*Sphenolithus heteromorphus*	17.71		Lourens et al., 2004
Tc	*Sphenolithus belemnos*	17.95	NN4	Lourens et al., 2004
T	*Triquetrorhabdulus carinatus*	18.28	NN3	Lourens et al., 2004
B	*Sphenolithus belemnos*	19.03		Lourens et al., 2004
B	*Helicosphaera ampliaperta*	20.43		Lourens et al., 2004
X	*Helicosphaera euphratis/H.carteri*	20.92		Lourens et al., 2004
B	*Sphenolithus disbelemnos*	22.76		Lourens et al., 2004
Oligocene-Miocene boundary		**23.03**		
T	*Sphenolithus delphix*	23.11		Lourens et al., 2004
B	*Sphenolithus delphix*	23.11		Lourens et al., 2004
T	*Dictyococcites bisectus*	29.9		Perch-Nielsen,1985

Abbreviations

B = Base, B c= Base common
Br =Base re-entrance
FO = first occurrence datum
LO = last occurrence datum
T =Top, Tc = Top common
X = abundance cross-over

Neogene ages and duration of stages (Lourens et al., 2004) used in dating Sonne 213 samples:

Eon, Era, System, Series, Stage	Age of base (Ma)	Duration (Ma)
PHANEROZOIC		
Cenozoic Era		
Neogene System		
Holocene Series	11.5 ka	0.0115
Pleistocene Series:		
Late (Upper Pleist. subseries)	0.126 Ma	0.115
Middle (Middle Pleist. subseries)	0.781 Ma	0.655
Early (Lower Pleist. subseries)	1.806 Ma	1.025
Pliocene Series:		
Late (Gelasian Stage)	2.588 Ma	0.782
Middle (Piacenzian Stage)	3.600 Ma	1.01
Early (Zanclean Stage)	5.333 Ma	1.73
Miocene Series:		
Late (Messinian+Tortonian Stage)	11.608 Ma	1.92+4.36
Middle (Serravallian+Langhian Stage)	15.970 Ma	2.04+2.32
Early (Burdigalian+Aquitanian Stage)	23.030 Ma	4.46+2.60

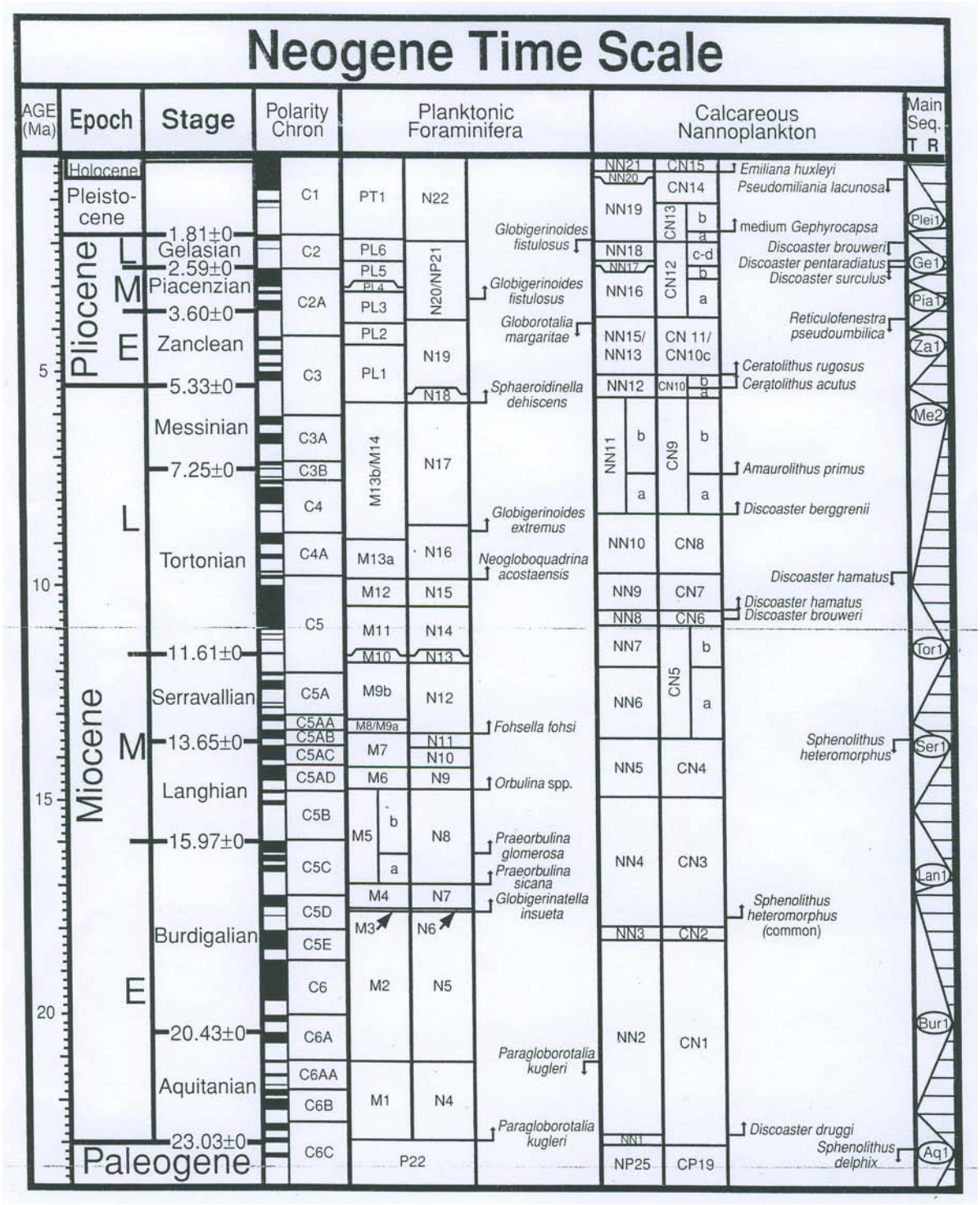

Fig. 4.7.3-2. Neogene Time Scale used for this report (Lourens et al., 2004). It includes stratigraphic subdivisions, geomagnetic polarity scale, and selected datums of planktonic foraminifera and calcareous nannoplankton.

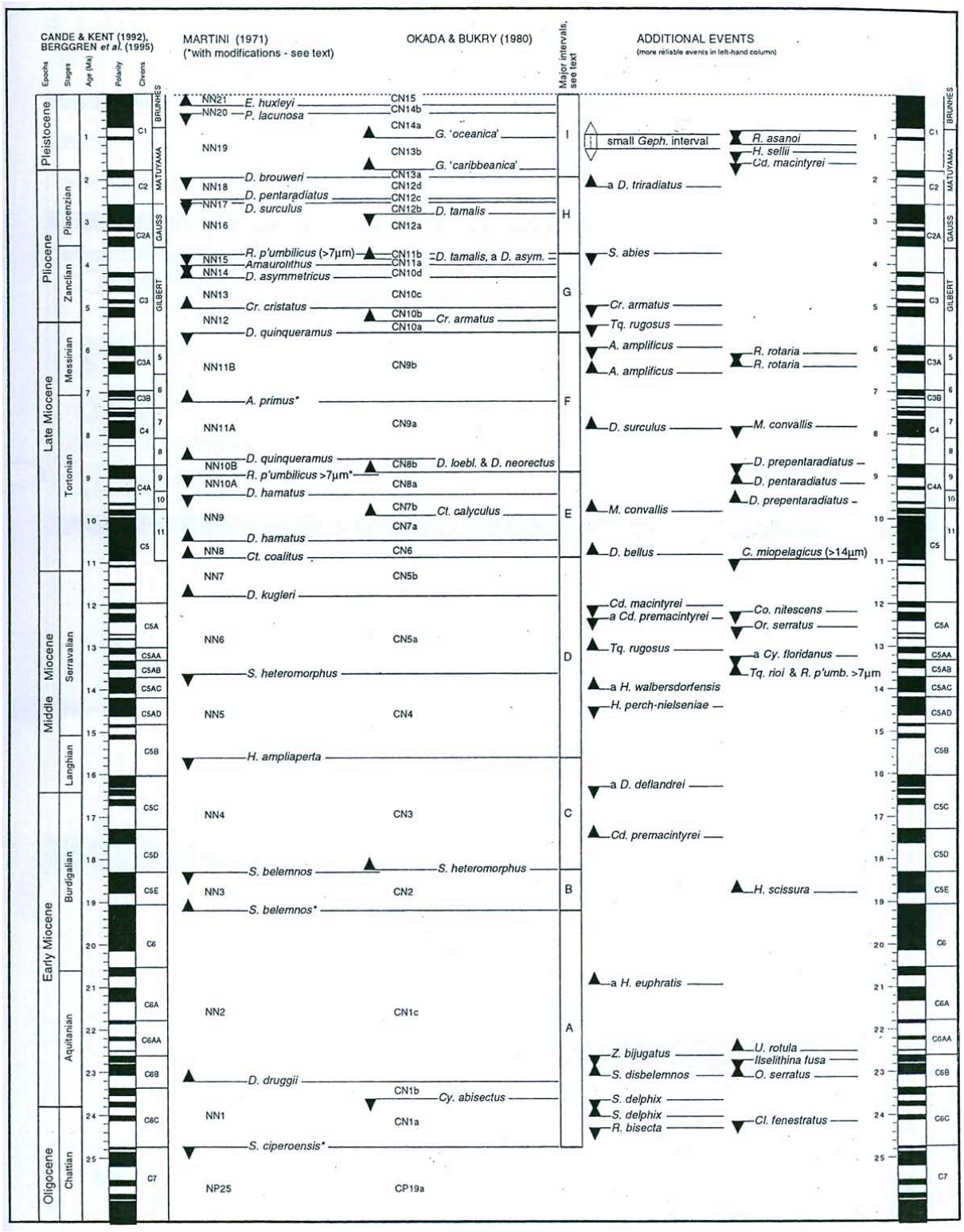

Fig. 4.7.3-3. Summary of Neogene nannofossil biostratigraphic zonation schemes and bioevents (Bown, 1998) used for this report (a=acme).

Samples and procedures
Calcareous nannoplankton species listed in this report are mostly those which are abundant and/or useful to constraint an accurate age.

The first core retrieved during Leg 1 of SOPATRA 213 expedition (SO213 -1-2 KOL) was sampled every meter. It has been examined relatively detailed with regard to: abundance, preservation, name of the different species of calcareous nannoplakton (ranging from dominant to scarcest ones) and ages inferred.

For the rest of the cores retrieved, just some "key" species (used as markers) and ages inferred are indicated within the text, generally every meter. In some cases, constraining an accurate age involved additional analyses of selected smear slides from the opened cores. This procedure is indicated in the text as "detailed biostratigraphy". A few samples are highlighted in grey and were not commented in the text to avoid that the biostratigraphy section becomes too extensive.

All the information collected during the expedition is displayed in the tables (see appendix), where "key" species are highlighted and some extra information is shown (i.e., carbonate dissolution, reworked material, etc).

For this study, a visual estimation of the abundance of calcareous nannofossils specimens (cc) in the smear slides was done and characterized by:
VA = Very abundant (>100 cc/visual field)
A = Abundant (>10 cc/visual field)
C = Common (>1 cc/visual field)
F = Few (1 cc/some visual fields)
R = Rare (1 cc/>10l visual fields)
B = Barren
(Note that the order of the species within the text range from more abundant to scarcer ones).

Preservation of calcareous nannofossils was characterized by:
VG= Very Good, exceptional
G = Good
M = Intermediate, Moderate
P = Poor
VP = Very Poor
(See tables in the appendix)

4.7.4. Results summary of nannoplankton biostratigraphy

SO213 -1-2 KOL (piston core)
<u>0 cm</u>
Abundance of calcareous nannofossils: Abundant
Preservation: Good
Species: *Reticulofenestra minuta, Reticulofenestra minutula Calcidiscus leptoporus*, *Gephyroocapsa oceanica*, *Coccolithus pelagicus*, *Helicosphaera carteri*, *Syracosphaera* spp., *Pseudoemiliania lacunosa*, *Reticulofenestra* spp.*, Dictyococcites* spp.
Age: Mid Pleistocene (>0.44 Ma, NN19), as indicates the presence of *P. lacunosa*. *Dictyococcites* spp. is linked with rare reworked material (Paleogene?).
<u>78 cm</u>
Abundance of calcareous nannofossils: Abundant
Preservation: Good
Species: *R. minuta*, *R. minutula*, *C. leptoporus*, *H. carteri*, *Syracosphaera* spp., *C. pelagicus*, *P. lacunosa*, *Reticulofenestra* spp., *Ceratolithus* spp, *Reticulofenestra pseudoumbilica*,

Age: Mid Pleistocene (>0.44 Ma, NN19), as indicates the presence of *P. lacunosa. Reticulofenestra pseudoumbilica* indicates slight mixing with Pleistocene material (>3.8Ma).

178 cm

Abundance of calcareous nannofossils: Abundant/Intermediate

Preservation: Good

Species: *R. minuta*, *R. minutula*, *C. leptoporus*, *P. lacunosa*, *G. oceanica*, *H. carteri C. pelagicus*, *Calcidiscus macintyrei*, *Reticulofenestra asanoi* (?), *Ceratolithus* spp., *Syracosphaera* spp., *R. pseudoumbilica*, *Dictyococcites bisectus*.

Age: Pleistocene (>1.6 Ma, NN19), as indicates the presence of *C. macintyrei*, probably close to 1.6 Ma.

Note that there is slight mixing with rare reworked material (Paleogene? and >3.8 Ma).

278 cm

Abundance of calcareous nannofossils: Very Abundant

Preservation: Good

Species: *R. minuta*, *R. minutula*, *C. leptoporus*, *P. lacunosa*, *C. macintyrei, Syracosphaera* spp., *Ceratolithus* spp., *Scyphosphaera* spp., *R. pseudoumbilica.*

Age: Pleistocene (>1.6 Ma, NN19), as indicates the presence of *C. macintyrei* with rare reworked Pleistocene material (>3.8 Ma).

381 cm

Abundance of calcareous nannofossils: Intermediate

Preservation: Moderate

Species: *R. minuta*, *R. minutula*, *C. leptoporus*, *P. lacunosa*, *C. macintyrei, Syracosphaera* spp., *C. pelagicus*, *Reticulofenestra rotaria* (?)

Age: Pleistocene (>1.6 Ma, NN19), as indicates the presence of *C. macintyrei.*

481 cm

Abundance of calcareous nannofossils: Abundant

Preservation: Moderate to Good

Species: *R. minuta*, *R. minutula*, *C. leptoporus*, *C. macintyrei, Syracosphaera* spp., *P. lacunosa*, *Discoaster* spp., *Discoaster brouweri* (?), *Discoaster triradiatus*, *Helicosphaera* spp., *Ceratholithus* spp., *R. rotaria* (?), *R. pseudoumbilica*.

Age: Pliocene (>2.14 Ma, NN18), as indicates the presence of *D. triradiatus,* with rare reworked material.

581 cm

It was not possible to analyze this sample, since there was some problem concerning the preparation of this smear slide.

681 cm

Abundance of calcareous nannofossils: Abundant

Preservation: Good

Species: *R. minuta*, *R. minutula*, *C. leptoporus*, *C. macintyrei, Syracosphaera* spp., *P. lacunosa*, *C. pelagicus*, *Discoaster* spp., *D. brouweri* (?), *D. triradiatus*,

Age: Middle-Late Pliocene (>2.14 Ma, NN18), as indicates the presence of *D. triradiatus.*

781 cm

Abundance of calcareous nannofossils: Abundant

Preservation: Good

Species: *R. minuta*, *R. minutula*, *Discoaster* spp., *C. leptoporus*, *C. macintyrei, P. lacunosa*, *D. triradiatus, Discaoaster decorus, Discoaster tamalis, Discoaster pentaradiatus.*

Age: Middle Pliocene (>2.4 Ma, NN18), as indicates the presence of *D. pentaradiatus*, being more accurated >2.8 Ma (NN16) as indicated by *D. decorus* and *D. tamalis.*

882 cm

Abundance of calcareous nannofossils: Abundant

Preservation: Good

Species: *R. minuta*, *R. minutula*, *Discoaster* spp., *Reticulofenestra* spp., *C. leptoporus*, *C. macintyrei*, *C. pelagicus*, *D. pentarradiatus*, *P. lacunosa*, *Syracosphaera* spp., *D. tamalis*, *Discoaster quinqueramus* (?).

Age: Middle Pliocene (>2.8 Ma, NN16) as indicated by *D. decorus* and *D. tamalis.* The presence of *D. quinqueramus* is probably due to an error in the recognition of this species.

983 cm

Abundance of calcareous nannofossils: Abundant

Preservation: Good

Species: *R. minuta*, *R. minutula, P. lacunosa*, *C. pelagicus, C. leptoporus, D. brouweri, D. decorus, D. tamalis, Syracosphaera* spp., *H. carteri*, *Calciosolenia* spp., *C. macintyrei*, *D. quinqueramus* (?),

Age: Middle Pliocene (>2.8 Ma, NN16) as indicated by *D. decorus* and *D. tamalis*. It has to be <3.54 Ma because any *Sphenolithus* spp. was observed. The presence of *D. quinqueramus* is probably due to an error in the recognition of this species.
1083 cm
Abundance of calcareous nannofossils: Abundant to Intermediate
Preservation: Good
Species: *R. minuta*, *R. minutula, Reticulofenestra* spp., *P. lacunosa, C.leptoporus, C. pelagicus, Syracosphaera* spp., *D. decorus, D. surculus, D. tristellifer, H. carteri.*
Age: Middle Pliocene (>2.8 Ma, NN16) as indicated by *D. decorus*, and also <4.2 Ma as indicated by the FO of *P. lacunosa*. It should be <3.54 Ma because any *Sphenolithus* spp. was observed.
1183 cm
Abundance of calcareous nannofossils: Abundant
Preservation: Good
Species: *R. minuta*, *R. minutula, Discoaster* spp., *C. leptoporus, C. pelagicus, Reticulofenestra pseudoumbilica, Syracosphaera* spp., *C. macintyrei*, *Discoaster challengeri*, *Helicosphaera* spp.,
Age: Early Pliocene (>3.7 Ma, NN16) as indicated by *R. pseudoumbilica*, and <4.2 Ma as indicated by the absence of *P. lacunosa*.
1283 cm
Abundance of calcareous nannofossils: Abundant
Preservation: Good
Species: *R. minuta*, *R. minutula, Reticulofenestra* spp., *Ceratholithus* spp., *C. leptoporus*, *Discoaster* spp., *D. pentarradiatus*, *D. quinqueramus*, *D. surculus*, *Helicosphaera* spp., *R. pseudoumbilica*, *Sphenolithus abies*.
Age: Early Pliocene (>3.8 Ma, NN16) as indicated by *Sphenolithus abies*, >3.7 Ma, (NN16) as shown by *R. pseudoumbilica* and >4.2 Ma as suggested by the absence of *P. lacunosa*.
Note also that *Triquetrorhabdulus rugosus* was not observed, which would mean an age <5.28 Ma for the core catcher.

Detailed biostratigraphy SO213 -1-2 KOL
80 cm, 100 cm
Age: Early Pleistocene as indicates the presence of *Reticulofenestra asanoi* (>0.91 Ma and <1.14 Ma, NN19)
120 cm
Age: Early Pleistocene, >1.26 Ma and <1.56 Ma as indicate the presence of “large” Gephyrocapsa (>5.5µm), NN19.
140 cm, 160 cm
Age: Early Pleistocene (<1.6 Ma, NN19) as displayed by the absence of *C. macintyrei*.
180 cm, 200 cm, 220 cm
Age: Early Pleistocene (>1.6 Ma, NN19), as indicates the presence of *C. macintyrei.*
440 cm, 520 cm, 560 cm, 580 cm, 640 cm, 660cm
Age: Late Pliocene, >2 Ma, as indicated by *D. brouweri*, and < 2.5 Ma as shown by *D. triradiatus.* At 660 cm depth the age should be closer to 2.5 Ma.
740 cm
Age: Middle Pliocene as suggested by *Discoaster pentaradiatus* (>2.4Ma, NN18) together with *Discoaster tamalis* and *Discoaster decorus*. (>2.8 Ma, NN16).
860 cm
Age: Middle Pliocene as indicated by the presence of *Discoaster tamalis* and *Discoaster decorus* (>2.8 Ma, NN16). The absence of *Sphenolithus* spp. points to an age <3.54 Ma.
882 cm
Age: Middle Pliocene as indicated by the presence of *Discoaster tamalis* (>2.8 Ma, NN16). The absence of *Sphenolithus* spp. points to an age <3.54 Ma.
1080 cm
Age: Middle Pliocene. The presence of *Sphenolithus* spp. points to an age close to 3.54 Ma (NN16).
1200 cm
Age: the presence of *Sphenolithus* spp. indicates an age >3.54 Ma (NN16), probably close to 3.70 Ma as shown by some of specimens of *Reticulofenestra pseudoumbilica* (>7µm) found.
1240 cm, 1260 cm
Age: Early Pliocene (>3.7 Ma, NN16) as indicated by *R. pseudoumbilica*, and <4.2 Ma as indicated by the presence of *P. lacunosa*.
1280 cm

Age: Early Pliocene (>4.2Ma), as suggested by the presence *R. pseudoumbilica*, and the absence of *P. lacunosa* (FO at 4.2 Ma). The lack of *Ceratholithus acutus* indicates an age <5.04 Ma (LO of this species at that time).

1300 cm

Age: Early Pliocene as suggested by the presence of *Discoaster tamalis*, *Amaurolithus primus* (FO at 8.6 Ma and LO at 4.7 Ma) and the absence of *Ceratholithus acutus* (LO at 5.05Ma). Note also that *Triquetrorhabdulus rugosus* was not observed, which means an age <5.28 Ma, which corroborates the age proposed.

SO213 -24-3 SL

0 cm

Age: >0.44 Ma as shown by *P. lacunosa* and also >1.6 Ma as indicated by the presence of *C. macintyrei*.

34 cm

Age: See discussion below.

123 cm

Age: Late Pliocene, around 2.4 Ma (NN18) as displayed by the LO of *D. pentaradiatus.*
The specimens of *R. pseudoumbilica, Dictyococcites* spp. and *R. umbilica* would be interpreted as reworked material.
(See discussion below)

223 cm

Age Late Pliocene, >2 Ma as indicated by *D. brouweri*, and < 2.5 Ma as shown by *D. triradiatus.*

309 cm

Age: Middle Pliocene (>2.8 Ma, NN16) as indicated by *D. decorus* and *D. tamalis*.
The age has to be <4.2 Ma because FO of *D. tamalis* happened at that time, and probably the age of the sample is <3.54 Ma because any *Sphenolithus* spp. was observed.

Detailed biostratigraphy SO213 -24-3 SL:

A more detailed study was carried out regarding the following samples: MUC: 1-2 cm (assemblage and age similar to 0 cm depth) and 25-26 cm (assemblage and age close to 34 cm depth); Core (24-3): 155 cm, 170 cm, 220 cm, 250 cm, 282 cm, 286 cm, 296 cm, 305 cm.

155 cm, 170 cm

Age: (see discussion below)

220 cm

Age Late Pliocene, >2 Ma as indicated by *D. brouweri*, and < 2.5 Ma as shown by *D. triradiatus* (see discussion below)

250 cm

Age Late Pliocene, >2 Ma as indicated by *D. brouweri*, and < 2.5 Ma as shown by *D. triradiatus* (see discussion below).

282 cm

Age Midle Pliocene, 2.9 Ma aprox. as suggested by the high abundance of *D. pentaradiatus,* (if we consider *P. pseudoumbilica* as rare reworked material, see discussion below).

286 cm

Age: Midle Pliocene, 2.9 Ma aprox. as suggested by the high abundance of *D. pentaradiatus,* (if we consider *P. pseudoumbilica* as rare reworked material, see discussion below).

296 cm

Age: Middle Pliocene, > 2.8 Ma as indicated by the presence of *D. decorus*.

305 cm

Age: Mid-Early Pliocene: <4.2 Ma (indicated by *D. decorus*, *P. lacunosa* and *D. tamalis*), but since there are any *Sphenolithus* spp., the age would be even <3.54 Ma.

Discussion

There are two possibilities to estimate the age of this core:

1. There is no mixing in the first m (let's regard 0-155 cm). Therefore the presence of *Reticulofenestra pseudumbilica* (which we consider *in situ* and was not reworked for this case) at 0 cm would indicate a top age of >3.8 Ma. And the maximum age of the whole core would be of 4.2 Ma, date indicated by the FO of *P. lacunosa*, species always present in this core.
2. There is mixing in the upper part of the core (0-170 cm aprox., when *R. pseudoumbilica* disspears). Therefore we would have a "younger" age than the one proposed in the first case for 0 m depth, that has to be >0.44 Ma and >1.6 Ma as indicated by LO of *P. lacunosa* and LO of *C. macintyrei*. The basis of the core (309 cm) would have then an age of 3.8 – 4.2 Ma aprox. In between, the sample from 282 cm would have an age of 2.9 cm coincident with the Paracme of *Discoaster pentaradiatus*.

In short, it is also possible an age of >1.6 Ma at 0 m depth, 24.4 Ma at 123 cm depth (LO of *D. pentaradiatus*), 2.9 Ma at 282 cm (paracme of *D. pentaradiatus*) and <4.2 Ma at 309 cm (indicated by *D. decorus, P. lacunosa and D. tamalis*), but since there are any *Sphenolithus* spp., the age would be even <3.54 Ma.
For more details, see tables (Appendix)

SO213 -26-2 SL
0 cm
Age: Late Pleistocene-Holocene (<0.29 Ma, NN21), as indicates the presence of *E. huxleyi*
100 cm
Age: Middle Pleistocene (Close to 0.44 Ma, NN20) as indicates the presence of *P. lacunosa* (although just a couple of specimens were found).
200 cm
Age: Middle Pleistocene (> 0.44 Ma, NN20) as indicates the presence of *P. lacunosa.* The very scarce presence of *Reticulofenestra pseudoumbilica* would be linked to contamination when the smear slide was prepared in the Geo-lab.
300 cm
Age: Middle Pleistocene >0.44 Ma (NN20) as indicates the presence of *P. lacunosa and* <0.9 Ma shown by the absence of *Reticulofenestra asanoi.*

Detailed biostratigraphy SO213 -26-2 SL:
A more detailed study was carried out to perfectly define LO of *Pseudoemiliania lacunosa* and FO of *Emiliania huxleyi* in this core, studying the following samples:
MUC: 0-1 cm and 30-31 cm (both <0.29 Ma).
Core (26-2): 49 cm (<0.29 Ma), 55 cm(<0.29 Ma; FO of *Emiliania huxleyi*), 65 cm (>0.29 Ma), 86 cm (0.44Ma aprox; LO of *Pseudoemiliania lacunosa* between 86 cm and 100 cm), 108 cm (>0.44Ma),118 cm (>0.44 Ma), 150 cm (>0.44Ma), and 180 cm (>0.44 Ma).

SO213 49-2 SL
5 cm, 16 cm, 32 cm
Age: Late Pleistocene-Holocene (<0.29 Ma, NN21), as indicates the presence of *E. huxleyi*
50 cm, 79 cm
Age: Middle-Late Pleistocene (?) (<0.44, >0.29, close to NN20-NN21 transition) as indicate the absence of *E. huxleyi* and *P. lacunosa.*
105 cm, 120 cm, 141 cm
Age: Middle Pleistocene (>0.44 Ma, NN19), as indicates the presence of *P. lacunosa.* It was inferred that the sample corresponding to 141 cm is close to 0.91 Ma owing to the scarce specimens of *Reticulofenestra asanoi* found.
164 cm, 190 cm, 205 cm,
Age: Early Pleistocene as indicates the presence of *Reticulofenestra asanoi*. (>0.91Ma and <1.14 Ma, NN19)
499 cm
Age: Pleistocene (>1.6 Ma, NN19), as indicates the presence of *C. macintyrei.*
698 cm, 699 cm
Age Late Pliocene, as suggested by the presence of *D. pentaradiatus, D. assymetricus* (>2.4 Ma, NN18) and *Discoaster surculus* (>2.5 Ma, NN17), the last one just found at 698 cm.
cc
Age Mid-Late Pliocene, as suggested by the presence of *D. surculus* (>2.5 Ma, NN17), *D. tamalis* and *D. decorus* (>2.8 Ma, NN16). The absence of *Sphenolithus* spp. indicates an age <3.54 Ma.

SO213 49-4 KOL
0 cm (Core and Trigger Core)
Age: Late Pleistocene-Holocene (<0.29 Ma, NN21), as indicates the presence of *E. huxleyi*
100 cm
Age: Middle Pleistocene (>0.44 Ma, NN19), as indicates the presence of *P. lacunosa.*
203 cm
Age: Early Pleistocene as indicates the presence of *Reticulofenestra asanoi*. (>0.91Ma and <1.14 Ma, NN19)
304 cm
Age: Early Pleistocene as indicates the presence of *Reticulofenestra asanoi*. (>0.91Ma and <1.14 Ma, NN19)

604 cm
Age: Pleistocene (>1.6 Ma, NN19), as indicates the presence of *C. macintyrei.*
804 cm
Age: Late Pliocene, as suggested by the presence of *D. brouweri* (>2 Ma, NN19).
906 cm
Age: Late Pliocene, as suggested by the presence of *D. assymetricus* (>2.4 Ma, NN18).
1004 cm
Age Late Pliocene, as suggested by the presence of *D. pentaradiatus* and *D. assymetricus* (>2.4 Ma, NN18).
1104 cm
Age Middle-Late Pliocene, as suggested by the presence of *D. decorus* (>2.8 Ma, NN18). The absence of *Sphenolithus* spp. indicates an age <3.54 Ma.
cc
The lack of *Discoaster* spp. in the samples did not allow us to get an accurate age. But we consider that the age is similar to the one for 1104 cm depth (Middle-Late Pliocene).

SO213 52-1 KOL
0 cm, 16 cm, 42 cm, 68 cm (white material), 68 cm (dark material)
Age: Late Pleistocene-Holocene (<0.29 Ma, NN21), as indicates the presence of *Emiliania huxleyi*
114 cm
Age: Middle-Late Pleistocene (<0.44, >0.29, close to NN20-NN21 transition) as indicate the absence of *Emiliania huxleyi* and *P. lacunosa.*
150 cm
Age: Middle Pleistocene (>0.44 Ma, NN19), as indicates the presence of *P. lacunosa.*
183 cm, 198 cm
Age: Early Pleistocene as indicates the presence of *Reticulofenestra asanoi*. (>0.91 Ma and <1.14 Ma, NN19)
293 cm
Age: Early Pleistocene? (>1.6 Ma, NN19), as indicates the presence of *C. macintyrei.*
393 cm
Age: Late Pliocene-Early Pleistocene (>1.6 Ma, NN19), as indicates the presence of *C. macintyrei.*
450 cm
Age: Late Pliocene-Early Pleistocene (>1.6 Ma, specifically >2 Ma, NN19), as indicates the presence of *C. macintyrei* and *D. brouweri.*
493 cm
Age Late Pliocene, as suggested by the presence of *D. assymetricus* (>2.4 Ma, NN18).
593 cm
Age Mid-Late Pliocene, as suggested by the presence of *D. decorus* (>2.8 Ma, NN16).
623 cm
Age: (>2.5 Ma, NN17) indicated by *D. surculus*.
693 cm
Age: Late Pliocene (>2.8 Ma, NN16) as indicated by *D. tamalis.* The maximum age would be 4.2 Ma as displays the presence of *P. lacunosa* (also FO of *D. tamalis*).
878 cm, 879 cm, 880 cm
Age: Middle Pliocene (>3.7 Ma, NN16) as indicated by *R. pseudoumbilica* and <4.2 Ma as shown by the presence of *D. tamalis* (FO of *D. tamalis*).
892 cm
Age: Middle Pliocene (>3.7 Ma, NN16) as indicated by *R. pseudoumbilica*, and <4.2 Ma as indicated by *P. lacunosa*.
992 cm
Age: Early-Middle Pliocene (<4.2 Ma, but close to this age) as indicated by the presence of *P. lacunosa*.
1092 cm
Age: Early Pliocene (>4.2 Ma) as indicated by the absence of *P. lacunosa* and *D. decorus*
1120 cm, 1150 cm
Age: In those samples, we could not find any *Discoaster* spp., to well constraint the age. However both samples correspond to Early Pliocene, specifically >4.7 Ma, indicated by *Amaurolithus delicatus* (LO at 4.7 Ma) & *Amaurolithus primus* (LO at 4.7 Ma), and >5.1 Ma, as suggested by the absence of *Ceratolithus rugosus* (FO at 5.1 Ma and LO at 1.7 Ma).

1192 cm
Age: Early Pliocene (>5.1Ma and <5.35 Ma, NN12-NN13) as indicated by the presence of the following species: *Amaurolithus delicatus* (LO at 4.7 Ma), *Amaurolithus amplificus* (LO at 5.1 Ma), *Ceratholithus acutus* (FO at 5.35 Ma and LO at 5.04 Ma).
cc
Age: Early Pliocene-Late Miocene (>4.7 Ma and <5.58 Ma, NN12) as indicated by the presence of *Amaurolithus delicatus* (LO at 4.7 Ma), *Amaurolithus amplificus* (LO at 5.1Ma) and the absence of *Discoaster quinqueramus* (LO at 5.58 Ma).

SO213 54-5 KOL
0 cm (from TC), 0 cm (from core), 0 cm (from MUC), 10-12 cm (MUC), 28-29 cm
Age: Late Pleistocene-Holocene (<0.29 Ma, NN21), as indicates the presence of *Emiliania huxleyi.* There is important mixing, displayed by the following species: *Sphenolithus* spp. (Middle-Early Pliocene, >3.54 Ma), *Reticulofenestra pseudoumbilica* (early Pliocene, >3.7 Ma), *Dictyococcites bisectus* (Oligocene, >23.9 Ma).
35 cm
Age: *P. lacunosa* suggests an age>0.44 Ma, and *D. decorus* indicates Middle Pliocene age (>2.8 Ma). There is mixing, displayed by the presence of *Reticulofenestra pseudoumbilica* (early Pliocene, >3.7 Ma) and *Dictyococcites bisectus* (Oligocene, >23.9 Ma).
235 cm (note the carbonate dissolution)
Age: *P. lacunosa* suggests an age >0.44 Ma, and *D. decorus* indicates Middle-Early (?) Pliocene (>2.8 Ma). There is mixing, displayed by the presence of *Dictyococcites bisectus* (Oligocene, >23.9 Ma).
285 cm (note the high carbonate dissolution)
Age: *D. decorus* indicates at least Middle Pliocene age (>2.8 Ma) and the absence of *P. lacunosa* suggests an age >4.2 Ma (Early Pliocene), although the carbonate dissolution is intense.
There is mixing, as shown by *Dictyococcites bisectus* (Oligocene, >23.9 Ma).
385 cm (note the carbonate dissolution)
Age: *D. decorus* indicates at least Middle Pliocene age (>2.8 Ma) and the absence of *P. lacunosa* suggests an age >4.2 Ma (Early Pliocene?). There is important mixing, as shown by the abundant specimens of *Dictyococcites bisectus* (Oligocene, >23.9 Ma), some of them partially dissolved and looking like large *Reticulofenestra*.
486 cm cm (note the carbonate dissolution)
Age: *Sphenolithus* spp. suggest an age >3.54 Ma (Early Pliocene?), although the mixing continues, as shown by the abundant specimens of *Dictyococcites bisectus* (Oligocene, >23.9 Ma), some of them partially dissolved and looking like large *Reticulofenestra*.
586 cm, 686 cm (note the carbonate dissolution)
Age: The presence of *Calcidiscus tropicus* (NN4-NN10) indicates Middle-Late Miocene (?), >9.67Ma and <17.95 Ma. Mixing continues, as shown by the abundant specimens of *Dictyococcites bisectus* (Oligocene, >23.9 Ma), some of them partially dissolved and looking like large *Reticulofenestra*.
786 cm
Age: *D. brouweri* indicates a maximum age of 10.8 Ma (NN8). Specimens of *Dictyococcites bisectus* (Oligocene, >23.9 Ma) are common, also dissolved.
886 cm
Age: *Dictyococcites bisectus* dominate clearly the assemblage, therefore we assume an Oligocene age (>23.9 Ma).
cc (white material), cc (grey material)
Age: Late Oligocene (>23.9 Ma and <29.9 Ma) as indicated by the clear dominance of *Dictyococcites bisectus* and the presence of *Coccolithus miopelagicus* (FO at 29. 9 Ma) in the whitest core catcher sample.

SO213 59-2 SL
0 cm, 11 cm
Age: Late Pleistocene-Holocene (<0.29 Ma, NN21), as indicates the presence of *Emiliania huxleyi*
111 cm
Age: The acme of *E. huxleyi* observed here would correspond to an age close to 0.075 Ma or even younger (Pleistocene-Holocene, <0.29 Ma, NN21).
211 cm, cc
Age: Late Pleistocene-Holocene (<0.29 Ma, NN21), as indicates the presence of *E. huxleyi*

SO213 60-1 SL
0 cm, 83 cm,
Age: Late Pleistocene-Holocene (<0.29 Ma, NN21), as indicates the presence of *Emiliania huxleyi*

182 cm
Age: Late Pleistocene-Holocene (close to 0.29 Ma, NN21), as indicates the scarce specimens of *Emiliania huxleyi*
232 cm, 245 cm, 260 cm
Age: Middle-Late Pleistocene (<0.44 Ma, >0.29 Ma close to NN20-NN21 transition) as indicate the absence of *Emiliania huxleyi* and *P. lacunosa.*
282 cm ("small" *Gephyrocapsa* ooze).
Age: Middle Pleistocene (>0.44 Ma, NN19), as indicates the presence of *P. lacunosa.*
382 cm (note the carbonate dissolution), 482 cm, 582 cm
Age: Age: Middle-Early Pleistocene (>0.44 Ma, <0.91 Ma, NN19), as indicates the presence of *P. lacunosa* and the absence of *Reticulofenestra asanoi*. (LO at 0.91 Ma)
681 cm ("small" *Gephyrocapsa/Reticulofenestra* ooze), cc
Age: Age: Middle-Early Pleistocene (>0.44 Ma, <0.91 Ma, NN19), as indicates the presence of *P. lacunosa* and the absence of *Reticulofenestra asanoi* (LO at 0.91 Ma).

SO213 61-2 SL
Note the presence of diatoms.
0 cm
Age: Late Pleistocene-Holocene (<0.29 Ma, NN21), as indicates the presence of *Emiliania huxleyi*
67 cm (*Emiliania huxleyi* ooze)
Age: This ooze would correspond to an age close to 0.075 Ma or even younger (Pleistocene-Holocene, <0.29 Ma, NN21).
135 cm. (note the carbonate dissolution)
Age: Not clear (<0.29 Ma?, NN21). *E. huxleyi* is not recognized here, probably due to the poor preservation observed.
162 cm, 177 cm
Age: Middle-Late Pleistocene (<0.44 Ma, >0.29 Ma, close to NN20-NN21 transition) as indicate the absence of *Emiliania huxleyi* and *P. lacunosa.*
211 cm, 234 cm ("small" *Gephyrocapsa* ooze, specially at 234 cm).
Age: Middle-Late Pleistocene (<0.44 Ma, >0.29 Ma, close to NN20-NN21 transition) as indicate the absence of *Emiliania huxleyi* and *P. lacunosa.*
252 cm, 261 cm ("small" *Gephyrocapsa* ooze).
Age: Middle Pleistocene (close to 0.44 Ma, or >0.44 Ma, NN19), as indicates the presence of *P. lacunosa* (it appears sporadically in both samples).
361 cm (note the carbonate dissolution and the abundant terrigenous material)
Age: Middle Pleistocene (>0.44 Ma, NN19), as indicates the presence of *P. lacunosa.*
461 cm, 561 cm, 661 cm (note the carbonate dissolution and the abundant terrigenous material in those samples)
Age: Middle-Early Pleistocene (>0.44 Ma, <0.91 Ma, NN19), as indicates the presence of *P. lacunosa* and the absence of *Reticulofenestra asanoi*. (LO at 0.91 Ma). The presence of *R. pseudoumbilica* and *Dictyococcites* spp. indicate mixing with Pleistocene (>3.8 Ma) and Oligocene (>23.9 Ma) material, especially at 661 cm depth.
cc (mixed *Emiliania huxleyi* ooze?)
The core catcher looks mainly like the sediment sample corresponding to 67 cm depth (mixed with some older species). This information is inconsistent, and we link the calcareous nannoplankton assemblage found here to contamination while retrieving the core.

SO213 62-1
Note the presence of diatoms. In general, there is poor to moderate preservation of the calcareous nannofossils.
0 cm, 14 cm, 105 cm, 110 cm, 130 cm, 150 cm, 170 cm, 180 cm (note the carbonate dissolution)
Age: Late Pleistocene-Holocene (<0.29 Ma, NN21), as indicates the presence of *Emiliania huxleyi*. The presence of *Dictyococcites* spp. indicates slight mixing with reworked material.
190 cm, 195 cm, 200 cm(note the carbonate dissolution),
Age: FO of *E. huxleyi* takes place in this frame, but it was difficult to constraint it more accurately. However we can assign an age close to 0.29 Ma to those samples.
205 cm (note the carbonate dissolution)
Age: Middle-Late Pleistocene (<0.44 Ma, >0.29 Ma, close to NN20-NN21 transition) as indicate the absence of *E. huxleyi* and *P. lacunosa.* The presence of *Dictyococcites* spp. indicates slight mixing with reworked material.

280 cm, 290 cm, 305 cm (“small” *Gephyrocapsa* ooze).
Age: Middle Pleistocene (>0.29 Ma, <0.44 Ma, but close to 0.44 Ma, NN19), as indicates the absence of *P. lacunosa*).
405 cm, 505 cm, 605 cm, 705 cm (note the carbonate dissolution and the abundant terrigenous material)
Age: Middle-Early Pleistocene (>0.44 Ma, NN19), as indicates the presence of *P. lacunosa.* Slight mixing is also suggested by the reworked material.
cc (note the carbonate dissolution and the abundant terrigenous material)
Age: Early Middle Pleistocene (>0.44 Ma, <0.91Ma, NN19), as indicated by the presence of *P. lacunosa* and the absence of *Reticulofenestra asanoi* (LO at 0.91 Ma).

SO213 63-2
Note the presence of diatoms.
0 cm, 53 cm, 140 cm (note the carbonate dissolution in the last one)
Age: Late Pleistocene-Holocene (<0.29 Ma, NN21), as indicates the presence of *Emiliania huxleyi*. The presence of *Dictyococcites* spp. indicates slight mixing with reworked material.
153 cm (“small” *Gephyrocapsa* and *E. huxleyi* ooze).
Age: Late Pleistocene-Holocene (<0.29 Ma, NN21), as indicates the scattered specimens of *E. huxleyi*.
155, 167 cm (note the carbonate dissolution and the abundant terrigenous material)
Age: Late Pleistocene-Holocene? (<0.29? Ma, NN21), as indicates the scattered specimens of *E. huxleyi*, which were not observed in both samples (probably owing to dissolution).
One specimen of *P. lacunosa* was observed at 167 cm depth, therefore the age suggested is not so clear.
180 cm (note the carbonate dissolution and the abundant terrigenous material)
Age: Late Pleistocene-Holocene? (<0.29? Ma, maybe close to 0.29 Ma, NN21), as indicate the scattered specimens of *E. huxleyi* poorly preserved. There is mixing as displayed by the presence of *C. macintyrei*, *Sphenolithus* spp. and *Dictyococcites* spp.
241 cm (note the carbonate dissolution)
Age: Middle-Late Pleistocene (>0.44 Ma, NN19) as indicate the presence of *P. lacunosa*. There is slight mixing with reworked material (i.e., *Sphenolithus* spp. *Dictyococcites* spp, *R. pseudoumbilica*)
253 cm (note the carbonate dissolution and the reworked material)
Age: Unknown
283 cm cm (note the carbonate dissolution and the reworked material)
Age: Not clear. Middle-Late Pleistocene (>0.44 Ma, NN19) as shown by *P. lacunosa* and probably >1.6 Ma (?) as indicated by the presence of *C. macintyrei*. There is important mixing with reworked material (i.e., *Coccolithus miopelagicus, Dictyococcites* spp, *Reticulofenestra gelida*).
298 cm
Age: Not clear. The presence of *D. decorus* and *D. challengeri would s* indicate at least Middle Pliocene age (>2.8 Ma) which would reach back to 3.54 Ma (as suggested by *Sphenolithus* spp.), or even 3.7 Ma (as suggested by *R. pseudoumbilica*). There is important mixing with reworked material (i.e., *Dictyococcites bisectus*).
312 cm (note the carbonate dissolution and the reworked material)
Age: Unknown
350 cm 353 cm (note the very poor preservation of carbonate).
Age: Not clear. *D. decorus* suggest an age >2.8 Ma and <4.2 Ma. There is mixing with reworked material (i.e., *Dictyococcites bisectus*).
cc (361 cm, note the carbonate dissolution)
Age: Not clear.
Initially, an age >0.44 Ma and <1.01 Ma, was assigned, as indicated by the presence of *P. lacunosa* and *R. asanoi* (note that just one specimen of *R. asanoi* was observed), but this is inconsistent with the previous younger smear slides analyzed.

SO213 64-1
depth: 3925 m
0 cm, 1 cm, 7 cm, 17 cm, 27 cm, 37 cm.
Age: Probably late Pleistocene-Holocene (<0.29 Ma, NN21), as indicates the presence of *E. huxleyi*. The presence of *Dictyococcites* spp. indicates mixing with reworked material.
45 cm, 74 cm, 92 cm (note the poor to moderate preservartion of the calcareous nannofossils)
Age: Not clear. Any clear calcareous nannofossil marker was found. Some specimens of *E. huxleyi* found there would suggest an age <0.29 Ma? (NN21). Any specimen of *P. lacunosa* was observed, pointing out an age <0.44 Ma.

There is reworked material or mixing as indicates the presence of *Dictyococcites* spp. and *Coccolithus miopelagicus.*
106 cm, 119 cm, 132 cm 174 cm (note the high carbonate dissolution in all the samples)
Age: The presence of *Sphenolithus* spp. would suggest at least Middle Pliocene, >3.54 Ma (NN16), also indicated by *D. decorus* (>2.8 Ma, NN16) at 132 cm. *Dictyococcites* spp. (in all the samples), *Coccolithus miopelagicus* (just at 174 cm) indicate mixing with reworked material.
190 cm
Age: *D. variabilis* and *D. tristellifer* (LO at 2.8 Ma, NN16) together with *Amaurolithus primus* and *Ceratolithus acutus* (this last species not so clear) suggest Early Pliocene: >4.7 Ma and <5.1 Ma. This generates a conflict with the presence of *D. decorus* (FO at 4.2 Ma) but a misunderstanding with *D. variabilis* is possible.
214 cm
Age: *D. variabilis* (LO at 2.8 Ma, NN16) together with *Amaurolithus primus* (LO at 4.7 Ma) and *Ceratolithus armatus* (FO at 5.2 and LO at 5.1 Ma) suggest Early Pliocene.
The already known conflict concerning *D. decorus/D. variabilis* (FO of the first one at 4.2 Ma) still remains.
274 cm, 274 cm (base), cc (=274 cm)
Age: *D. variabilis* indicates a minimum age of 2.8 Ma (LO). The scarce presence of *A. primus suggest* an age >4.7 Ma, which again generates a conflict with the presence of *D. decorus* (FO at 4.2 Ma), probably due to a misunderstanding with *D. variabilis.*
Some specimens of *D. brouweri* and *Reticulofenestra haqii* suggest an age younger than 10.8 Ma, coincident with both FO.
There is important mixing, as shown by the very abundant specimens of *D. bisectus* (Oligocene, >23.9 Ma), some of them partially dissolved and looking like large *Reticulofenestra* spp.

SO213 66-5
There is not carbonate at all to suggest an approximate age.
Note the presence of diatoms.

SO213 68-2
0 cm, 17 cm, 117 cm, 217 cm
Age: Late Pleistocene-Holocene (<0.29 Ma, NN21), as indicates the presence of *Emiliania huxleyi*
294 cm, 394 cm
Age: The presence of *E. huxleyi* is not so clear, but the absence of *P. lacunosa* clearly indicates an age <0.44 Ma (NN20).
493 cm ("small" *Gephyrocapsa* ooze).
Age: Middle-Late Pleistocene (<0.44 Ma, >0.29 Ma, close to NN20-NN21 transition) as indicate the absence of *Emiliania huxleyi* and *P. lacunosa.*
Base (there is not cc for this core).
Age:Not clear (?). There is mixing. The presence of *E. huxleyi* is in consistent with the sequence previously observed. However the absence of *P. lacunosa* clearly indicates an age <0.44 Ma (NN20).

SO213 73-1
Note the presence of diatoms.
TC 0 cm, 0 cm, 93 cm, 193 cm
Dissolution: carbonate is not preserved.
293 cm, 393 cm (note the poor to moderate preservation)
Age: Late Pleistocene-Holocene (<0.29 Ma, NN21), as indicates the presence of *E. huxleyi*.
493 cm, 593 cm (note the poor to moderate preservation)
Age: Not clear.
693 cm, 793 cm, 894 cm, 994 cm
Dissolution: carbonate is not preserved.
1094 cm, 1194 cm (note the moderate preservation)
Age: Not clear.
1294 cm, 1394 cm, 1495 cm, 1594 cm, 1694 cm,
Dissolution: carbonate is not preserved.
1793 cm: smear slide missing
cc (1793 cm)
Age: the absence of *P. lacunosa* suggest an age <0.44 Ma (NN20).

4.8 SEISMICS

The seismic reflection measurements comprise two objectives: 1) Mapping of sedimentary structures such as sediment drifts to image modifications in the bottom water circulation. 2) A high-resolution seismic pre-site survey in the southern Pacific on drill sites located north of 50°S as proposed in the paleoceanographic IODP proposal no. 625 (Gersonde et al. 2002).

4.8.1 Multi-channel reflections seismics (MCS)

We used a standard multi-channel seismic reflection technique (Tab. 4.8.1-1) to image the outline and reflectivity characteristics of the sedimentary layers and the structure of the sub-sedimentary basement.

Seismic sources, triggering and timing
High-resolution seismic reflections lines were shot using a cluster of 4 GI-Guns^{TM} to resolve the sedimentary layers (Fig. 4.8.1-1). A single GI-Gun is made of two independent airguns within the same body. The first airgun ("Generator") produces the primary pulse, while the second airgun ("Injector") is used to control the oscillation of the bubble produced by the "Generator". We used the "Generator" with a volume of 0.72 litres (45 in^3) and fired the "Injector" (1.68 litres = 105 in^3) with a delay of 33 ms. This leads to an almost bubble-free signal. The guns were towed 20 m behind the vessel in 2 m depth and fired every 10 s (25 m shot interval) with a working pressure between 135 and 140 bar. Firing was started with gradually increasing working pressure (ramping up) at the beginning of a profile and after shot interruptions.

***Fig. 4.8.1-1**: Two high frequency 2 GI-Airgun cluster used for the seismic surveys (Photo: T. Ronge)*

Seismic data acquisition requires a very precise timing system, because seismic sources and recordings systems must by synchronized. A combined electric trigger-clock system was in operation in order (1) to provide the firing signal for the electric airgun valves, and (2) to provide the time-control of the seismic data recording. Due to the variable time difference in the NMEA format of the ship-provided clock and the DVS system, a separate Meinberg GPS clock was used with an antenna mounted on the upper deck. The clock provides UTC date and time (minute and second) pulses.

Multi-channel reflection recording system

For multi-channel reflection data acquisition a 3000 m long digital solid streamer of 240 channels, type Sentinel by SERCEL was used (Fig. 4.8.1-2). The data were recorded by the SEAL system of SERCEL and stored parallel on LTO-2 tapes and on NAS disk system for backup in SEGD-format. On-track quality control was done with the eSQC-Pro system displaying every shot record as well as single-channels (here Chan. 16) along profiles.

A constant streamer depth of 10 m was kept with the help of 12 DigiCourse depth-control birds (Model 5010) mounted at 300 m intervals along the streamer. The Digicourse software gives a continuously updated graphical display of depths and wing angles of the Digibirds. Additionally, two streamer life-saving-systems were mounted at 1000 m intervals to prevent hazardous sinking of the streamer below 40 m. At the streamer end a floatation buoy with a diameter of 120 cm was attached.

Fig. 4.8.1-2*: Deployment of the 3000 m long digital streamer (Type SERCEL), and montage of the Digibirds and rescue system (Photos: T. Ronge).*

Mitigation for marine mammals

According to the *'Guidelines for Minimising Acoustic Disturbances to Marine Mammals from Seismic Survey Operations of the New Zealand Department of Conservation'* mitigation for marine mammals was conducted during seismic profiling (Tab 5.8.1-2). The main procedures include (1) constant visual monitoring of the area in a radius of 1.5 km around the vessel for possible marine mammal appearance before and during seismic profiling, (2) soft-start procedures for the airgun cluster for the duration of 15 minutes and (3) immediate shutdowns of airgun operations in cases of detected marine mammals within a safety distance from the ship.

Profile Name	*Active Length*	*Lead-in*	*Shot intervall*	*Record Length*	*Sample Rate*
AWI-20110001	3000 m	191 m	12 s	10 s	1 ms
AWI-20110002	3000 m	191 m	10 s	9 s	1 ms
AWI-20110003	3000 m	191 m	10 s	9 s	1 ms
AWI-20110004	3000 m	191 m	10 s	9 s	1 ms
AWI-20110005	3000 m	191 m	10 s	9 s	1 ms
AWI-20110006	3000 m	191 m	10 s	9 s	1 ms
AWI-20110007	3000 m	191 m	10 s	9 s	1 ms
AWI-20110008	3000 m	191 m	10 s	9 s	1 ms
AWI-20110009	3000 m	191 m	10 s	9 s	1 ms

Tab. 4.8.1-1*: The data were recorded with the following parameters*

Table 4.8.1-2 Marine mammal observations.

Date	Time [UTC]	Latitude	Longitude	Info	Observation	seismic stop	seismic start	Name
Central South Pacific								
03.02.2011	01:18	- 43° 50.49‘	- 120° 21.81‘	softstart (4 airguns)	-	-	02:18	D. Korte L. Hoffsommer U.Büchele
05.02.2011	20:56	- 46° 13.94‘	- 116° 02.46‘	stop shoting (profile end)	-	20:56	-	D. Korte L. Hoffsommer U.Büchele
New Zealand Waters								
24.02.2011	16:43	- 46° 39.78‘	- 177° 14.84‘	softstart (4 airguns)	-	-	-	D. Korte
25.02.2011	01:49	-46 °16.58’	-177° 55.23’	stop & start shoting	7-8 Pilot Whales occur suddenly 200m stb. disappear fast after shoting stop	01:49	01:58	U.Büchele
25.02.2011	20:36	-46°13.78’	-179°33.04	stop & softstart	Only 2 tall blows observed ~ 1 nm , 050° stb. not observed anymore	20:36	21:05	L. Hoffsommer
26.02.2011	21:17	45°35.47’	+178°54.35	stop & softstart	1 whale, grey back, tall blow ~ 1nm, 020° portside 5 blasts and dived away	21:17	21:47	L. Hoffsommer
27.02.2011	17:00	45° 59.85	-179° 30.00	stop shoting (profile end)	-	17:00	-	D. Korte

4.8.2 First Results

As detailed seismic processing is time-consuming and could not be carried out on board. Only single channel plots of some seismic sections had been produced which allow a first, preliminary interpretation. All further seismic processing will be performed at the AWI.

Seismic profiling
A total of 1131 km of seismic reflection profiles were recorded in two sequences in the (1) Central South Pacific, and (2) along the Bounty Trough east off New Zealand (Tab. 4.8.2-1). Technical problems of the seismic gear were almost negligible, allowing continuous profiling over both transects. The data quality is generally at a good level, although sometimes a high swell caused lifting and lowering of the streamer, which could not be regulated by the depth-control birds.

First profile sequence, Central South Pacific
Seismic data of the Eltanin-Cruises recorded between 1965 and 1970 showed that sediments with a relevant thickness of more than 100 m occurred more than 200 km west off the EPR. Thus, a sequence of 5 seismic reflection profiles was recorded starting 650 km west off the EPR (Fig. 4.8.2-1) with a total length of almost 560 km (Tab. 4.8.2-1). The aim was to perform a pre-site survey for a potential IODP drilling location, and further to approach the EPR until sedimentary thickness decreases below the resolution of seismics.

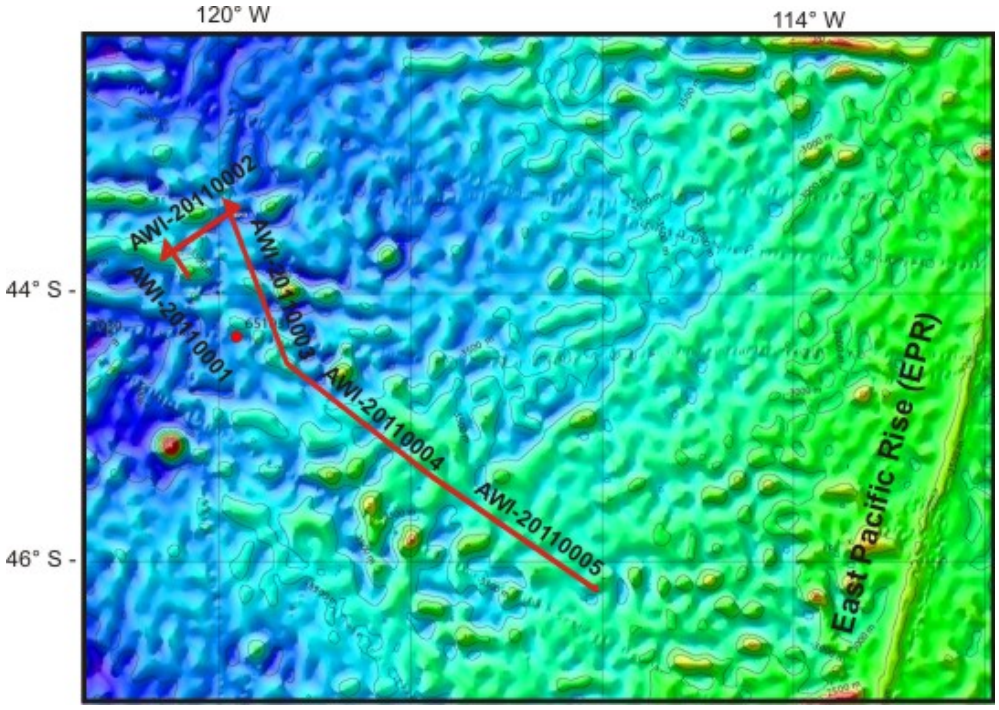

Fig. 4.8.2-1: *Bathymetric map of the Central South Pacific Ocean. The red lines mark the location of the seismic reflection Profiles AWI-20110001 to AWI-20110005.*

Profiles 20110001-20110003 were mainly recorded to perform the pre site survey. The data show an undulating basement with a sedimentary cover between 0.16 - 0.25 s two-way-travel time (twt) (130m - 220m) (Figs. 4.8.2-2 and 4.8.2-3). The sedimentary cover follows mostly the basement topography, but also at some locations it is interrupted by smooth basement elevations. In some parts stratification is indicated by parallel reflector sequences (Fig. 5.8.2-3).

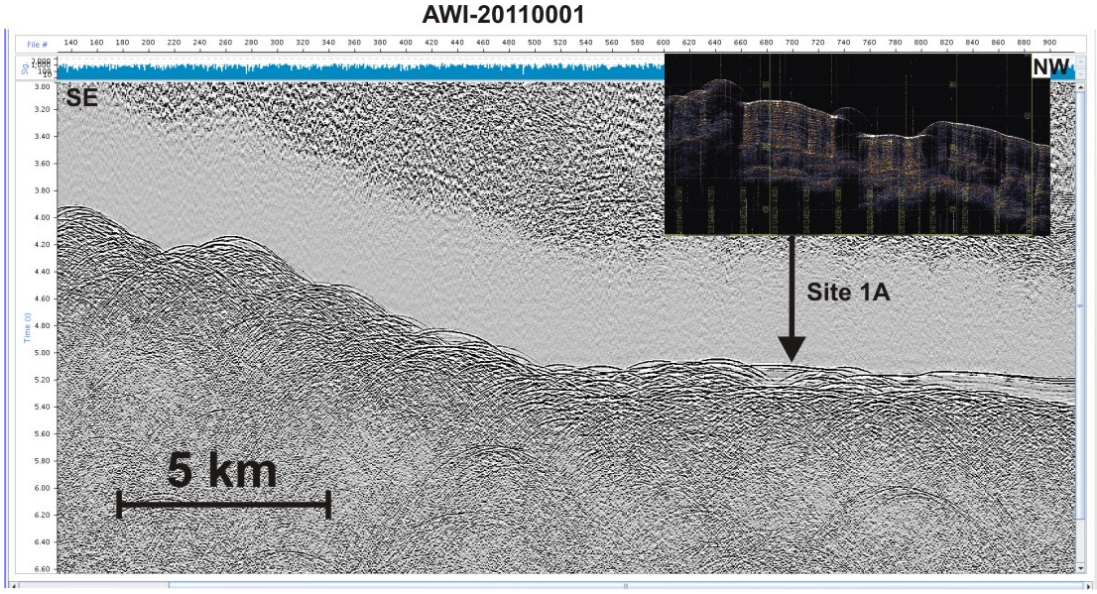

Fig. 4.8.2-2: *Part of line AWI-20110001. The figure shows a screen shot of the single-channel display. The vertical axis is two-way travel-time in seconds. The location of the proposed IODP-Site 1A is marked by a black arrow. The inclusion shows the corresponding Parasound profile.*

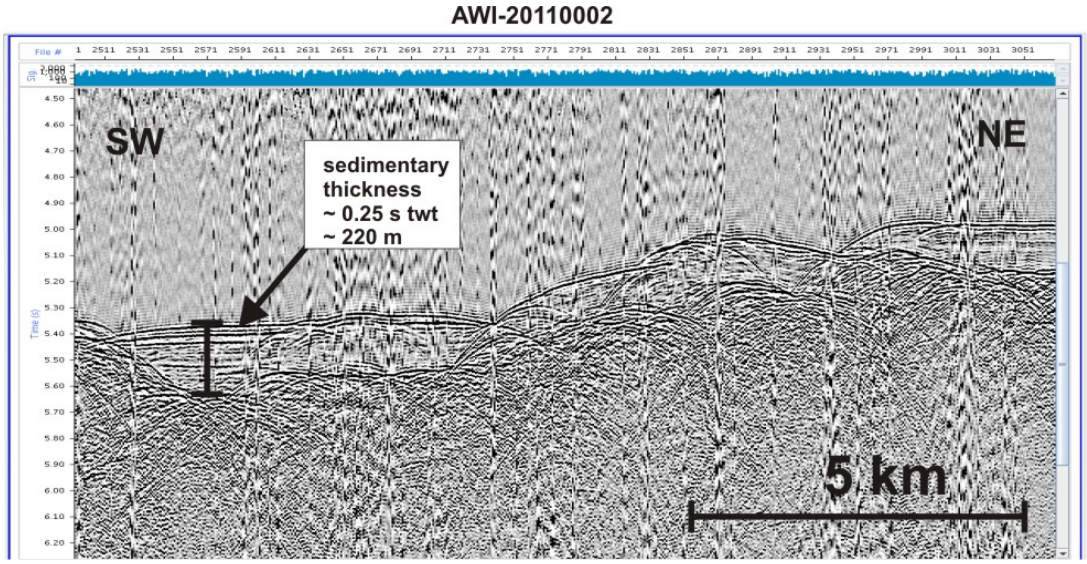

Fig. 4.8.2-3*: Part of line AWI- 20110002 located approximately 650 km west off the East Pacific Rise. The vertical axis of this single channel screen shot is in two-way travel-time in seconds.*

Profiles 20110004 and 20110005 were recorded perpendicular towards the EPR to detect any sedimentary drifts for bottom-current reconstructions. The basement age reaches from Middle Miocene at the start of the lines to Pliocene at the end of line 20110005. The depth of the seafloor rises gently along this transect from 5.2 s twt to 4.5 s twt (3900 -3300m). The basement topography along the whole transect is undulated as indicated by numerous diffraction hyperbolas. The thickness of the sedimentary cover decreases from 0.15 s twt

below the resolution of the seismic records approaching the EPR (Fig. 4.8.2-4). Initial screening of the single channel data onboard did not reveal any significant drift bodies, thus a careful inspection of the processed data is necessary to clarify this.

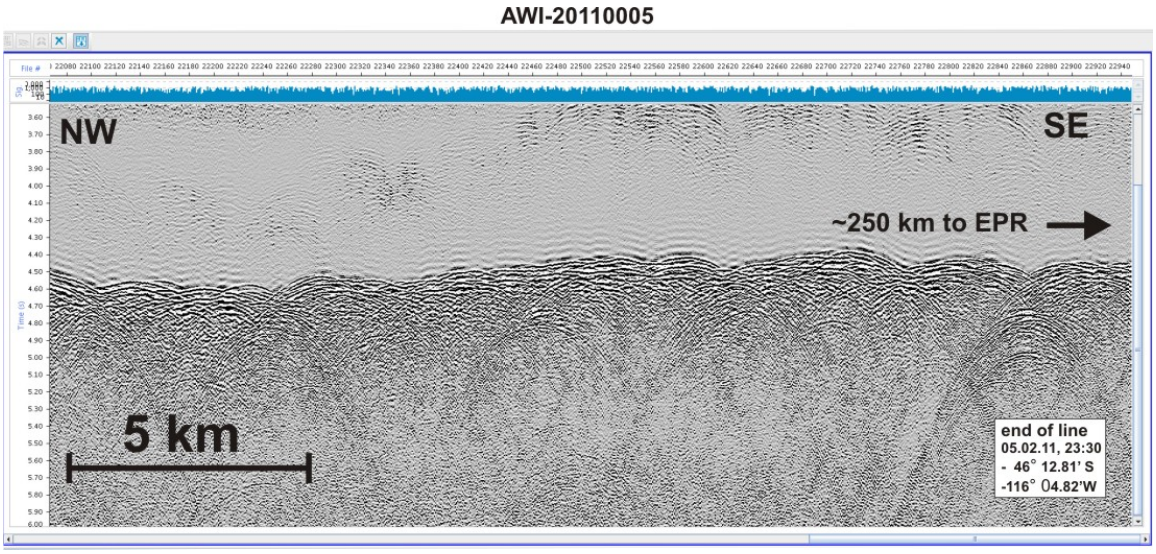

***Fig. 4.8.2-4**: Part of line AWI- 20110005 located approximately 250 km west off the East Pacific Rise. The vertical axis of this single channel screen shot is in two-way travel-time in seconds. Diffraction hyperbolas indicate a rough topography of outcropping basement. The thickness of any sedimentary cover is below the resolution of the seismic records.*

Second profile sequence, Bounty Trough

The second area of interest aimed the mouth of the Bounty Trough (BT) and the Bounty Fan (BF) around ODP Site 1122. This region is characterized by a high sedimentary input from the New Zealand Mountains. Sediments were transported downslope by turbidity channels and entrained into the north-ward flowing Deep Western Boundary Current (DWBC). The interaction of both, lateral current controlled deposition and downslope transport led to the building of a complex sedimentary drift system. Processing and interpretation of the seismic profiles will allow to derive the geometry and internal structure of the drifts in order to reconstruct the path and strength of the current system. Individual reflectors can be dated by a correlation with ODP Site 1122 data. Originally, the seismic survey was planned to cover the region around the BF, but due to an upcoming Taifun seismic profiling had to be shifted towards the centre of the BT. A sequence of 5 seismic reflection profiles with a total length of 570 km was recorded along the Bounty Trough and Bounty Channel off New Zealand (Fig. 4.8.2-5). For a few times air-gun operation had to be stopped due to some whale occurrence close to the ship (Tab. 4.8.1-2).

The easternmost line AWI-20110006 runs from the left bank levee of the abyssal Bounty Fan towards its centre crossing the location of ODP Site 1122 (Fig. 4.8.2-6). A gently undulating basement reflector is overlain by a series of reflectors indicating a sedimentary cover with a total thickness of 1.5 s twt (~ 1300 m). This package can be subdivided at least into three different acoustic units. The uppermost unit is about 0.4 s twt thick (300-400m) and consists of reflector series with wavy character indicating current controlled deposition. The sequence below with a thickness of 0.3 s twt (~ 250 m) shows horizontal, conform and continuous layering. The third unit has a gently undulating surface and exhibits a transparent reflection pattern. Its thickness amounts about 0.8 s twt (750 m).

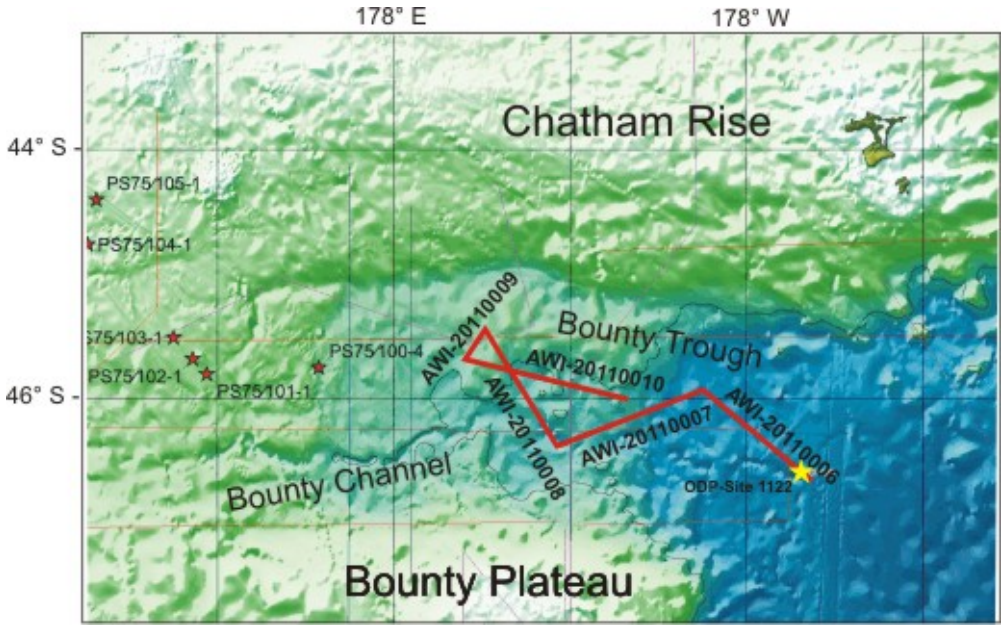

Fig. 4.8.2-5: *Bathymetric map of the Bounty Trough east off New Zealand. Thick red lines mark the location of the seismic reflection profiles AWI-20110006 to AWI- 201100010. Thin red lines show former tracks. Stars mark the location of Sediment cores of* RV Polarstern *cruises (red) and the ODP Site 1122 (yellow).*

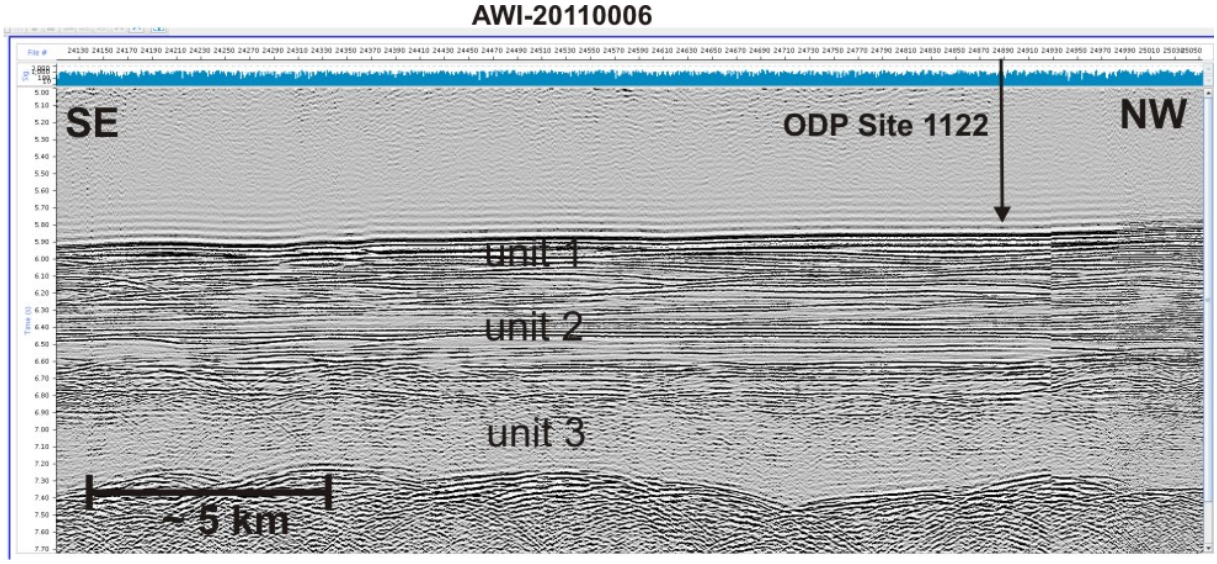

Fig. 4.8.2-6*: Part of line AWI- 20110006 located in the Bounty Trough off New Zealand. The vertical axis of this single channel screen shot is in two-way travel-time in seconds. The location of ODP site 1122 is marked by an arrow.*

Line AWI-20110007 runs from the centre of the Bounty Fan southwards crossing the northern half of the Bounty Channel. The seafloor topography rises gently towards the southwest and is more and more interrupted by vertical displacements, which reach up to 0.1 s twt (80 m) (Fig. 4.8.2-7). Towards the Bounty Channel the basement reflector become less undulated and rises from 6.9 s to 5.3 s twt depth. At the same time the sedimentary package thins from 1.5 s twt to 0.8 s twt thickness. Due to numerous diffraction hyperbolas the subdivision of the sedimentary package becomes less clear.

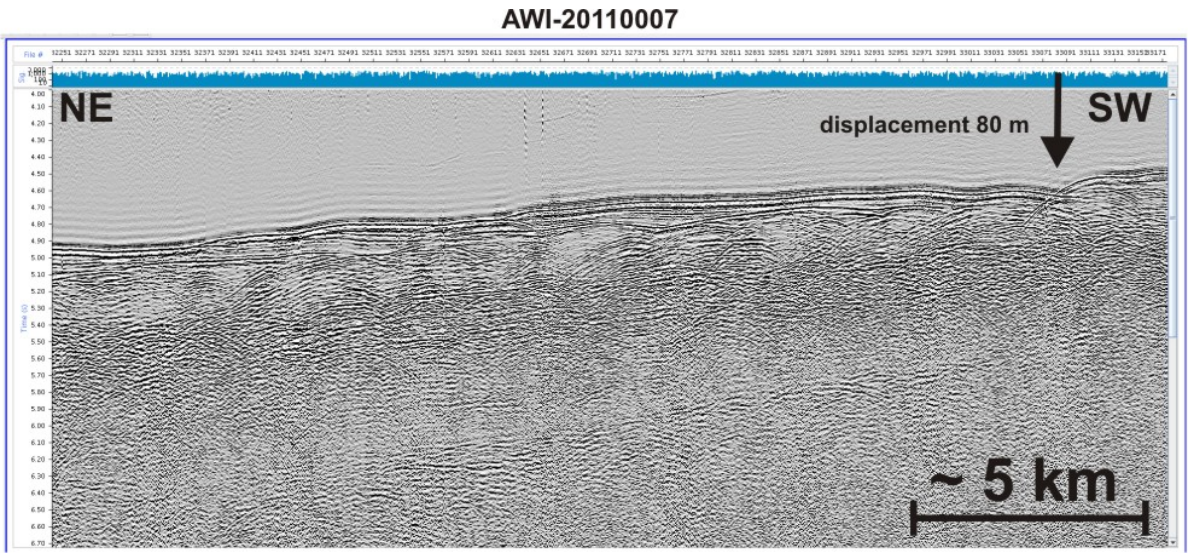

***Fig. 4.8.2-7**: Part of line AWI- 20110007 located showing several surface undulations and a vertical displacement (arrow). The vertical axis of this single channel screen shot is in two-way travel-time in seconds.*

Line AWI-20110009 is the westernmost profile of our seismic survey and runs from the centre of the Bounty Trough southwestwards (Fig. 4.8.2-8). In the northeast, the basement has a significant depth of 4.6 s twt overlain by a thick sedimentary package of 1.1 s twt (almost 1000 m). This package can be subdivided into four acoustic units. The deepest one shows an undulated surface, owns a scattered reflection pattern, and onlaps the base reflector in the southwest. In the second unit the reflectors amplitudes are much lower but indicate a continuous and conformable layering. The third unit is also quite transparent with reflectors series of low amplitude running through. It has an undulated surface and onlaps also on the rising basement. The uppermost unit consists of strong amplitude reflectors, which rest on the undulations of the layer below. Its uppermost reflectors show in some parts truncation at the seafloor.

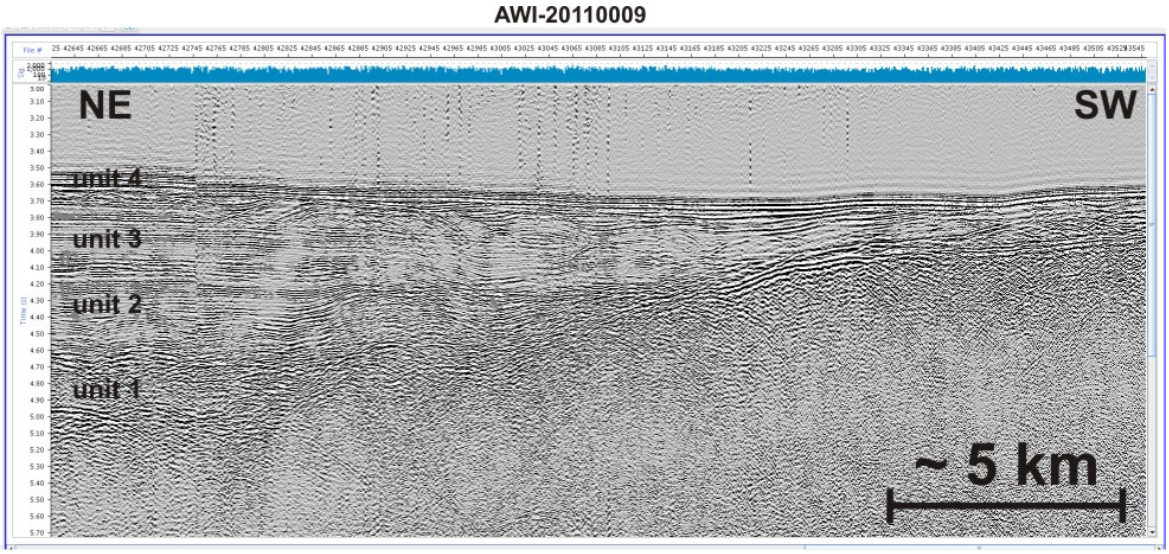

***Fig. 4.8.2-8**: Part of line AWI- 20110009 showing four acoustic units. The vertical axis of this single channel screen shot is in two-way travel-time in seconds.*

Table 4.8.2-1. Summary of seismic reflection profiles

Profile #	Start end	Date (UTC)	Time (UTC)	Latitude	Longitude	Shot #	Record Length [s]	Samp. Rate [ms]	Shot Interval [s]	Profile Length [km]	GI-Gun array	Tape	Comment
20110001	Start End	03.02.11 03.02.11	01:33:40 04:45	-43.827000 -43.6328333	-120.377231 -120.5583333	75 1035	10	1	12	26	4 x 2.7 ltr.	P00000 P00001	GI-4 Injector defect Time Difference: UTC-ship: 12:27:51 CMXL-operation report: 12:33:17 CMXL-recording report: 12:33:17 CMXL-disc report: 12:33:17
20110002	Start End	03.02.11 03.02.11	06:57 15:33	-43.7476667 -43.3571667	-120.5896667 -119.7965000	1804 4895	9	1	10	77.4	4 x 2.7 ltr.	P00000 P00001	GI-4 Injector defect Time Difference: “
20110003	Start End	03.02.11 04.02.11	17:26 10:27	-43.3230000 -44.5480000,	-119.9323333 -119.2798333	5753 11515	9	1	10	145.8	4 x 2.7 ltr.	P00000 P00001	GI-4 Injector defect Time Difference: UTC-ship: 11:35:59 CMXL-operation report: 11:41:27 CMXL-recording report: 11:35:59 CMXL-disc report: 11:35:59
20110004	Start End	04.02.11 05.02.11	10:27 02:44	-44.5480000 -45.3915000	-119.2798333 -117.7785000	11516 17561	9	1	10	151	4 x 2.7 ltr.	P00000 P00001	GI-4 Injector defect Time Difference: “
20110005	Start End	05.02.11 05.02.11	02:44 20:30	-45.3915000 -46.2135333	-117.7785000 -116.0803667	17562 23958	9	1	10	160.5	4 x 2.7 ltr.	P00000/P00001 P00002/P00003	GI-4 Injector defect Time Difference: “
20110006	Start End	24.02.11 25.02.11	15:06 08:42	-46.650000 -45.969500	-177.2683333 -178.4528333	24201 29763	9	1	10	133.4	4 x 2.7 ltr.	P00002 P00003	GI-4 Injector defect No time difference
20110007	Start End	25.02.11 26.02.11	10:24 01:10	-45.971500 -46.354516	-178.6078333 -179.9785000	30370 35513	9	1	10	136.9	4 x 2.7 ltr.	P00002 P00003	GI-4 Injector defect No time difference
20110008	Start End	26.02.11 26.02.11	03:16 17:42	-46.343833 -45.438833	+179.0166666 +179.0243333	36283 41467	9	1	10	121.2	3 x 2.7 ltr.	P00002 P00003	GI-4 defect No time difference
20110009	Start End	26.02.11 26.02.11	18:53 22:58	-45.479000 -45.701333	+179.0211666 +178.8080000	41893 43163	9	1	10	32.5	3 x 2.7 ltr.	P00002/P00003 P00004/P00005	GI-4 defect No time difference
20110010	Start End	26.02.11 27.02.11	23:20 17:00	-45.723000 -46.019000	+178.8293333 -179.3528333	43303 49664	9	1	10	147.1	3 x 2.7 ltr.	P00004 P00005	GI-4 defect No time difference

4.9 Volcanology

4.9.1 Rock sampling - Methods

Rock sampling on seamounts and volcanic ridges during SO213 was carried out using chain bag dredges (Fig. 4.9.1-1). Chain bag dredges are similar to large steel buckets with a chain bag attached to their bottom and steel teeth at their openings, which are dragged along the ocean floor by the ship or the ship's winch. Volcanic glass sampling along the active PAR was carried out using a 'Vaseline' rock corer. The rock corer used during SO213 (Fig. 4.9.1-2) consisted of 7 steel cups, each 6 cm in diameter, screwed to the base of 40 cm diameter steel plate that was attached to a ~1500 kg weight. The sampling cups were filled with chilled Vaseline prior to the rock corer being lowered at 1.0 metre/sec until it hit the PAR and volcanic glass shards became embedded in some or all of the Vaseline filled cups.

Fig. 4.9.1-2: Rock corer. The shattered pieces of rock stick to the small containers, which are filled with Vaseline and demonstrate a successful sampling of the volcanic crust.

Fig. 4.9.1-1: Chain bag dredge

Once the rock corer was on-board the glass shards were combined together from the various sample cups for later cleaning with warm water. In the case of each dredge-haul large rocks were measured and then broken into manageable sizes. A selection of the rocks were cleaned and cut open using a rock saw. The rocks were then grouped according to all aspects of their lithology, including the primary mineralogy and degree of alteration/weathering, and/or the presence of Mn encrustations. The immediate aim of these observations was to determine the material most suitable for geochemistry and isotopic age dating. Fresh glass extracted whenever it was present and blocks of the freshest representative samples were then cut for thin section and microprobe preparation, geochemistry and isotopic dating.

SO213 rock and glass samples will be analyzed using a variety of different geochemical methods and, in the of rock samples, by $^{40}Ar/^{39}Ar$ laser dating. Major element geochemistry measured by X-ray fluorescence (XRF) and electron microprobe (EMP) will constrain magma chamber processes within the crust, and also yield information on the average depth of melting, temperature and source composition to a first approximation. Trace element data measured by inductively coupled plasma mass spectrometry (ICP-MS) may help to define the degree of mantle melting and to characterize the chemical composition of the source. Long-lived radiogenic isotopic ratios measured by Thermal Ionization Mass Spectrometry (TIMS) and Multi-Collector ICP-MS such as $^{87}Sr/^{86}Sr$, $^{143}Nd/^{144}Nd$, $^{206}Pb/^{204}Pb$, $^{207}Pb/^{204}Pb$,

$^{208}Pb/^{204}Pb$, and $^{187}Hf/^{188}Hf$ are independent of the melting process and reflect the long term evolution of a source region and thus serve as tracers to identify mantle (and recycled crust) sources. Through integration of the various geochemical parameters, age data, morphological and volcanological data the origin and evolution of the sampled structures can be reconstructed.

4.9.2. Sampling report and preliminary results

Sampling sites were selected on the basis of SIMRAD EM120 multibeam mapping and the GEBCO 8 dataset. The maps in this section were all created by W. Borchert and A. Ehmer (RF Forschungsschiffahrt GmbH, scientific and technical department) (WTD) onboard RV SONNE. This section gives background information and short summaries of the sampling and mapping together with some preliminary results. Refer to Appendices F, G and H for exact latitude, longitude, and depth of dredge sites and rock descriptions. An overview of the tectonic setting, bathymetry, volcanology sample stations and ship's track is shown on Figure 4.9.2-1.

Overlapping Spreading Ridge (VSR 1 – 5)
Rock corer sampling of fresh volcanic glass at five locations along the Overlapping section of the PAR successful filled a crucial sampling gap north of the active Foundation hotspot (Figs. 4.9.2-1 and 4.9.2-2). The geochemical composition of these samples will establish how far hotspot mantle flows to the north of the main locus of hotspot volcanism marked by the geoid anomaly and hotspot trail morphology. This information will address fundamental questions concerning the actual size of the hotspot melting zone influencing the PAR.

Westerly Seamounts (DR 1 – 6)
Dredge sampling recovered pillow and flow lavas from four of the five volcanoes in a 110 km-long, NE trending chain of seamounts and from a volcano offset about 35 kilometres to the west (Fig. 4.9.2-3). Detailed EM120 multibeam maps of the sampled seamounts and locations of dredge stations are shown in Figures 4.9.2-4 to 4.9.2-7. Calderas are evident on the tops of the second (Fig. 4.9.2-5), third (Fig. 4.9.2-6) and sixth (Fig. 4.9.2-7) seamounts sampled during SO213.

The age and geochemical composition of the Westerly Seamount samples should provide important new insights into whether these off-axis seamounts were created age-progressively, synchronously or in some random sequence above a region of NE flowing hotspot mantle. Another possibility is that the seamounts formed in response to episodes of increase plate stress associated with the Juan Fernandez Microplate (Fig. 1.3-1, Fig. 1.4-1). The Westerly Seamount Chain is potentially also an extension of a prominent NE trending Foundation Chain VER (Fig. 4.9.2-1), which has a NE age-progression from 3.5 Ma to 2 Ma (Fig. 1.4-3). This 290 km-long line of VERs and volcanoes crosses three posited zones of coeval volcanism (Fig. 1.4-3) so age and geochemistry data should test the concepts of elongate zones of coeval hotspot volcanism, ~1 Myr periodicity, and plate migration over a broad Foundation hotspot. A fascinating possibility is that the progression from VER to seamounts shows for the first time that VERs form initially as progressive lines of seamounts or volcanic centres. As these volcanic centres continue growing, their lavas fill in the gaps between them to create a VER. Mapping of the Diagonal Ridges, discussed in the following section, shows evidence of a similar mechanism for VER formation.

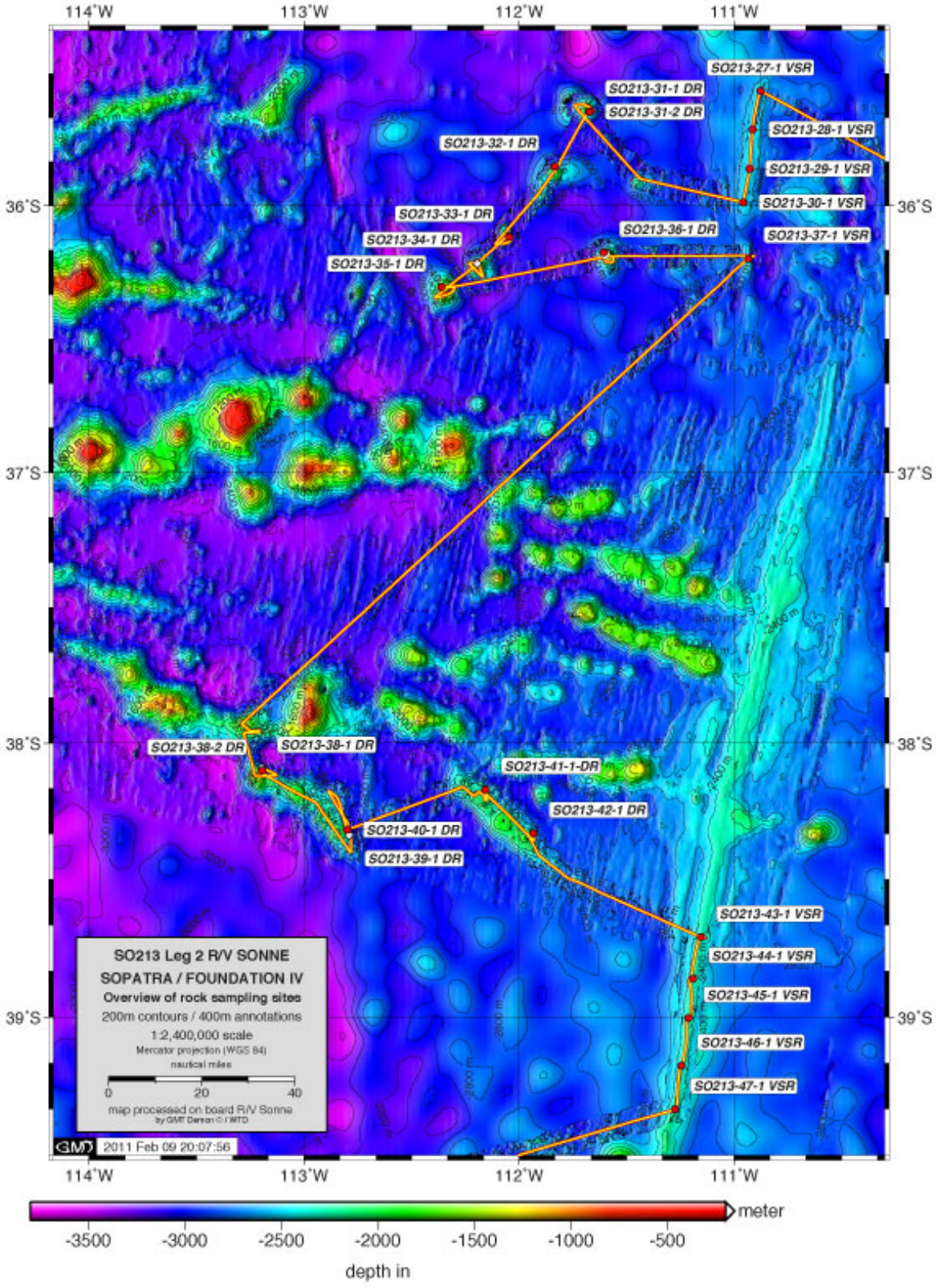

Fig. 4.9.2-1: Tectonic setting, bathymetry and volcanology sampling stations on the Foundation Chain and the Pacific-Antarctic Ridge (PAR) (yellow line is for ship's track). SO213 expedition station numbers are show. DR = Dredge Station, VSR = Rock Coring Station. Red disks = in situ rocks or glass fragments, white disks = empty dredge. Map is mixed grid with EM120 multibeam data and GEBCO 8.

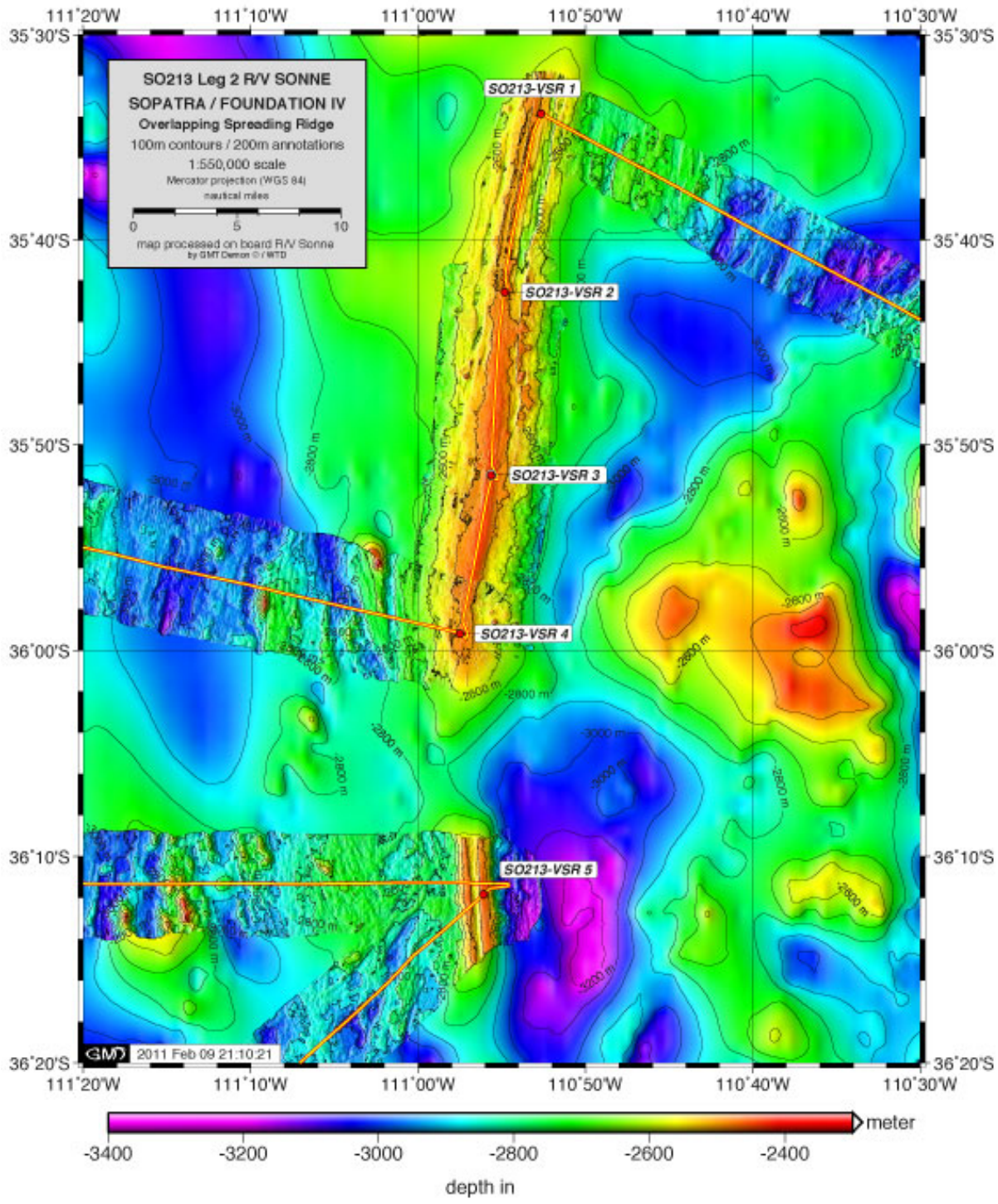

Fig. 4.9.2-2: Bathymetry and rock coring (VSR) stations on the Overlapping section of Pacific-Antarctic Ridge (PAR) located north of the Foundation Chain (yellow line is for ship's track). SO213 volcanology station numbers are shown. Note that sampling is on the 'axial-high' marking the most recent volcanism. Red disks = in situ glass sampled. Map is mixed grid with EM120 multibeam data and GEBCO 8.

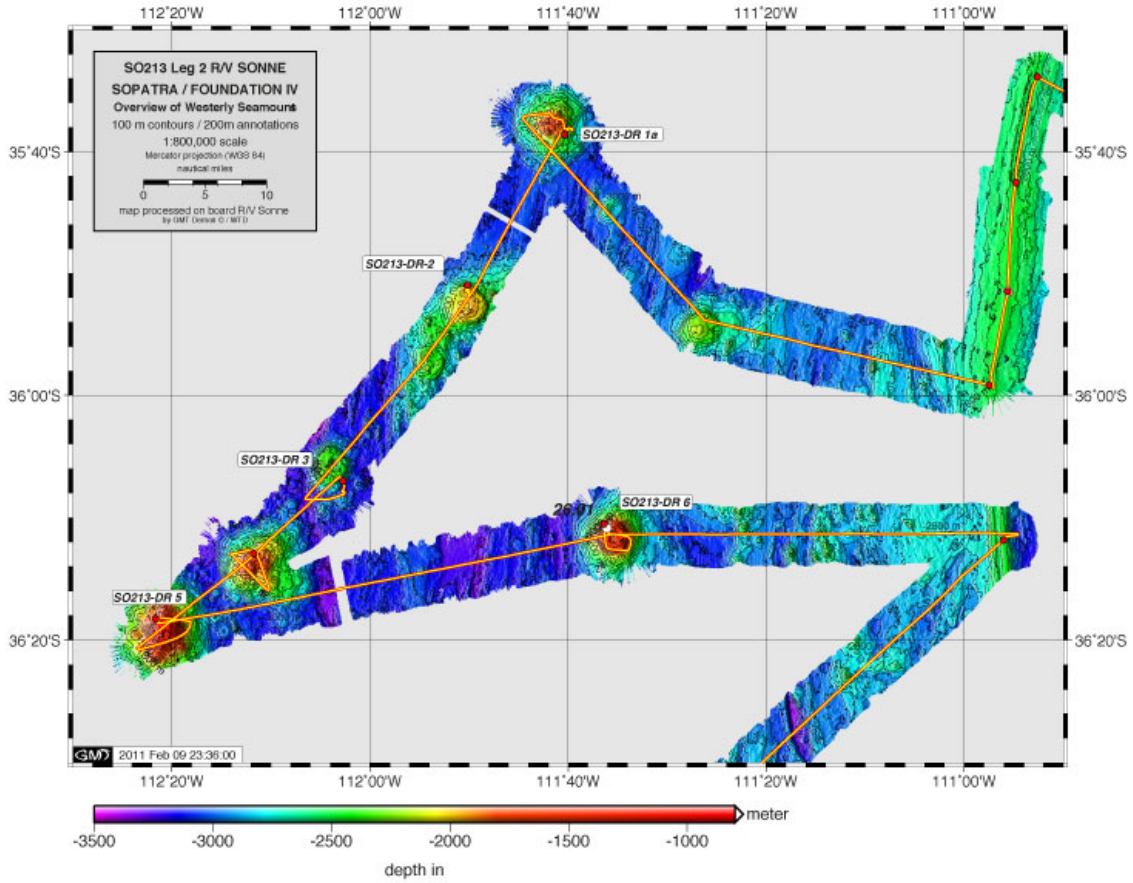

Fig. 4.9.2-3: Overview of bathymetry and dredge stations (DR) in the Westerly Seamounts. Note the NE trending Westerly Seamount Chain (yellow line is for ship's track). SO213 volcanology station numbers are shown only where in situ rocks were recovered. Map made with EM120 multibeam data.

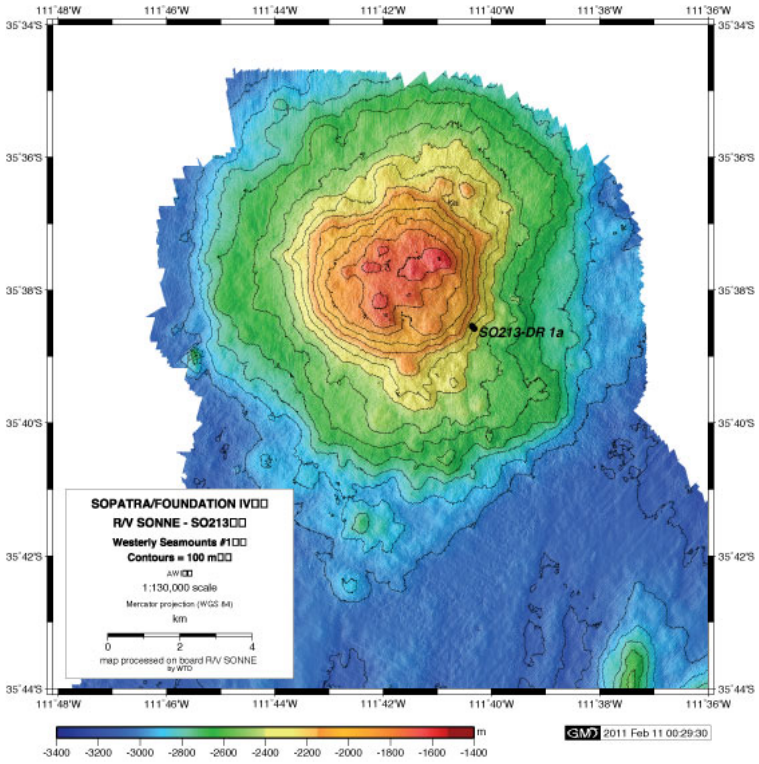

Fig. 4.9.2-4: Dredge station DR 1a on the seamount at the northern end of the Westerly Seamount Chain (see Fig. 4.9.2-3). Map made with EM120 multibeam data.

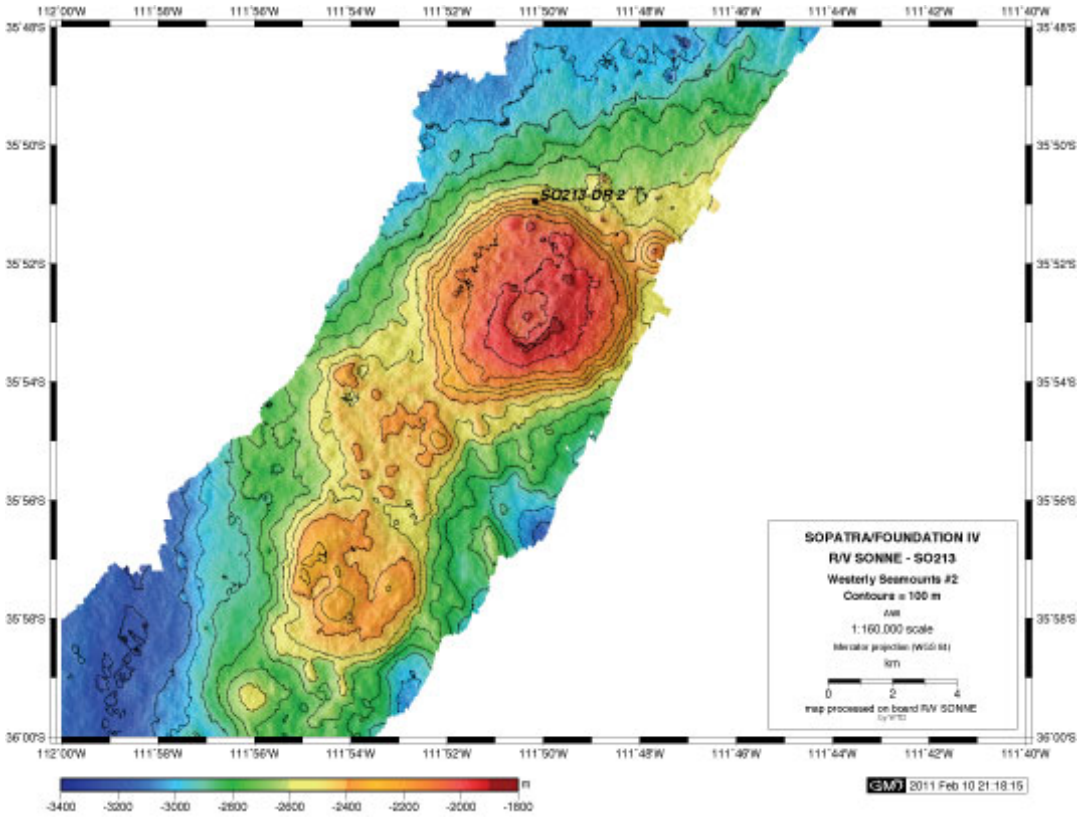

Fig. 4.9.2-5: Dredge station DR 2 on the second volcano sampled in the Westerly Seamount Chain (see Fig. 4.9.2-3). Note small caldera on the top. Map made with EM120 multibeam data.

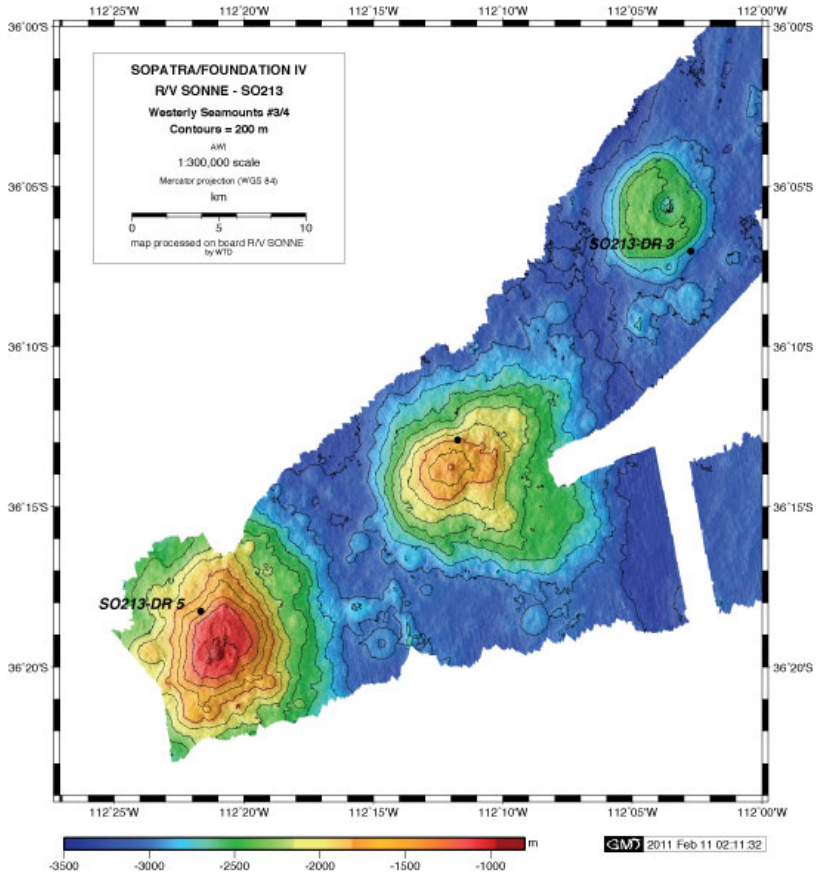

Fig. 4.9.2-6: Dredge stations DR 3 and DR 5 on the third and fourth volcanoes sampled in the Westerly Seamount Chain (see Fig. 4.9.2-3). Note the caldera on the volcano to the NE. Map made with EM120 multibeam data.

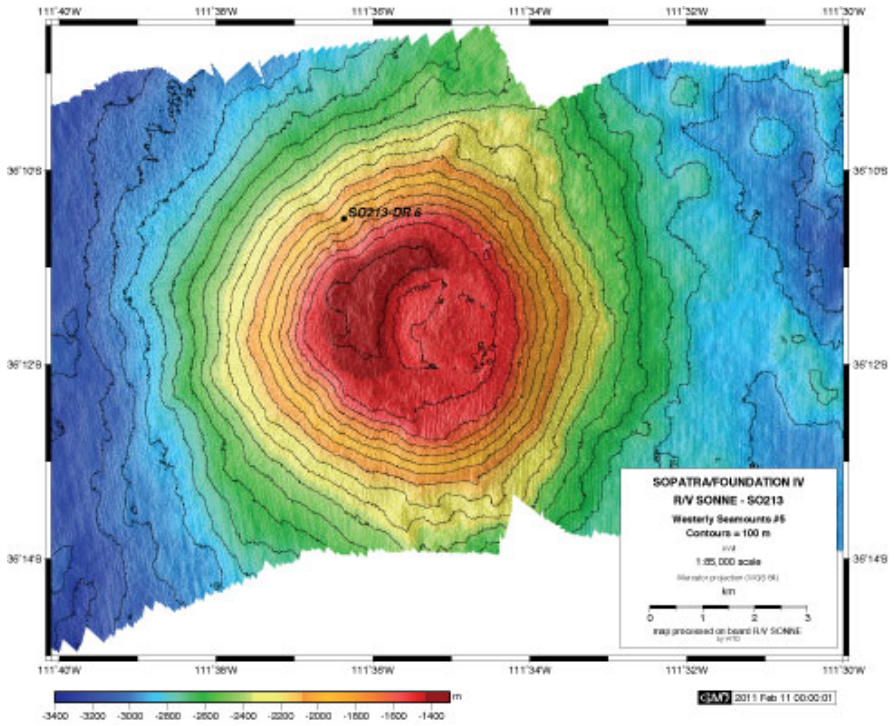

Fig. 4.9.2-7: Dredge station DR 6 on a Westerly Seamount offset 35 km east of the seamount chain (see Fig. 4.9.2-3). Note the caldera forming on the top. Map made with EM120 multibeam data.

Diagonal Ridges (DR 7a – 10)

Dredge sampling recovered pillow and flow lavas from the northern and southern ends of the SE trending co-parallel Diagonal Ridges (Figs. 4.9.2-8 - 4.9.2-10). The Diagonal Ridges are each ~60 km long, ~15 km wide, are located ~80 km apart and their midpoints are ~90 km (Diagonal Ridge #2) and ~170 km (Diagonal Ridge #1) from the active PAR (Fig. 4.9.2-8). Their unique SE trend compared to the E-W trend of the Foundation VERs to the north suggests that they might reflect a preferred SE flow direction of hotspot mantle at different times to the PAR. Existing ages show that the E-W trending VER to the north of Diagonal Ridge #1 and #2 is 2 Ma and 1 Ma, respectively (Fig. 1.4-3).

At the northern end of Diagonal Ridge #1 (Fig. 4.9.2-9) is a prominent volcano that rises to a depth of ~1500 m with a well-developed caldera (Fig. 4.9.2-11). In the middle of the ridge is a developing volcano that rises to a depth of about 1800 m with a small peak. The southern half of the ridge consists of less evolved volcanoes and lava flows rising to a depth of about 2000 m. The ridge-like structure of Diagonal Ridge #1 seems to have evolved (or be evolving) from three to four growing volcanic centres supplying lavas flows that are filling in gaps between them to form a VER.

The southern half of Diagonal Ridge #2 consists of two volcanoes rising to a depth of about 1800-1900 m. The one to the north is the better developed with a flat top and possibly a developing caldera while the other is less well evolved with a small peak (Fig. 4.9.2-10). The northern half of Diagonal Ridge #2 consists of lower relief volcanoes and/or lava flows rising to a depth of about 2200 m.

Age and geochemistry data for the Diagonal Ridges will establish if they are SE extensions of the prominent VERs to the north and if they formed age-progressively, synchronously or in some random sequence above a region hotspot mantle flowing to the SE. In conjunction with information from the Westerly Seamounts located on the opposite of the Foundation hotspot track, the concepts of elongate zones of coeval hotspot volcanism, ~1 Myr periodicity and plate migration over broad hotspot can all be tested using the SO213 rock samples and high resolution maps.

As proposed in the previous section, mapping of the Westerly Seamounts during SO213 has revealed first time that VERs form initially as (age-progressive?) lines of seamounts or volcanic centres, which continue growing and creating lava flows that fill in the gaps between them to create a VER. Interestingly, while the Diagonal Ridges show evidence of having

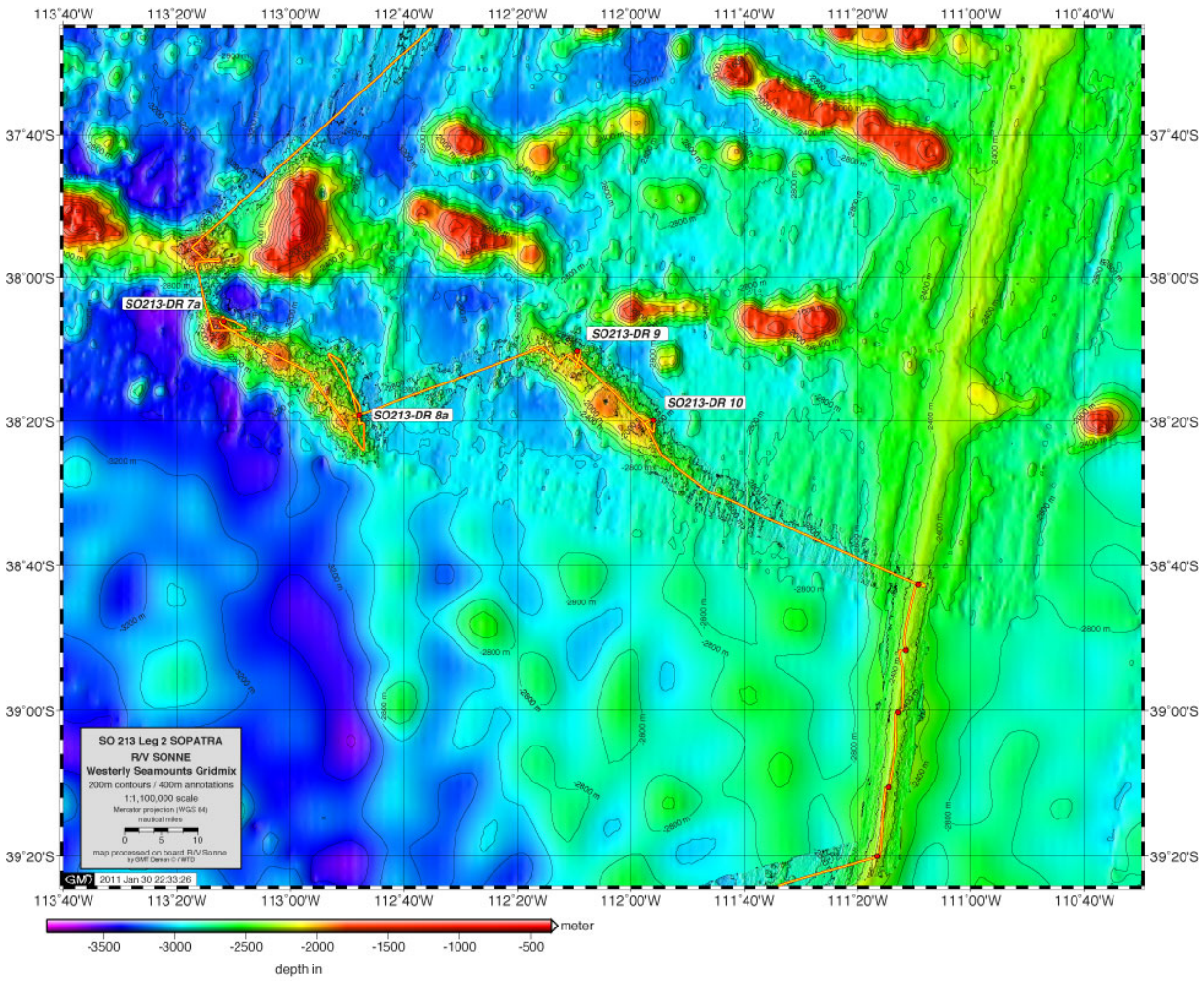

formed by this mechanism, they represent an intermediate stage between initial seamount and final VER formation.

Fig. 4.9.2-8: Overview of bathymetry and dredge stations (DR) on the Diagonal Ridges (yellow line is for ship's track). Map is mixed grid with EM120 multibeam data and GEBCO 8.

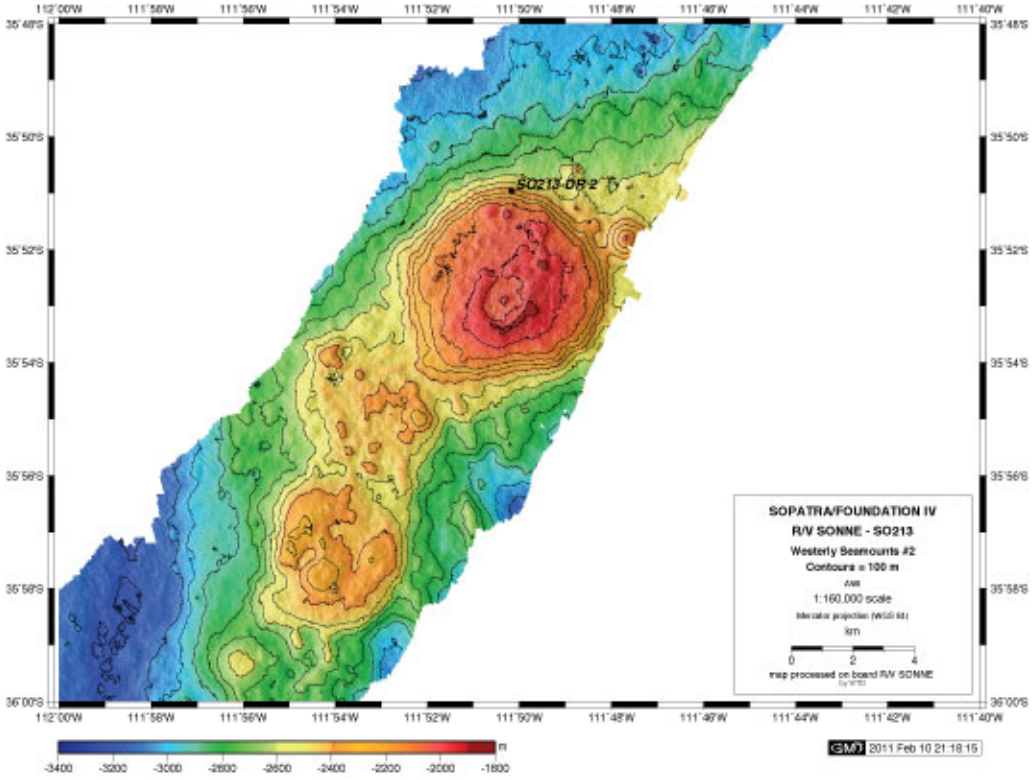

Fig. 4.9.2-9: Dredge sites DR 7a and DR 8a on the Diagonal Ridge (#1). Map is mixed grid with EM120 multibeam data and GEBCO 8.

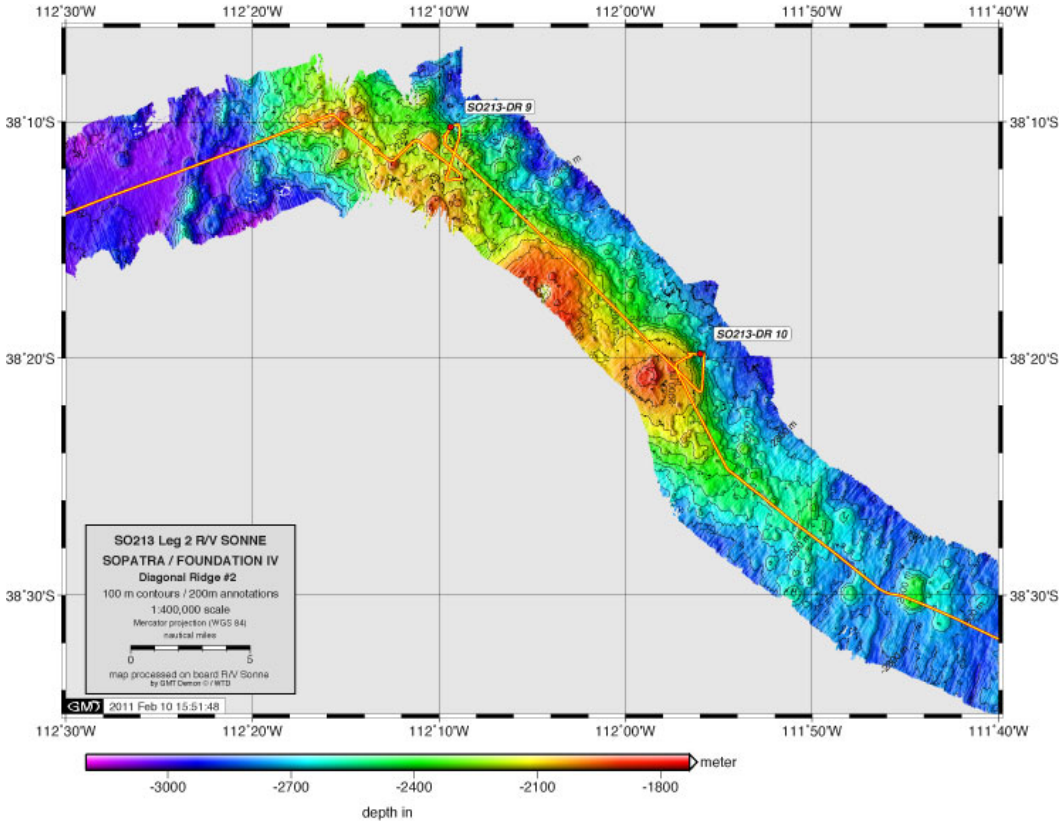

Fig. 4.9.2-10: Dredge sites DR 9 and DR 10 on the Diagonal Ridge (#2). Map made with EM120 multibeam data.

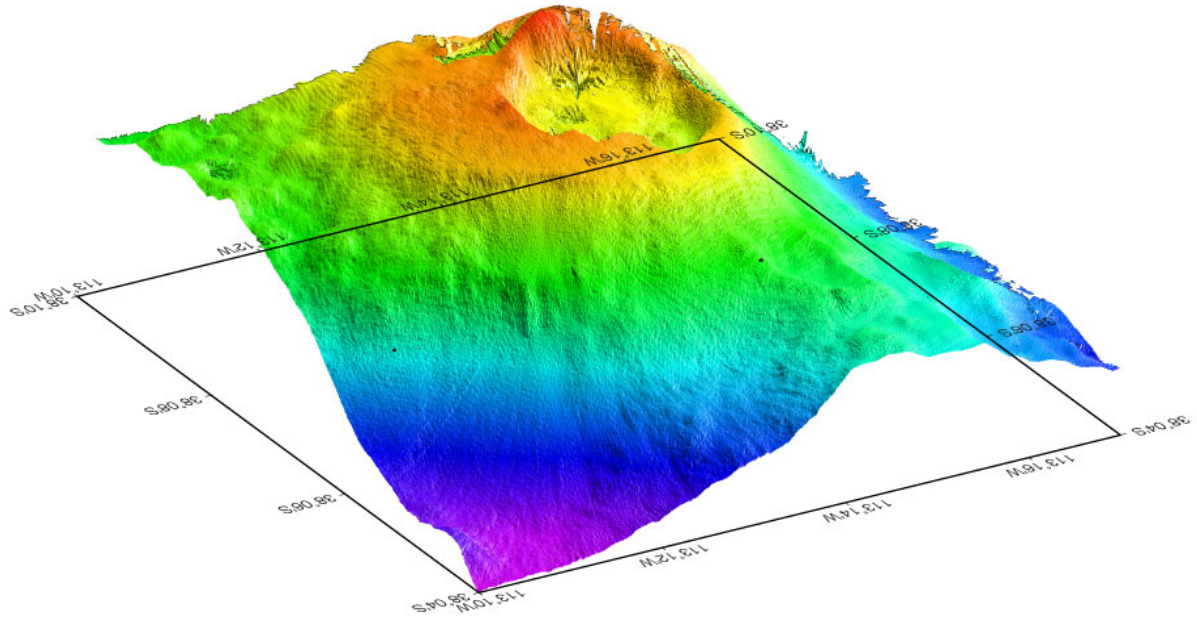

Fig. 4.9.2-11: Three-dimensional map shown caldera structure on seamount at the NW end of Diagonal Ridge #1. See Figure 4.9-9 for location of DR 7a on this volcano. Map made with EM120 multibeam data.

Southern PAR (VSR 6 – 10)

Rock corer sampling of fresh volcanic glass at five locations along the Southern PAR filled a crucial gap in sampling south of the Foundation hotspot (Fig. 4.9.2-12). One consequence of hotspot-ridge interactions is the presence of an additional hotspot-derived magma flux at the spreading-axis, which may enhance the development of a long-term robust magma chamber beneath the PAR crest. Such magma chambers permit processing and differentiation of primitive basaltic melts into more evolved andesitic and dacitic magmas. Elsewhere, highly differentiated lavas are erupted only at central volcanoes where the magma flux is the highest (e.g. Iceland). A cruise objective was to determine if there is SiO2-rich volcanism along the entire section of the PAR between 37°S and 40 °S, or are there two separate SiO2-rich areas linked to different regions of intraplate volcanism.

The geochemical composition of these samples will establish how far hotspot mantle flows to the south of the main locus of the hotspot volcanism marked by the geoid anomaly and hotspot trail morphology. This information will address fundamental questions concerning the size of the hotspot melting zone currently interacting with the PAR and test geochemical models linking the Foundation hotspot to a deep (plume?) or shallow mantle source.

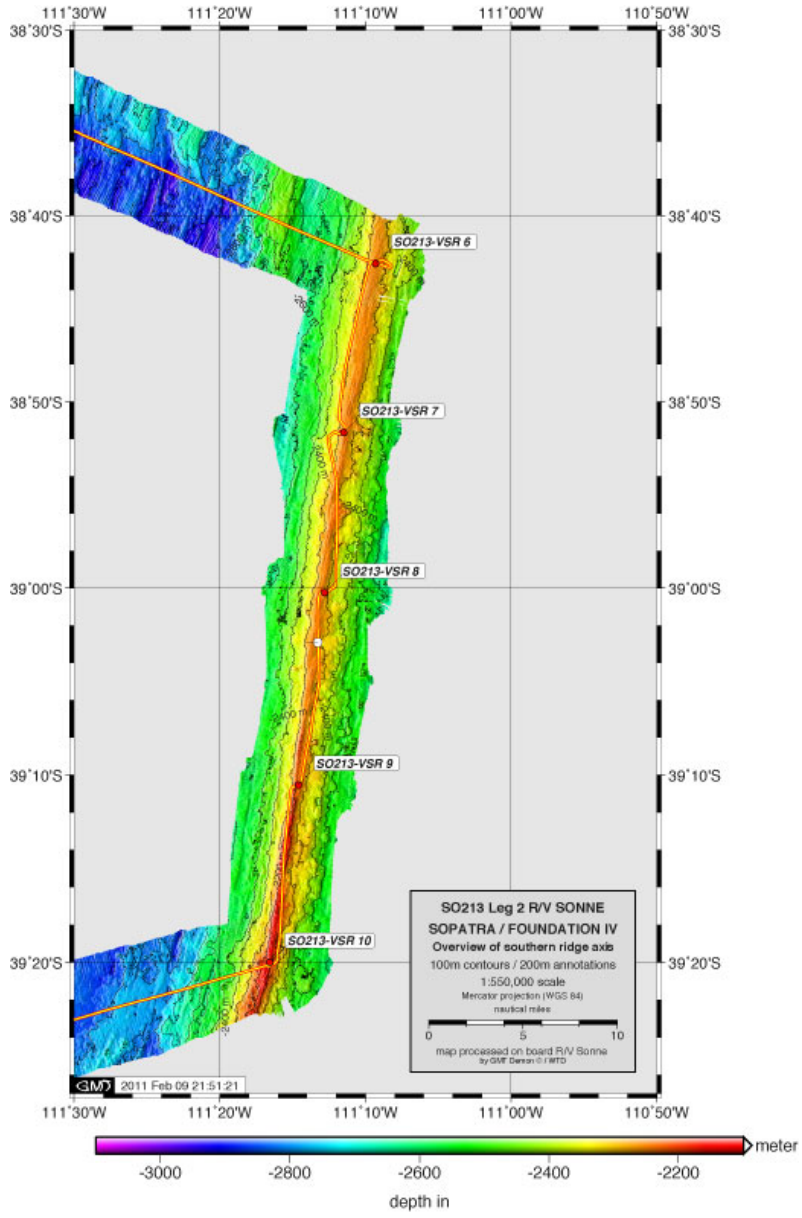

Fig. 4.9.2-12: Bathymetry and rock coring (VSR) stations on the section of the Pacific-Antarctic Ridge (PAR) south of the Foundation Chain sampled during the SO213 cruise (yellow line is for ship's track). Red disks = in situ glass sampled. Note that sampling is on the 'axial-high' marking the most recent volcanism. Map made with EM120 multibeam data.

4.9.3 Louisville Hotspot Trail (DR 11)

Background and sampling report

The Louisville Seamount chain in the SW Pacific (Fig. 4.9.3-1) formed over the last 80 Myr, at the same time as the Hawaiian-Emperor seamount chain. Age-progressive volcanism in the Hawaiian-Emperor seamount chain, and the fact that this is largely unaffected by the occurrence of the classic 'elbow' in the middle, the so-called Hawaiian-Emperor Bend (HEB), are the key observations underpinning the hypothesis that seamount chains form as tectonic plates that drift relative to fixed or slowly moving hotspots (Wilson, 1963). Hotspots are generally attributed to deep-seated mantle plumes or upwellings (Morgan, 1971) rising from a mantle boundary layer (either the core-mantle boundary, or the phase transition at 660 km depth). An alternative to this 'bottom-up' model is a 'top-down' plate-driven process in which

rifting of the lithosphere triggers shallow mantle melting (Anderson, 2000), although, as discussed by Tarduno et al. (2009), these alternative mechanisms (e.g., propagating cracks) may be insufficient (Sleep 2007) to explain the large volume flux and longevity of the Hawaiian hotspot and the geometry of its track. Seismic imaging of the mantle is still unable to distinguish between these possibilities, although recent seismic imaging of the mantle beneath the Hawaiian Islands (Wolfe et al., 2009) shows a several hundred kilometre-wide region of low velocities compatible with an upwelling high-temperature plume from the lower mantle.

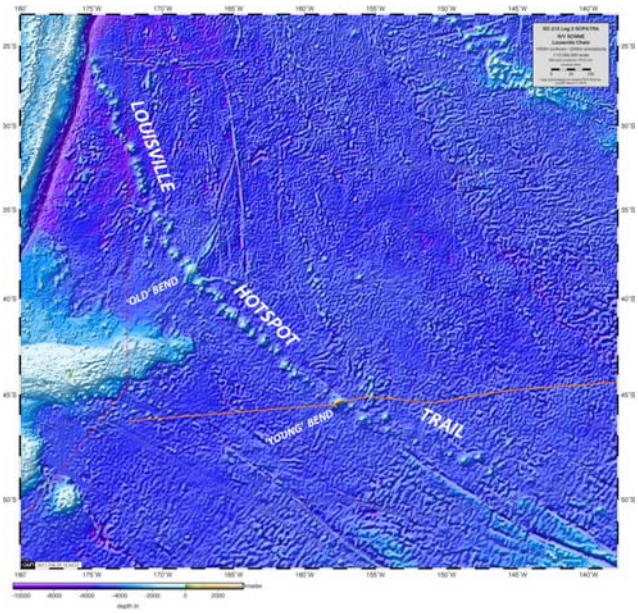

Fig. 4.9.3-1: Tectonic setting, bathymetry and volcanology working station (red symbol) on 157.6°W Guyot (Lonsdale, 1988) at the 'Young' Bend' in the Louisville hotspot trail (yellow line is for ship's track). Map made using GEBCO 8 database.

The relative motion between the Hawaiian and Louisville hotspots in the Pacific can be inferred by comparing the age records for their seamount trails. Estimates of their relative motion over time has consequences for understanding the role and character of deep mantle return flow in the largest continuous mantle region on Earth.

$^{40}Ar/^{39}Ar$ mineral ages for 18 lavas from 10 seamounts in the Hawaiian-Emperor seamount chain dredge sampled during the SO100 expedition of the RV Sonne (Ackermand et al., 2009) show that the slope of the along-track distance to the currently-active Hawaiian hotspot versus age plot is constant between ~59 and 25 Ma in the central ~1900 km of the seamount chain, including the HEB (O'Connor et al., submitted (a)). This linear model predicts that, between ~15 Ma and the present, age progression was twice as fast at the young end of the Hawaiian Chain. $^{40}Ar/^{39}Ar$ mineral ages for lavas dredge sampled from the Louisville hotspot trail during the SO167 expedition of the RV Sonne (Stoffers et al., 2003) show that the relation of age versus distance in this South Pacific seamount trail was also approximately linear between ~60 and 35 Ma (O'Connor et al., submitted (b)).

A very important question is whether age progression was also twice as fast between ~15 Ma and the present in the Louisville hotspot trail? Faster age-progression for the past 15 Myr on both hotspot trails would show that either the Pacific plate increase speed or both hotspots began moving in the opposite direction to the motion of the Pacific plate. If not, it would imply that faster age progression in the Hawaiian-Emperor chain reflects a local plate or mantle process related potentially related to recent seismic imaging of the mantle beneath the Hawaiian Islands (Wolfe et al., 2009) showing a several hundred kilometre-wide region of low velocities compatible with an upwelling high-temperature plume from the lower mantle.

Another possibility suggested by recent imaging is ponding of hot material near 670 km depth (and not by a narrow vertical lower mantle plume) beneath Hawaii (Li et al., 2008).

The track of the RV Sonne to the working area near New Zealand passed directly over a large guyot, named the 157.6°W Guyot by Lonsdale (1988) (Fig. 4.9.3-2) located at the 'Young Bend' at the virtually un-sampled young end of the Louisville hotspot trail (Fig. 4.9.3-3). We recovered rounded small boulders with excellent potential from dating and geochemistry studies embedded in breccia and coated with Mn-crust. $^{40}Ar/^{39}Ar$ dating and geochemical analysis of these samples will test for faster age-progress in the last 15-20 Myr, determine the age of the 'young Bend', and establish the geochemical composition of the Louisville mantle source (plume?) at the time of the young Louisville Bend.

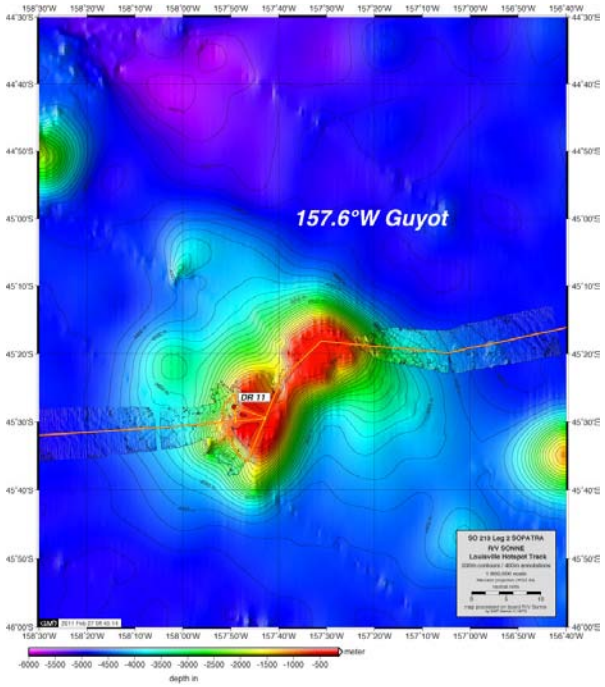

Fig. 4.9.3-2: Dredge site DR 11 on the 157°W Guyot (Lonsdale, 1988) marking the 'Young' Bend in the Louisville hotpot trail (yellow line is ship's track). Map is mixed grid using EM120 multibeam data and GEBCO 8.

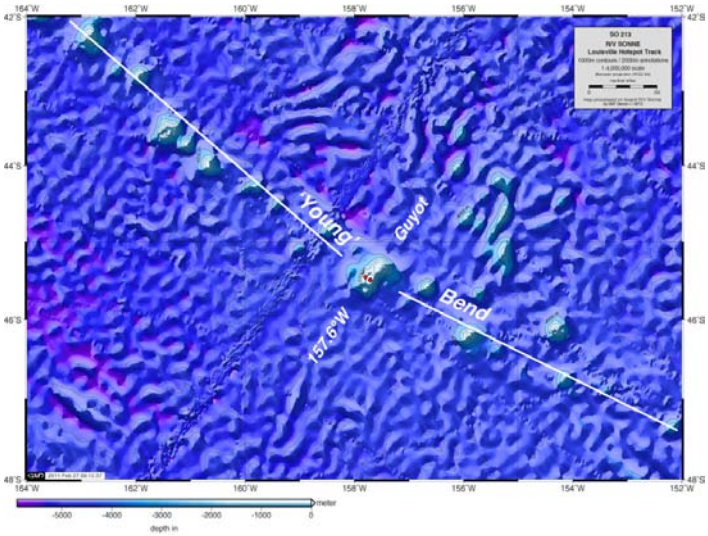

Fig. 4.9.3-3: Dredge site DR 11 on the 157.6°W Guyot. White lines show changed trending of the Louisville hotspot trails before and after formation of the 'Young Bend'. Map made using GEBCO 8 database.

5. REFERENCES

Ackermand et al., 1999. Cruise Report SONNE 141, HULA 1 Expedition. Report Nr. 8, Institute for Geosciences, University of Kiel, ISSN 0175-9302.

Anderson, D.L., 2000. The thermal state of the upper mantle; No role for mantle plumes. Geophys. Res. Lett. 27, 3623-3626.

Armand, L.K., 1997, The use of diatom transfer functions in estimating sea-surface temperature and sea-ice in cores from the southeast Indian Ocean [PhD thesis]: Canberra, The Australian National University.

Backman, J., and N. J. Shackleton (1983), Quantitative biochronology of Pliocene and early Pleistocene calcareous nannofossils from the Atlantic, Indian and Pacific oceans, Mar. Micropaleontol., 8 (2), 141-170, doi: 10.1016/0377-8398(83)90009-9.

Belkin, I.M. und Gordon, A.L., 1996. Southern Ocean fronts from the Greenwich meridian to Tasmania, J. Geophys. Res., 101, 3675-3696.

Berggren, W.A., Kent, D.V., Swisher, C.C., Aubrey, M.-P., 1995. A revised Cenozoic geochronology and chronostratigraphy. In "Geochronology, time scales and global stratigraphic correlation." (W. A. Berggren, and others, Eds.), pp. 129-212. SEPM Special Publication 54.

Boersma, A., 1986. Biostratigraphy and biogeography of Tertiary bathyal benthic foraminifers: Tasman Sea, Coral Sea and on the Chatham Rise (Deep Sea Drilling Project, Leg 90). In "Initial Reports of the Deep Sea Drilling Project." (J. P. Kennett, and C. C. von der Borch, et al, Eds.), pp. 961-1035. U.S. Govt. Printing Office, Washington.

Bown, P. R, Young, J.R., 1998. Introduction. In: Bown, P. R. (Ed.) Calcareous nannofossil biostratigraphy, Chapman & Hall, London, pp. 1-15.

Carter, L., Neil, H.L., McCave, I.N., 2000. Glacial to interglacial changes in noncarbonate and carbonate accumulation in the SW Pacific Ocean, New Zealand. Palaeogeography, Palaeoclimatology, Palaeoecology 162, 333-356.

Chaigneau, A. and Pizarro, O., 2005. Surface circulation and fronts of the South Pacific Ocean, east of 120 degrees W. Geophysical Research Letters, 32(8).

Cooke, P., Nelson, C.S., Crundwell, M., 2008. Miocene isotope zones, paleotemperatures, and carbon maxima events at intermediate water-depth, Site 593, Southwest Pacific. New Zealand Journal of Geology and Geophysics 51, 1-22.

Cooper, R.A. (Ed.) 2004. “The New Zealand Geological Timescale." Institute of Geological and Nuclear Sciences Monograph 22.

Crundwell, M.P. 2004. Miocene (Pareora, Southland and Taranaki Series). In "The New Zealand Geological Timescale." (R. A. Cooper, Ed.), pp. 165-194. Institute of Geological and Nuclear Sciences Monograph 22.

Crundwell, M.P., 2004. Pliocene-Pleistocene. In "The New Zealand Geological Timescale." (R. A. Cooper, Ed.). Institute of Geological and Nuclear Sciences Monograph 22.

Crundwell, M., Scott, G., Naish, T., Carter, L., 2008. Glacial–interglacial ocean climate variability from planktonic foraminifera during the Mid-Pleistocene transition in the temperate Southwest Pacific, ODP Site 1123. Palaeogeography, Palaeoclimatology, Palaeoecology 260, 202-229.

De Pol-Holz, R., Keigwin, L., Southon, J., Hebbeln, D. and M. Mohtadi, 2010. No signature of abyssal carbon in intermediate waters off Chile during deglaciation. Nature Geoscience, 3, 192-195. DOI: 10.1038/NGEO745.

Deacon G. E. R., 1982. Physical and biological zonation in the Southern Ocean. Deep-Sea Research, 29, l-15.

Devey, C.W. et al., 1997.The Foundation Seamount Chain: a first survey and sampling, Marine Geology 137, 191-200.

Faugeres, J.C., Stow, D.A.V., 1993. Bottom-current-controlled sedimentation: a synthesis of the contourite problem, Sediment. Geol., 82, 287-297.

Frank, M., Whiteley, N., Kasten, S., Hein, J.R., and O’Nions, R.K., 2002. North Atlantic Deep Water export to the Southern Ocean over the past 14 Myr: Evidence from Nd and Pb isotopes in ferromanganese crust. Paleoceanography, 17(2), 1022, 10.1029/2000PA000606.

Gersonde, R., Abelmann, A., Cortese G., Becquey, S., Bianchi, C., Brathauer, U., Niebler, Zielinski, U. und Pätzold, J., 2003. The late Pleistocene South Atlantic and Southern Ocean surface – A summary of time-slice and time-series studies, in Wefer, G., Mulitza, S., Ratmeyer, V., eds. The South Atlantic in the late Quaternary: Reconstruction of Material Budgets and Current Systems, Springer Berlin, 499-529.

Gersonde, R., Crosta, X., Abelmann, A. und Armand, L., 2005. Sea-surface temperature and sea-ice distribution of the Southern Ocean at the EPILOG Last Glacial Maximum – a circum-Antarctic view based on siliceous microfossil records, Quat. Sci. Rev., 24(7-9), 869-896, doi:10.1016/j.quascirev.2004.07.015.

Gersonde, R., Gohl, K., Billups, K., Tiedemann, R., Abelmann, A., Crosta, X., De La Rocha, C., von Eynatten, H., Filippelli, G.M., Flores, J.A., Koc, N., Kuhn, G., Kyte, F., Michel, E., Ninnemann, U., Shemesh, A. and G. Uenzelmann-Neben, 2010. Cenozoic Southern Ocean Pacific (CESOP): A full-proposal for drillingCenozoic history sites in the Pacific sector of the Southern Ocean.

Gildor, H., Tziperman, E., and Toggweiler, J.R., 2002, Sea ice switch mechanism and glacial-interglacial CO2 variations: Global Biogeochemical Cycles, v. 16, p. 10.1029/2001GB001446.

Gutjahr, M., Frank, M., Stirling, C.H., Keigwin, L.D., Halliday, A.N., 2008. Tracing the Nd isotope evolution of North Atlantic Deep and Intermediate Waters in the western North Atlantic since the Last Glacial Maximum from Blake Ridge sediments. Earth Planet. Sci. Lett., 266, 61-77.

Hays, J.D., Lozano, J.A., Shackleton, N.J., Irving, G., 1976. Reconstruction of the Atlantic and western Indian Ocean sectors of the 18,000 B. P. Antarctic Ocean , in Investigation of Southern Ocean Paleoceanography and Paleoclimatology, edited by R.M. Cline, J.D. Hays, Mem. Geol. Soc. Am., 145, 337–374.

Hayward, B.W., Kawagata, S., Grenfell, H.R., Sabaa, A.T., O'Neill, T., 2007. The last global extinction in the deep sea during the mid-Pleistocene climate transition. Paleoceanography 22, PA3103, doi:10.1029/2007PA001424.

Heezen, B.C., Hollister, C.D., Ruddiman, W.F., 1966. Shaping of the continental rise by deep geostrophic contour currents, Science, 152, 502-508.

Hékinian, R., Stoffers, P., Devey, C., Ackermand, D., Hemond, C., O'Connor, J., Binard, N., and Maia, M., 1997. Intraplate versus ridge volcanism on the Pacific-Antarctic Ridge near 37°S- 111°W, Journal of Geophysical Research 102, 12265-12286.

Hékinian, R., Stoffers, P., Ackermand, D., Revillion, S., Maia, M., and Bohn, M., 1999. Ridge-Hotspot interaction: The Pacific-Antarctic Ridge and the Foundation seamounts, Marine Geology 160, 199-223.

Hémond, C, and Devey, C.W., 1996. The Foundation Seamount chain, Southeastern Pacific: First isotopic evidence of a newly discovered hotspot track, VM Goldschmidt Conf J Conf Abstr.

Hémond, C., Maia, M., Gente, P., 1999. The Foundation Seamounts: Past and present ridge hotspot interactions? EOS Trans Am Geophys Union 80, 1056.

Hine, N., Weaver, P. P. E., 1998. Quaternary. In: Bown, P. R. (Ed.) Calcareous nannofossil biostratigraphy, Chapman & Hall, London, pp. 265-278.

Hornibrook, N.deB., 1982. Late Miocene to Pleistocene Globorotalia (Foraminiferida) from DSDP Leg 29, Site 284, Southwest Pacific. New Zealand Journal of Geology and Geophysics 25, 83-99.

Hornibrook, N.de.B, Brazier, R.C., Strong, C.P., 1989. Manual of New Zealand Permian to Pleistocene foraminiferal biostratigraphy.New Zealand Geological Survey Paleontological Bulletin 56, 175 p.

Hornibrook, N.deB., Jenkins, D.G., 1994. DSDP Site 594, Chatham Rise, New Zealand - Late Neogene planktonic foraminiferal biostratigraphy revised. Journal of Micropalaeontology 13, 93-101.

Hoskins, R.H., 1990. Planktonic foraminiferal correlation of the late Pliocene to early Pleistocene of DSDP Sites 284 and 593 (Challenger Plateau) with New Zealand stages. New Zealand Geological Survey Report Pal 149.

Howard, W.R., and Prell, W.L., 1992, Late Quaternary surface circulation of the southern Indian Ocean and its relationship to orbital variations: Paleoceanography, v. 7, p. 79-117.

Jeandel, C., 1993. Concentration and isotopic composition of Nd in the Southern Atlantic Ocean, Earth Planet. Sci. Lett., 117, 581-591

Kaiser, J., Lamy, F. and Hebbeln, D., 2005. A 70-kyr sea surface temperature record off southern Chile (Ocean Drilling Program Site 1233), Paleoceanography, 20, PA4009, doi:10.1029/2005PA001146.

Kennett, J.P., Srinivasan, M.S., 1983. "Neogene Planktonic Foraminifera: A Phylogenetic Atlas." Hutchinson Ross Publishing Company, Stroudsberg, Pennsylvania.

Koppers, A.A.P., Duncan, R.A. Steinberger, B., 2004. Implications of a nonlinear $^{40}Ar/^{39}Ar$ age progression along the Louisville seamount trail for models of fixed and moving hot spots. Geochem. Geophys. Geosys. 5, Q06L02, doi:10.1029/2003GC000671.

Labracherie, M., Labeyrie, L.D., Duprat, J., Bard, E., Arnold, M., JPichon, .-J., Duplessy, J.-C., 1989. The last deglaciation in the Southern Ocean. Paleoceanography, 4, 629–638.

Li, C., van der Hilst, R.D., Engdahl, E.R., Burdick, S., A new global model for P wave speed variations in Earth's mantle, Geochem. Geophys. Geosyst., 9, Q05018, doi:10.1029/2007GC001806, 2008.

Liu, Z. Y., Shin, S. I., Webb, R. S., Lewis, W. and Otto-Bliesner, B. L., 2005. Atmospheric CO2 forcing on glacial thermohaline circulation and climate. Geophys. Res. Lett. 32, 4, doi: 10.1029/2004gl021929.

Lonsdale, P., 1988. Geography and history of the Louisville hotspot chain in the Southwest Pacific. J. Geophys. Res. 93, 3078–3104

Lonsdale, P., 1994. Geomorphology and structural segmentation of the crest of the southern (Pacific-Antarctic) East Pacific Rise. J Geophys Res 99, 4683–4702.

Lourens, L. J., Hilgen, F. J., Shackleton, N. J., Laskar, J., Wilson, D., 2004. The Neogene Period. In: Gradstein, F. M., Ogg J. G., Smith, A. G. (Eds.), A Geological Time Scale, Cambridge University Press, Cambridge, pp. 409-440.

Maia, M., Ackermand, D., Dehghani, G.A., Gente, P., Hekinian, R., Naar, D., O'Connor, J., Perrot, K., Phipps Morgan, J., Ramillien, G., Revillon, S., Sabetian, A., Sandwell, D., and Stoffers, P., 2000. The Pacific-Arctic Ridge Foundation hotspot interaction: a case study of a ridge approaching a hotspot, Marine Geology 167, 61-84.

Maia, M., Hémond, C., and Gente, P., 2001. Contrasted interactions between plume, upper mantle, and lithosphere: Foundation chain case, Geochemistry Geophysics Geosystems, 2, 10.1029/2000GC000117.

Mammerickx, J., 1992. The Foundation Seamounts: tectonic setting of a newly discovered seamount chain in the South Pacific, Earth Planet Sci Lett 113, 293- 306.

Mazzullo, J.M., Meyer, A., and Kidd, R.B., 1988. New sediment classification scheme for the Ocean Drilling Program. In Mazzullo, J., and Graham, A.G. (Eds.), Handbook for Shipboard Sedimentologists:.ODP Tech. Note, 8:45-67.

Minolta Co. Ltd., 1995. Spectrophotometer CM-508d Instruction Manual, 32 pp.

Morgan, W.J., 1971. Convective plumes in lower mantle. Nature 230, 42–43.

Morgans, H.E.G., Scott, G.H., Beu, A.G., Graham, I.J., Mumme, T.C., St George, W., Strong, C.P., 1996. New Zealand Cenozoic Time Scale (version 11/96). In Institute of Geological and Nuclear Sciences Science Report 96/38, 12 p.

Morley, J.J., Prell, W.L., Howard, W.R., 1988. Response of the Southern Ocean over the Milankovitch frequency band. Eos Trans. AGU, 69, 299.

Morley, J.J., 1989. Variations in high-latitudes oceanographic fronts in the southern Indian ocean: An estimation based on faunal changes. Paleoceanography, 4, 547–554.

Ninnemann, U.S. und Charles, C.D., 2002. Changes in the mode of Southern Ocean circulation over the last glacial cycle revealed by foraminiferal stable isotopic variability, Earth Planet. Sci. Lett., 201, 383-396.

Niu, Y., Waggoner, D.G., Sinton, J.M., and Mahoney, J.J., 1996. Mantle heterogeneity and melting processes beneath seafloor spreading centers: The East Pacific Rise, 18°-19°S, J. Geophy. Res 101, 27711-27733.

Nürnberg, D. und Groeneveld, J., 2006. Pleistocene variability of the Subtropical Convergence Zone at East Tasman Plateau–Evidence from planktonic foraminiferal Mg/Ca (ODP Site 1172). Geochem., Geophys., Geosys. 7 (1), doi:10.1029/2005GC000984.

O'Connor, J.M., Stoffers, P., Wijbrans, J.R., 1998. Migration rate of volcanism along the Foundation Chain, SE Pacific, Earth Planet Sci Lett 164, 41–59.

O'Connor, J.M., Stoffers, P., and Wijbrans, J.R., 2001. En echelon volcanic elongate ridges connecting intraplate Foundation Chain volcanism to the Pacific-Antarctic spreading center, Earth Planet Sci Lett 192, 633-648.

O'Connor, J.M., Stoffers, P., and Wijbrans, J.R., 2002. Pulsing of a focused mantle plume: Evidence from the distribution of Foundation Chain hotspot volcanism, Geophy. Res Lett 29, DOI: 10.1029/2002GL014681.

O'Connor, J.M., Stoffers, P., and Wijbrans, J.R., 2004. The Foundation Chain: Inferring Hotspot- Plate Interaction from a Weak Seamount Trail, in Oceanic Hotspots, edited by R. Hekinian, P. Stoffers, und J.-L. Cheminee, pp. 349-374, Springer, Berlin.

O'Connor, J.M., Regelous, M., Koppers, A.A.P., Wijbrans, J.R., Haase, K., Stoffers, P., Steinberger, B., Mahoney, J.J., Re-dating the Hawaiian-Emperor bend: Implications for past mantle and plate motions, submitted (a).

O'Connor, J.M., Steinberger, B., Regelous, M., Koppers, A.A.P., Wijbrans, J.R., Haase, K., Stoffers, P. & Garbe-Schönberg, D., Widespread very-late rejuvenated volcanism on the western Louisville Seamounts, submitted (b).

Orsi, A.H., Whitworth, T. and Nowlin, W.D., 1995. On the meridional extent and fronts of the Antarctic Circumpolar Current. Deep-Sea Research Part I-Oceanographic Research Papers, 42(5): 641-673.

Pahnke, K. und Zahn, R., 2005. Southern Hemisphere Water Mass Conversion Linked with North Atlantic Climate Variability, Science, 307, 1741-1746.

Pahnke, K., Zahn, R., Elderfield, H., Schulz, M., 2003. 340,000-year centennial-scale marine record of Southern Hemisphere climatic oscillations. Science 301, 948-952.

Pahnke, K., Goldstein, S. & Hemming, S., 2008. Abrupt changes in Antarctic Intermediate water circulation over the past 25,000 years. Nature Geosci. 1, 870-874.

Perch-Nielsen, K., 1985. Cenozoic calcareous nannofossils. In: Bolli, H. M., Saunders, J. B., Perch-Nielsen, Y.K. (Eds.), Plankton Stratigraphy, Cambridge University Press, Cambridge, pp. 427-555.

Pichon, J.J., Bareille, G., Labracherie, M., Labeyrie, L.D. Baudrimont, A., Turon, J.L., 1992. Quantification of the biogenic silica dissolution in Southern Ocean sediments. Palaeogeogr. Palaeoclimatol. Palaeoecol., 61, 79–95.

Phipps Morgan, J., and Morgan, W.J., 1999. Two-stage melting and the geochemical evolution of the mantle: a recipe for mantle plum-pudding, Earth Planet Sci Lett 170, 215-239.

Phipps Morgan, J., W.J. Morgan, Y.-S. Zhang, und W.H.F. Smith, 1995. Observational hints for a plume-fed, suboceanic asthenosphere and its role in mantle convection, J. Geophys. Res. 100, 12753-12767.

Piepgras, D. J., and G. J. Wasserburg, 1982. Isotopic composition of neodymium in waters from the Drake Passage, Science, 217, 207-214.

Piotrowski, A.M., Goldstein, S.L. Hemming, S.R., and Fairbanks, R.G., 2005. Temporal relationships of carbon cycling and ocean circulation at glacial boundaries, Science, 307, 1933-1938.

Prell, W. L., Hutson, W.H., Williams, D.F., 1979. The Subtropical Convergence and late Quaternary circulation in the southern Indian Ocean. Mar. Micropaleontol., 4, 225–234.

Prell, W.L., Imbrie, J., Martinson, D.G., Morley, J.J., Pisias, N.G., Shackleton, N.J., Streeter, H.F., 1986. Graphic correlation of oxygen isotope stratigraphy application to the Late Quaternary. Paleoceanography, 1, 137–162.

Rutberg, R.L., S.R. Hemming, and S.L. Goldstein, 2000. Reduced North Atlantic Deep Water flux to the glacial Southern Ocean inferred from neodymium isotope ratios, Nature, 405, 935-938

Sandwell D.T., A detailed view of the South Pacific geoid from satellite altimetry, 1984. J Geophys Res 89, 1089–1104.

Sarmiento, J.L., and Toggweiler, J.R., 1984, A new model for the role of the oceans in determining atmospheric PCO (sub 2): Nature (London), v. 308, p. 621-624.

Schilling, J.-G., 1973. Iceland mantle plume: geochemical study of Reykjanes Ridge, Nature 242, 565-571.

Schilling, J.-G., 1985. Upper mantle heterogeneities and dynamics, Nature 314, 62-67.

Schilling, J.-G., 1991. Fluxes and excess temperatures of mantle plumes inferred from their interaction with migrating mid-ocean ridges, Nature 352, 397-403.

Schneider, W., R. Fuenzalida, E. Rodrıguez-Rubio, J. Garces-Vargas, and L. Bravo, 2003. Characteristics and formation of eastern South Pacific Intermediate Water, Geophys. Res. Lett., 30(11), 1581, doi:10.1029/ 2003GL017086.

Scott, G.H., Bishop, S., Burt, B., 1990. "Guide to some Neogene Globorotalids (Foraminiferida) from New Zealand." New Zealand Geological Survey Paleontology Bulletin 61, 135 p.

Scott, G.H., 1991. Revision of the boundary between Lillburnian and Waiauan Stages (middle Miocene, New Zealand). New Zealand Journal of Geology and Geophysics 34, 397-406.

Scott, G.H., 1995. Coiling excursions in Globorotalia miotumida: high resolution bioevents at the middle-upper Miocene boundary in southern temperate water masses? Journal of Foraminiferal Research 25, 299-308.

Scott, G.H., Kennett, J.P., Wilson, K., Hayward, B.W., 2007. Globorotalia puncticulata: population divergence, dispersal and extinction related to Pliocene-Quaternary water masses. Marine Micropaleontology 62, 235-253.

Sigman, D.M. und Boyle, E.A., 2000. Glacial/ interglacial variations in atmospheric carbon dioxide, Nature, 407, 859-869.

Sigman, D. M., Jaccard, S. L. and G.H. Haug, 2004. Polar ocean stratification in a cold climate. Nature 428, 59–63.

Sleep, N.H., 2007. Origins of the plume hypothesis and some of its implications. In: Foulger, G.R., Jurdy, D. M. (Eds.), Plates, plumes, and planetary processes, Geol. Soc. Am. Spec. Paper 430, 29–45.

Smith, W.H.F. and Sandwell, D.T., 1997. Global sea floor topography from satellite altimetry and ship depth soundings. Science 277,1956–1962.

Stoffers et al., 2003. Cruise Report SONNE 167 Louisville Ridge: Dynamics and Magmatism of a Mantle Plume and its Influence on the Tonga–Kermadec Subduction System. Report Nr. 20, Institute for Geosciences, University of Kiel, ISSN 0175-9302.

Daniel M. Sigman, D.M., Hain. M.P. and G.H. Haug, 2010. The polar ocean and glacial cycles in atmospheric CO_2 concentration. Nature 466, doi:10.1038.

Stephens, B.B., and Keeling, R.F., 2000. The influence of Antarctic sea ice on glacial-interglacial CO (sub 2) variations: Nature (London), v. 404, p. 171-174.

Stoffers, P., and Shipboard Party, Cruise Report SONNE 157, 2001. Foundation 3, Magmatic and Hydrothermal Processes at a Spreading Axis influenced by a Hotspot. The Pacifik-Antarctic Ridge and Off-Axis Seamounts near 37° S. Ber.-Rep. Inst. Für Geowiss. Universität Kiel, Nr. 17, 112p.

Stoffers, P., Worthington, T.J. and Shipboard Scientific Party of SO-157, 2002. Silicic Volcanism and Hydrothermal Activity on the Pacific-Antarctic Ridge. Eos, Trans. Am. Geophysical Union 83: No.28.

Tarduno, J., Bunge, H-P, Sleep, N., Hansen, 2009. The Bent Hawaiian-Emperor Hotspot Track: Inheriting the Mantle Wind. Science 324, 50-53.

Wentworth, C.K., 1922. A scale of grade and class terms of clastic sediments. J. Geol., 30, 377–392.

Wilson, J.T., 1963. A possible origin of the Hawaiian Islands. Can. J. Phys. 41, 863-870.

Wolfe, C.J., Solomon, S.C., Laske, G., Collins, J.A., Detrick, R.S., Orcutt, J.A., Bercovici, D., Hauri, E.H., 2009. Mantle shear-wave velocity structure beneath the Hawaiian hot spot. Science 326, 1388-1390, doi:10.1126/science.1180165.

Young, J., 1998. Neogene. In: Bown, P. R. (Ed.) Calcareous nannofossil biostratigraphy, Chapman & Hall, London, pp. 225-265.